

UFPS: A unified framework for partially-annotated federated segmentation in heterogeneous data distribution**Authors**

Le Jiang, Li Yan Ma, Tie Yong Zeng, Shi Hui Ying

Correspondence

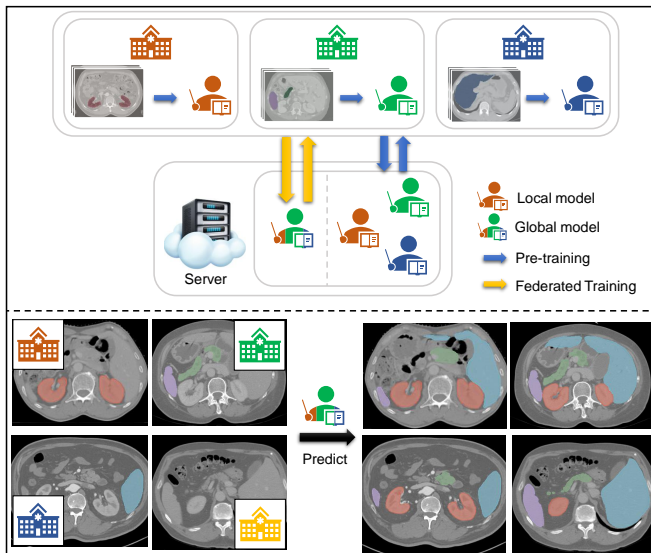
liyanma@shu.edu.cn

eTOC blurb

Partially supervised segmentation is a deep learning paradigm both frugal in label use and limited by data privacy issues and domain gaps in medical practice. This work presents a unified federated partially-labeled segmentation framework. By systematically analyzing challenges in federated partially supervised segmentation, we give more insights into how to generalize on different domains better without class collision based on partially-annotated datasets.

Highlights

- Challenges and solutions for federated partially supervised segmentation are provided
- Training a global model via heterogeneous datasets without class intersections
- Comprehensive experiments demonstrate the global model is effective on most classes for all domains

Graphical abstract

THE BIGGER PICTURE Labeling numerous data for segmentation tasks is labor prohibitive and requires expert knowledge for some classes. Partially supervised segmentation task seeks to solve this issue based on several partially-annotated datasets but is restricted in medical practice due to data privacy and domain gaps. Federated learning can be one solution to resolve privacy concerns but there is hardly any work on the combination of both technologies. The authors analyze underlying challenges and propose a unified federated partially-labeled segmentation framework to conduct federated partially supervised segmentation task. Extensive experiments validate the promising performance of the proposed solution with an application under a heterogeneous real-world setting in a privacy preserving manner where knowledge specific participators cooperate to train a universal global model.

Level 2. Proof-of-Concept: Data science output has been formulated, implemented, and tested for one domain/problem

UFPS: A unified framework for partially-annotated federated segmentation in heterogeneous data distribution

Le Jiang^a, Li Yan Ma^{a,*}, Tie Yong Zeng^b and Shi Hui Ying^c

^aSchool of Computer Engineering and Science, Shanghai university, Shanghai, China

^bDepartment of Mathematics, Chinese University of Hong Kong, Hongkong, China

^cDepartment of Mathematics, Shanghai university, Shanghai, China

ARTICLE INFO

Keywords:

Federated Learning
Medical Image Segmentation
Partial Label

SUMMARY

Partially supervised segmentation is a label-saving method based on datasets with fractional classes labeled and intersectant. However, it is still far from landing on real-world medical applications due to privacy concerns and data heterogeneity. As a remedy without privacy leakage, federated partially supervised segmentation (FPSS) is formulated in this work. The main challenges for FPSS are class heterogeneity and client drift. We propose a Unified Federated Partially-labeled Segmentation (UFPS) framework to segment pixels within all classes for partially-annotated datasets by training a totipotent global model without class collision. Our framework includes Unified Label Learning and sparsed Unified Sharpness Aware Minimization for unification of class and feature space, respectively. We find that vanilla combinations for traditional methods in partially supervised segmentation and federated learning are mainly hampered by class collision through empirical study. Our comprehensive experiments on real medical datasets demonstrate better deconflicting and generalization ability of UFPS compared with modified methods.

1. INTRODUCTION

Promoted by the progress of deep learning¹, techniques in the field of computer aided diagnosis^{2,3} have assisted clinicians with effective routine. Most of these techniques need large-scale data with abundant diversity to maintain reliability^{4,5}. Nevertheless, it requires specialized knowledge and intensive labor to collect annotations for medical data, especially for dense pixel-level tasks. Recently, partially supervised segmentation (PSS)^{6,7,8,9} has emerged as a label-saving means in allusion to the problem. Unlike traditional learning paradigm, PSS aims to achieve segmentation tasks on datasets with only a subset of all classes annotated for each dataset. Besides, there can be hardly any intersectant labeled classes between datasets in PSS, while the union includes all classes concurrently.

Existing works for PSS^{6,7,8,9} mainly count on centralized datasets, which are against privacy regulations in real-world medical applications¹⁰. Federated learning (FL)¹¹, a distributed learning framework, can serve as a promising solution to this challenge. It allows all clients (e.g., hospitals or apartments) to cooperate in training a global model with similar function as the one in centralized learning by aggregating model weights or gradients without data disclosure. However, utilizing partially-annotated labels to train a global segmentation model in the FL scenario is under-explored. In this work, we extend the formulation of PSS to an FL manner, i.e., federated partially supervised segmentation (FPSS). Apart from low demands for label integrity and protection for data privacy, this setting has the potential to boost model generalization through knowledge communication as well.

*Correspondence: liyanma@shu.edu.cn

^aThese authors contributed equally.

The learning process for FPSS encounters two major challenges, namely, class heterogeneity and client drift. The class heterogeneity problem is caused by inconsistency of annotated classes among clients. To give a straightforward illustration of solutions in centralized learning to the class heterogeneity problem, we present an example in Figure 1. When all unannotated classes are merged into the background class to calculate loss functions (Opt 1), the global model suffers severe class conflict. It comes to the fact that foreground annotations for each client are mistaken as background ones in other clients. When clients only use foreground classes to calculate loss (Opt 2), foreground channels without supervision can be optimized to any false direction. One simple but feasible solution for the class conflict issue is to aggregate part of the whole model globally and keep rest parts local, e.g., excluding the segmentation head from global model aggregation. However, some classes may be relevant in the medical field (e.g., relative organ position in CT image^{12,13,14}). This approach may hinder potential interaction between classes in the course of training and requires extra computational cost during evaluation.

In FL, client drift is caused by the assumption that data across clients are in non-independent and identically distributed distribution (non-IID)^{15,16}. It can be ascribed to multiple factors in the medical field like differences in data collection protocols¹⁷ or devices¹⁸, population diversity¹⁹, etc. When weights or gradients with a huge divergence between clients are aggregated under the non-IID setting, the global model can be optimized to a suboptimal solution and the convergence speed can also be decelerated. Previous methods to tackle the problem in FL can be categorized into three major directions: local optimization rectification^{20,21,22,23,24,25,26}, client selection^{27,28}, and contrastive learning^{29,30,31,32,33}. While client selection is mainly de-

signed for full class supervised learning, contrastive learning is costly both in computational time and memory, especially for Unified Federated Partially-labeled Segmentation (UFPS) in the medical field. Although there are lots of works about local optimization rectification, most of them only emphasize on optimization, ignoring the importance of local data distribution.

To resolve the aforementioned two challenges, we propose a framework called Unified Federated Partially-labeled Segmentation (UFPS). It alleviates effects of class heterogeneity and client drift via Unified Label Learning (ULL) and sparse Unified Sharpness Aware Minimization (sUSAM), respectively.

In FPSS, only a subset of all classes are labeled for each client, and common PSS methods in centralized learning fail to generalize. Therefore, to exploit underlying class intersections without class conflict problem, ULL labels all classes in a unified manner based on pretrained class-specific teachers. Since the pretraining step is executed locally, clients can train their models at any time, which is free from communication burden and stability in FL³⁴. Different from traditional pseudo labeling process, we filter the intersection part within pretrained teachers in the background channel as the ground truth to avert concept collision among clients. It is the first attempt to bring the pseudo labeling idea into FPSS. Thus, the class heterogeneity problem is translated to a noisy label learning issue.

We tackle the noisy label learning issue from both global and local perspectives. Since the global model benefits from overall data distribution and class interactions, it can serve as a more reliable source of pseudo labels. By increasing model aggregation weights of clients with high-quality data, the global model is more likely to concentrate on credible knowledge, thus better guiding local models. For local models, their common bottleneck is mainly caused by the coupling between noise and hard classes in pseudo labels. A loss weight scheduler is then proposed to alleviate side effects of noises while better fitting hard classes.

As a counterpart for the non-IID issue, Adaptive Sharpness Aware Minimization (ASAM), as an effective two-step approach has been proven in previous work FedASAM³⁵. Despite the good performance of ASAM, some directions may be far from global cliffy ways since these two steps are both based on the plain local dataset. When each local model is optimized towards the sharpest local direction, parts of these directions may be relevant to some client-specific attributes, thus restricting the generalization ability of the global model. Besides, the training time of FedASAM is doubled compared with FedAvg. For better generalization, our proposed sUSAM allows local models to approximate a unified optimization target for all clients through strong data augmentation. The effect of data augmentation is merely studied in the field of FL since underlying data information is banned from sharing. Besides, attempts to transfer traditional data augmentation to FL either promote the global model performance limitedly through slight augmentation or worsen it through strong augmentation³⁵. By

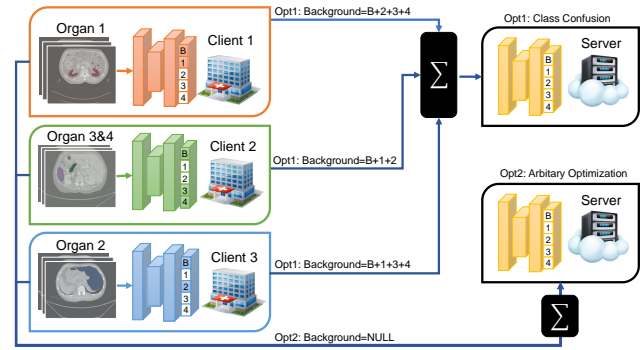


Figure 1: Illustration of solutions in centralized learning to class heterogeneity problem for FPSS on CT images.

Each client has only two or three classes annotated, which are colored in the segmentation head. 'Opt 1' merges unannotated classes into the background class to calculate the loss. 'Opt 2' only uses the foreground class(es) to calculate the loss.

decoupling training data for two steps in ASAM, local models can be free from training instability caused by strong data augmentation. To accelerate the ASAM based framework and avoid overfitting local-specific attributes, we only concentrate on the most essential ascent directions to optimize with and explore latent ones to enhance generalization ability of the global model. Through our experiments, we demonstrate our approach is capable of getting a large margin beyond previous methods. Our contributions can be concluded as:

- We investigate challenges for federated partially-annotated segmentation (FPSS) systematically and propose a heterogeneous benchmark based on our solutions.
- We propose a Unified Federated Partially-annotated Segmentation (UFPS) framework for FPSS based on pseudo labeling technology for the first time, in which unified label learning (ULL) and sparse Unified Sharpness Aware Minimization (sUSAM) are designed to cope with class heterogeneity and client drift issues, respectively.
- The comprehensive experiments on the benchmark validate the effectiveness of our proposed method.

2. RELATED WORK

2.1. Partially Supervised Segmentation in Medical Domain

Many efforts have been made to conduct PSS in the medical domain. Deep Learning (DL) based approaches can be divided into three main branches, i.e., prior guided segmentation, index conditioned segmentation, and pseudo label based segmentation.

Priori guided segmentation methods like PaNN⁶ distills the volume ratio of target organs based on a fully labeled dataset, which may be hard to collect in real applications.

PRIMP³⁶ proposes to use average masks for several groups as a priori, but it relies on manual preprocessing for start and end slices. These methods can be hard to implement in an FL scenario once such priori varies significantly between domains.

Cond-dec³⁷ and DoDNet³⁸ integrate organ indexes into the network. While the former encodes indexes to hash values and takes them as additional activations for each layer, the latter combines the bottleneck feature and an index vector to dynamically generate weights and bias for the segmentation head. Both of them require repetitive forward steps for all organs during the process of reference, which is time-consuming, especially in the medical domain.

CPS³⁹, a pseudo label based segmentation method, proposes to use siamese networks supervising each other to correct potential noises in pseudo labels. Another way in this research field is MS-KD⁴⁰, designing a framework that pre-trains teacher models based on several datasets, each for one organ, to give pseudo labels. Features in all layers are distilled along with final logits in MS-KD to ease model training when the loss function is mere Kullback-Leibler (KL) loss⁴¹. Other methods belong to none of these branches like PIPO⁹ utilizing multi-scale inputs and features to capture details and global context. For all methods mentioned above, the domain gap issue is not taken into consideration which is common in the medical domain.

2.2. Federated Learning

One of the most serious challenges in FL is statistical heterogeneity of decentralized data. In order to surmount this barrier, numerous works are put forward. For instance, a regularization term between the global model and local models is proposed in FedProx²⁰. SCAFFOLD²¹ uses control variants to mitigate local gradient drift. These two methods are limited in highly non-IID scenarios.

MOON²⁹ performs contrastive learning based on positive pairs between the local and global models, and on negative pairs between the current local model and the one in a previous round. FedCRLD³¹ reinforces the positive correlation in MOON and stability of local models via cross-attention and the local history distillation module, respectively. Nevertheless, they are costly both in computational time and memory.

Recently, several works have presented solutions based on high order information and managed to promote generalization ability of the global model to a great extent. FedAlign²⁵ proposes to distillate Lipschitz constant between the original network block and a slimmed one. FedASAM²⁶ combines Adaptive Sharpness Aware Minimization (ASAM)³⁵ and Stochastic Weight Averaging (SWA)⁴² in FL, which is prolonged in training.

Existing methods in FL mostly ameliorate the optimization process but seldom concentrate on data relevant techniques since data sharing among clients is prohibited. Direct data augmentation may even lead to model degradation in FL as proven in FedASAM.

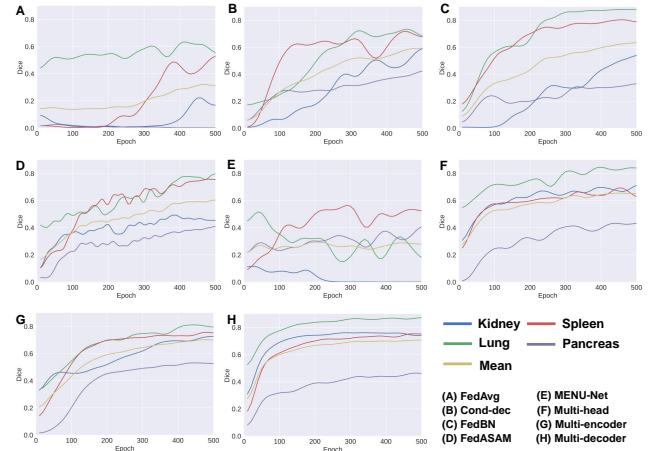


Figure 2: Mean test dice curves over all clients for different combinations between PSS and FL.

2.3. Federated Partially Supervised Segmentation

MENU-Net⁴³, as the early work in FPSS, trains a model with multiple encoders and deep supervision layers via marginal and exclusive loss. However, some foreground channels for one client may be within a background one for other clients, which is also mentioned in⁴⁴. The global segmentation head for all organs with direct aggregation is doomed to incur class conflict problem, which is demonstrated in the empirical study of our work. Besides, the global model with multiple encoders⁴⁵ is inferior to the one with multiple decoders⁴⁶. The same theory is verified in personalized federated learning (pFL)⁴⁷.

Naturally, a superior global model generalizes better than locally trained models to clients who may join FL in the future, which is common in the FL setting. Therefore, our main purpose is to train a global model instead of personalized ones for FPSS. Compared with MENU-Net, we represent comprehensive results based on originally fully labeled datasets in our experiment. To our best knowledge, it is also the first time that the global model is trained by clients with partially-annotated non-IID datasets but the benchmark performance for all organs in each client is reported. Our method only needs to forward the global model once for evaluation no matter how many organs are segmented and the global model in our approach generalizes better than local models on unseen clients.

3. RESULTS

3.1. Empirical study

Before formulating FPSS, we first study rationality of directly combining some methods for PSS with FL (Figure 1). Opt 1 in Figure 1 corresponds to (E) in Figure 2, that is, MENU-Net. Opt 2 in Figure 1 corresponds to (A), (B), (C), (D) in Figure 2. Implementation details can be found in Note S6.

To investigate the effect of solutions in centralized learning on the class heterogeneity issue, we start from the simplest case where locally trained segmentation networks are

completely aggregated in each communication round. We observe that FedAvg (Figure 2A) fails to segment pancreas in CT images, which is the hardest class among all organs since its anatomical morphology is highly varied between domains. Besides, FedAvg suffers tremendous oscillation and low convergence speed compared with the rest. We put the blame on the fact that foreground channels without supervision can be optimized to any false direction. Even with client index input into each layer of the decoder (Figure 2B) as auxiliary information or with batch normalization layers separated for each client (Figure 2C) as feature decoupling to ease training, the severe oscillation can still not be alleviated. When the method designed for highly non-IID setting (Figure 2D) is used, successive fluctuation caused by class heterogeneity still exists. It proves that the class heterogeneity issue is a more critical challenge than the client drift in FPSS.

When unannotated classes are merged into the background channel, MENU-Net (Figure 2E) suffers the most serious oscillation among all methods because foreground annotations for each client are mistaken as background ones in other clients when there exists no class intersections between clients. Thus, it can be concluded that both options in Figure 1 are not suitable for FPSS since Opt 1 and Opt 2 cannot deal with class conflict for all classes and the background class, respectively.

As long as some certain part of the local model is separated from aggregation and the part is updated based on the loss for complete partial labels (e.g., one annotated class as foreground and its inverse set as background), the oscillation can be remarkably reduced. This phenomenon stresses the significance of dealing with class heterogeneity and client drift simultaneously in FPSS. Furthermore, personalizing decoder (Figure 2H) achieves better performance than personalizing encoder (Figure 2G). The reason for this phenomenon is that global representations are closely related to better generalization ability of models in FL, which has also been proven in previous work in personalized federated learning⁴⁶. It is a priori that some classes are relevant in the medical field (e.g., relative organ position in CT image) and that layers around the bottleneck of the network usually extract high level information. Hence, personalizing such parts may hinder potential interactions between classes in the course of training. Despite the success of pFL based methods, they suffer from long inference time which is proportional to the number of classes.

Therefore, we aim to segment all classes without class conflict by filling up missing labels in a unified manner. Different from training personalized models, we also hope to train a generalized global model to forward once during testing, no matter how many target classes there are, by absorbing knowledge from all classes and all clients to learn organ interactions.

3.2. Problem formulation

In this subsection, we review objectives of PSS and FL and then define the formulation of FPSS based on empirical

study.

We first give a short review on PSS. Let $x \in X$ be the input and $y \in Y$ be its corresponding annotated label map. Suppose the entire dataset $D^p = \{D_i^p\}_{i=1}^N$ can be divided into N partially-annotated datasets where each subset D_i^p includes N_i data samples, i.e., $D_i^p = (X_i, Y_i^p) = \{(x_{ij}, y_{ij}^p)\}_{j=1}^{N_i}\}_{i=1}^N$. We denote $C_i \subset C$ as the label set of Y_i , where $|C|$ is the total number of classes. Here, we conclude some properties about classes in PSS.

Property 1. *The number of classes for the joint label space Y is fixed to N_c : $|\bigcup_{i=1}^N C_i| = N_c = |C|$.*

Property 2. *The amount of partially-annotated classes for any subset Y_i^p is usually limited: $0 < |C_i| \ll N_c$.*

Property 3. *The intersection of classes is restricted: $\forall i, j \in [1, N], i \neq j, C_i \cap C_j = c_{i,j}$, where $0 \leq |c_{i,j}| \ll N_c$.*

Consider the FL setting with N clients and the overall dataset D with N_c classes. Each client has the dataset D_i separated from D . Let w_i, w_0 denote the local model from client i and the global model, respectively. In each round, all clients upload their trained local model to the server for aggregation, and the server distributes the global model to clients as the initial local model at the next round. The global objective is to minimize the average of local empirical risks:

$$\min_{w_0 \in W} f(w_0) = \frac{1}{N} \sum_{i=1}^N f_i(D_i, w_0), \quad (\text{Equation 1})$$

where $f(\cdot)$ is the loss function.

Now, we give the formulation of FPSS and list feasible solutions for it. Suppose each client has a partially-labeled dataset D_i^p separated from D^p . The global objective for FPSS is almost same as the one for FL, i.e., Equation 1, but with more constraints (i.e., three properties listed in PSS setting):

$$\min_{w_0 \in W} f(w_0) = \frac{1}{N} \sum_{i=1}^N f_i(D_i^p, w_0), \quad (\text{Equation 2})$$

Without any preliminary step or part model aggregation, it is impossible to achieve global minimal in Equation 2 based on partially-annotated datasets due to class heterogeneity problem. Thus, one simple but feasible way is to separate part of the whole model from aggregation:

$$\min_{w_0^G \in W^G, w_i^L \in W^L} f(w_0^G, w_i^L) = \frac{1}{N} \sum_{i=1}^N f_i(D_i^p, w_0^G, w_i^L). \quad (\text{Equation 3})$$

The whole model w can be divided into $w_0^G, \{w_i^L\}_{i=1}^N$, denoting model parts aggregated globally and kept local, respectively.

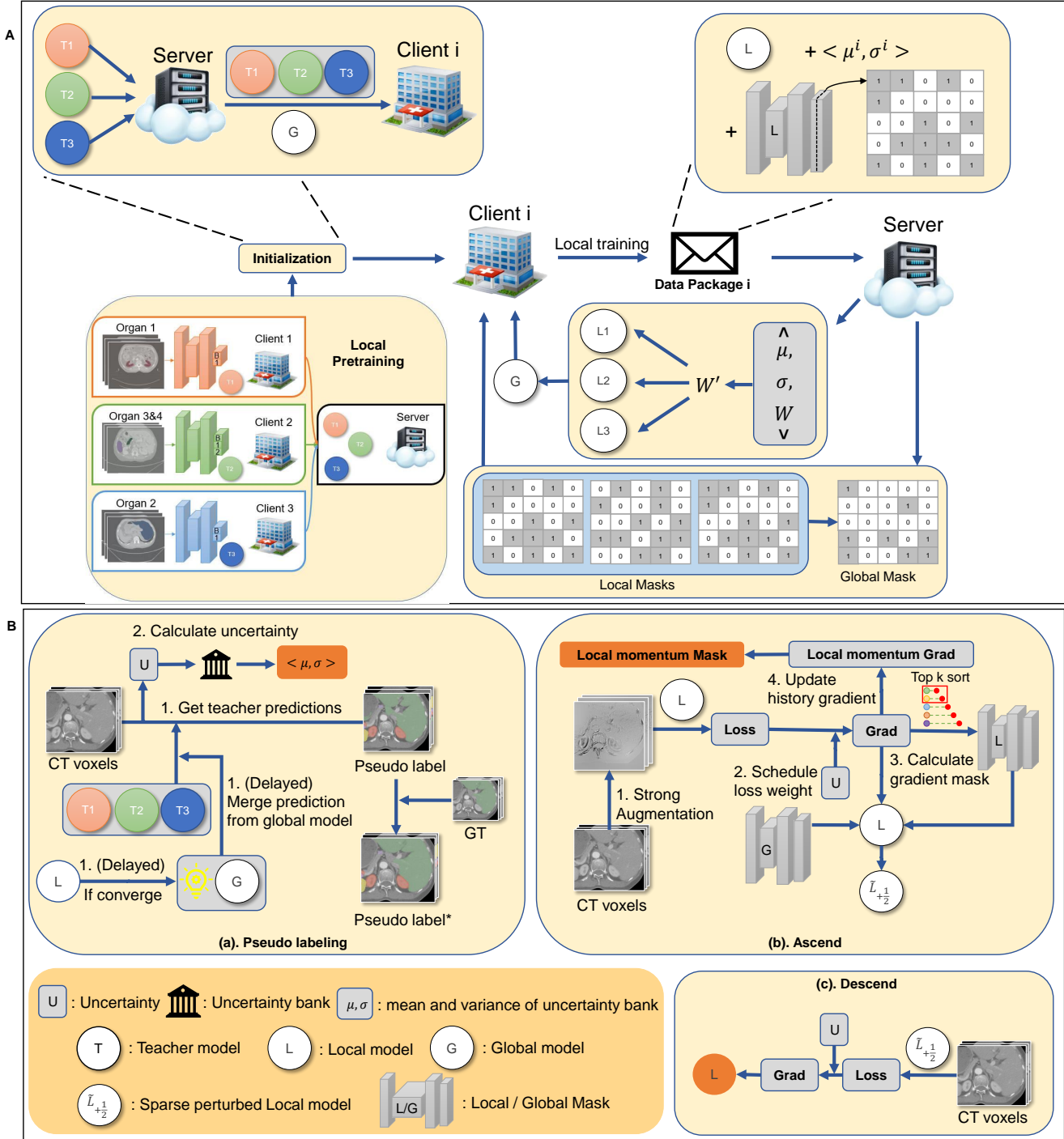


Figure 3: The overall flow of our proposed UFPS framework.

(A) Federated learning process. Operations in pseudo labeling are condensed in the 'initialization' box. The 'data package' refers to the local mask, the mean and variance of uncertainty bank for client *i*, and the local model. The low right part denotes taking the non-intersection part as the global mask. Aggregation weights are recomputed with statistics of the uncertainty bank and the original proportion weight.

(B) Local training loop. Uncertainty score for each batch is deposited into the uncertainty bank and used to reweight loss. The local mask acquired in the ascent step is combined with part of the global mask to perturb the clean model. The local momentum mask is the mask sent to the server after local training. When local training converges, the global model replaces pretrained teachers as the main teacher.

3.3. Unified Label Learning

In this subsection, we propose the pseudo labeling process for class heterogeneity problem and mechanisms for the noisy label learning issue from both global and local perspectives. The overall flow is depicted in Figure 3.

Denosing pseudo label generation. A better solution to the class heterogeneity issue should be free from class confliction and learn class interactions for better segmentation ability of the global model. In ULL, each client i first pretrains a local model as a class-specific teacher for other clients with partially-annotated labels before federation. After sending the pretrained local teacher and receiving pretrained teachers w^T from others, at each local round in FL, each client uses all pretrained teachers to get pseudo labels for all classes except ones with ground truth kept local. The background class for the pseudo label is the intersection of all teachers' background predictions, and foreground classes are merged in the predefined sequence. FL is then performed as:

$$\min_{w_0 \in W} f(w_0) = \frac{1}{N} \sum_{i=1}^N f_i(X_i, Y_{i,gt}, PL_i(X_i, w^T), w_0), \quad (\text{Equation 4})$$

where PL_i represents the operation to predict pseudo labels for X_i by w^T . $Y_{i,gt}$ denotes the annotated ground-truth labels within foreground classes for each client i . However, even though the annotated class is replaced by the ground truth, noise in rest channels may still be severe as the process of pseudo labeling is hindered by domain gaps. For this reason, the class heterogeneity problem is naturally transformed into a noisy label learning issue.

As the direct source of pseudo labels, a noise-robust teacher model can play an important role in the noisy learning problem. Otherwise, local models for full-organ segmentation may overfit misguided information in noisy pseudo labels, thus stuck at a local minimum. In⁴⁸, the global model trained on a labeled public dataset serves as the teacher model to give pseudo labels as it is more reliable than local models. However, such a public dataset is not always available in the medical domain due to privacy concerns. Even though a fully annotated public dataset to enhance model reliability is not available in our setting, predictions from the global model may still become less noisy than ones from local teacher models at some point in time since the global model absorbs knowledge from multiple organs and global data distribution. Thus, we use the global model as the main teacher (global main teacher, GMT) in the training course at that time to better supervise local models.

Although the ability of the global model to locate organs is promoted, its prediction for segmentation boundaries may be weakened. This phenomenon can be explained that the global model in FL is usually smoother than locally trained models since client drifts result in counteractions in some dimensions. Therefore, we use locally pretrained models as auxiliary teachers to refine boundary areas. Specifically, when the foreground prediction intersection of a patch be-

tween the global model and auxiliary teachers is greater than the volume percentage threshold ν , we use the intersection as the pseudo label. Otherwise, we only use forecast of the global model as convincing pseudo supervision:

$$\tilde{q} = \begin{cases} \tilde{q}^G, & \left| \tilde{q}_{c \neq 0}^{w^T} \cap \tilde{q}_{c \neq 0}^G \right| < \nu \cdot \left| \tilde{q}_{c \neq 0}^G \right|, \\ \tilde{q}_{c \neq 0}^{w^T} \cap \tilde{q}_{c \neq 0}^G, & \text{else,} \end{cases} \quad (\text{Equation 5})$$

where \tilde{q}^G denotes one-hot pseudo label from the global model and $|\cdot|$ here represents volume of the prediction.

Enlarging impact of less noisy local models. The denoising effect of GMT counts on a reliable global model, which is directly affected by the noise degree of local models. Considering that, we propose uncertainty-aware global aggregation (UA) to enhance reliability of the global model by enlarging aggregation weights of less noisy local models.

It is a common occurrence in FL that aggregation weights A^w only depend on the number of samples. However, clients with a large amount of data are not necessarily with high quality data. For FPSS, data quality can be reflected by confidence of pseudo labels. Using merged prediction from all teacher models, we first calculate data-wise uncertainty U for each sample j :

$$U_j = \frac{1}{N_c} \sum_{c=0}^{N_c-1} \frac{\sum_{vox} E_{vox} \cdot \tilde{q}_{vox,c}^{w^T}}{\sum_{vox} \tilde{q}_{vox,c}^{w^T} + 1}, \quad (\text{Equation 6})$$

where E_{vox} is average entropy across all classes and vox denotes voxel. Uncertainty scores for each client are then deposited in their individual uncertainty bank.

Besides, since local teachers are pretrained at different sites and for different organs, using only uncertainty of pseudo labels may not correctly rectify the aggregation weights. Thus, we calculate both mean μ_i and variance σ_i of the uncertainty bank for each site and combine them with the number of samples to decide the aggregation weight of each client i :

$$\hat{A}_i^w = \frac{1}{3} \left(\frac{e^{-\frac{\mu_i}{\tau^\mu}}}{\sum_j^N e^{-\frac{\mu_j}{\tau^\mu}}} + \frac{e^{-\frac{\sigma_i}{\tau^\sigma}}}{\sum_j^N e^{-\frac{\sigma_j}{\tau^\sigma}}} + A_i^w \right), \quad (\text{Equation 7})$$

where τ^μ, τ^σ are temperature hyper-parameters for mean and variance, respectively. By giving higher aggregation weights to these clients with reliable pseudo labels, the global model is less likely to be affected by these label noises. Direct assignment of \hat{A}_i^w can be improper because not all parts of the whole model are closely coupled with uncertainty. Consequently, we only apply this module to the decoder, which is most relevant to the final prediction.

Uncertainty-guided loss weight scheduler and noise robust loss. Another key factor restricting reliability of the global model is the inadequate learning for hard classes, resulting in even more severe noise than one of head classes. Pseudo labels with low confidence are more likely to be noisy or hard to segment. To avoid underfitting hard classes

and overfitting pure noise, we propose to use weight scheduler (WS) based on self-entropy for loss functions. The proposed scheduler, named tail shift (TS), is formulated as:

$$w(U_j) = \begin{cases} 2 - e^{\text{norm}(U_j) - \frac{r}{R}}, & U_j > U_{\mathcal{T}}, \\ 2 - e^{\text{norm}(U_j)}, & \text{else,} \end{cases} \quad (\text{Equation 8})$$

$$\text{where } \text{norm}(U_j) = \frac{U_j - \mu}{U_{\max} - U_{\min}},$$

where $U_{\mathcal{T}}$ corresponds to the uncertainty value at lowest \mathcal{T} percentage. μ, U_{\max}, U_{\min} represent mean, maximal, minimal uncertainty in the uncertainty bank of the current client, respectively. $w(U_j)$ is then multiplied with the overall loss function to ensure enough fitting emphasis on hard classes. Other schedulers and their impact are introduced in Note S8.

Pseudo labels given by teacher models can be quite noisy under some circumstances (e.g., restricted amount of labeled data)^{49,50}. As predictions from student models may become even more reliable than ones from teacher models during training, we use reverse cross entropy (RCE)⁵¹ loss and reweight it based on current training epoch r and total training epoch R (adaptive RCE loss, aRCE):

$$f_{aRCE} = e^{-20(1-\frac{r}{R})} \cdot (q(x) \log(p(x))), \quad (\text{Equation 9})$$

where $q(x)$ is model prediction and $p(x)$ is ground truth.

3.4. Sparse Unified Sharpness Aware Minimization

In this subsection, to alleviate the client drift problem, we introduce a unified ASAM (USAM) and its accelerating version, sparse USAM (sUSAM), based on the ASAM framework.

Optimizing towards global direction with strong data augmentation. FedASAM has been proven as an effective method for the client drift problem. In the ascent step, the objective is to approximate the steepest optimization direction. By further optimizing from the sharpest direction for the original parameter in the descent step, the global model achieves flatter minima and smoother loss landscape at each iteration.

However, local models in FedASAM may overfit some local-specific attributes, thus failing to generalize on the non-IID global distribution. Therefore, we aim to find the steepest global direction in a unified manner while maintaining the modeling capacity of local datasets. Unlike previous methods dealing with data heterogeneity in FL, we alleviate the model drift issue by approximating the underlying global data distribution through data augmentation.

From Theorem 1 in Note S2, it can be concluded that the gap between D_{global} and D_{aug} is mainly decided by constant g and its increment, caused by excessive data augmentation. Local models thus incur larger error of the upper bound for generalization on D_{global} . *Our key insights are that local models can be free from performance degradation when optimized on strongly augmented datasets indirectly and that the global model generalizes for unseen*

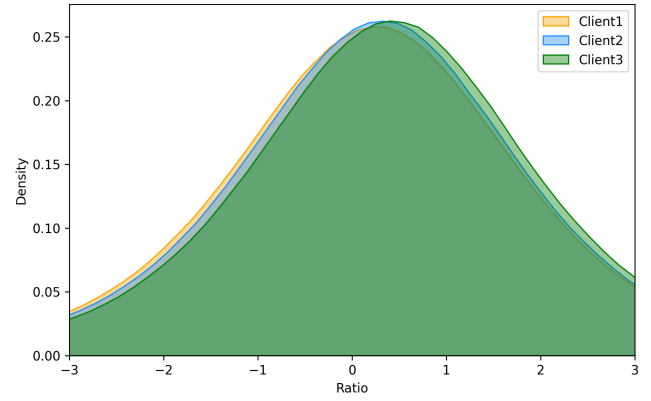


Figure 4: Relative difference ratio of gradients between the pseudo label baseline and USAM.

clients better when the local data distribution is extended to the global one through comprehensive augmentations in a privacy-preserving manner.

Thus, we propose USAM to optimize local models towards the global direction. As our setting for FPSS concentrates on medical images, we apply CMIDG⁵², a causality-inspired data augmentation method designed for the single-source domain medical image segmentation (e.g., CT and MRI), to local datasets to imitate the underlying global data distribution. CMIDG integrates medical priors and simulates real-world data from various data centers by inflicting non-linear medical noises on data. Thus, we can naturally treat CMIDG as a strong and reasonable data augmentation method to explore global cliffy ways. When CMIDG is used for both steps in ASAM in our experiment, the global model is more unstable just as what is verified in Theorem 1. Unlike FedASAM inputs the same data for ascent and descend steps, we perform the ascent step of ASAM on the augmented data through CMIDG.

Since the time complexity of USAM is about two times of FedAvg in our experiment, we only use USAM when the global model converges in late communication rounds and find it works almost as well as used for more rounds.

Accelerating and supplementing USAM with gradient mask. Although USAM has its potential to alleviate the effects of data heterogeneity, some sharp directions found in the ascent step may be relevant to attributes that only exist in a single local dataset. Besides, the time complexity of USAM is large even performed in limited rounds. We propose sUSAM focusing only on the most essential parts of perturbation to tackle both issues. Note that the principle of accelerating effect is discussed in the previous paper⁵³.

To illustrate whether all gradients deserve perturbation, we show the relative difference ratio of gradients between the pseudo label baseline and USAM:

$$r = \log \left| \frac{\nabla f_{USAM} - \nabla f_{\text{base}}}{\nabla f_{\text{base}}} \right|. \quad (\text{Equation 10})$$

As is demonstrated in Figure 4, about 60% gradients are steep (ratio more than 0). Hence, we introduce a gradient

mask M_L to only reserve gradients with top $T_L\%$ absolute value in the ascent step for USAM.

However, the sparse mask may erase some gradients accounting for vital global factors, which may be too hard to emphasize on for some clients but commonly stressed by others. To bridge this semantic gap, we propose to replace part of local masks with the nonintersecting global mask, which consists of three main steps, i.e., update of local masks and momentum gradients, communication for local and global masks, and merge of local and global masks.

Local masks are always updated in the top-k manner. In the meantime, each client maintains local momentum gradients G_{mo} on the ascent step, which is further used to calculate a momentum local mask $M_{L,mo}$. The local momentum gradients are updated at each iteration:

$$G_{mo} = \alpha_{mo} G_{mo} + (1 - \alpha_{mo}) \nabla f, \quad (\text{Equation 11})$$

where α_{mo} is hyper-parameter empirically set to 0.9.

After finishing local training, each client sends $M_{L,mo}$ to the server to represent dominant positions of local features. When receiving momentum local masks from all clients, the server merges them as a global mask M_G following the rule that nonintersecting parts of momentum local masks are set to 1 and the rest to 0:

$$\begin{aligned} (M_G)_0 &= \left(\sum_{i=1}^N M_{L,mo} \right)_0 \cup \left(\sum_{i=1}^N M_{L,mo} \right)_N, \\ (M_G)_1 &= 1 - (M_G)_0, \end{aligned} \quad (\text{Equation 12})$$

where $(\cdot)_i$ denotes positions with their values equal to i . The global mask ensures no redundant perturbation while exploring underlying global features in a unified manner. Compared with gradients of the float type, the global mask is of the bool type so the extra communication burden and privacy leakage can be almost negligible.

For these gradients G_N not in top $T_L\%$ of M_L but in the nonintersecting part of M_G , we randomly choose part of them as content for the extra perturbation mask M_E and the total length is:

$$|M_E| = \min(T_G |\nabla f|, |G_N|), \quad (\text{Equation 13})$$

where T_G is hyper-parameter to decide the proportion of the extra mask. The final descent step at the k -th iteration based on sparse disturbance is formulated based on the merge of masks:

$$w_{k+1} \leftarrow w_k - \nabla_{w_k} f(D, w_k) \Big|_{w_k + \hat{\epsilon}_k \cdot (M_L \cup M_E)}. \quad (\text{Equation 14})$$

To further save computational cost and stabilize training, the update for all masks is conducted every r_{fre} rounds. Otherwise, G_{mo} is not accumulated and a history local mask M_L got in the last update is used. In our experiment, the average computational overhead of the local mask is only 5%

Dataset	WORD	AbdomenCT-1K	AMOS	BTCV
Total selected	120	266	200	30
Partial Target	Kidney	Spleen & Pancreas	Liver	All
in-FL/out-FL	in-FL	in-FL	in-FL	out-FL
Client index	1	2	3	4

of the one for local global, which can be almost neglected. Next, we provide a summary convergence analysis for both full and part participating scenarios. Detailed assumption, proof, discussion are in Note S3 and Note S4.

It can be concluded for Theorem 2 and Theorem 3 in Note S4 that the sparse ratio for masks explicitly influences partial high order terms. Since the mask in sUSAM constrains sparse gradients, additional square and two-thirds terms are also negligible in magnitude. Besides, sUSAM is potential to generalize better by the dynamic mask, thus alleviating weight shifts in dominant terms for convergence.

3.5. EXPERIMENTAL PROCEDURES

3.5.1. Resource availability

3.5.1.1. Lead contact

Any further information, questions, or requests should be sent to Li Yan Ma (liyanma@shu.edu.cn).

3.5.1.2. Materials availability

Our study did not generate any physical materials.

3.5.1.3. Data and code availability

This study uses previously published datasets. Our source code is available at GitHub (https://github.com/tekap404/unified_federated_partially-labeled_segmentation) and has been archived at Zenodo⁵⁴.

3.5.2. Datasets

Main information of datasets is listed in Table 1. We conduct our experiments with four fully-annotated CT image datasets: WORD (<https://github.com/HiLab-git/WORD>), AbdomenCT-1K (<https://github.com/JunMa11/AbdomenCT-1K>), AMOS (<https://amos22.grand-challenge.org>) and BTCV (<https://www.synapse.org/@Synapse:syn3193805/wiki/217752>). Annotations for four organs are extracted from each dataset to serve as foreground classes, i.e., liver, kidney (left + right), spleen, pancreas. Whether a client is in the training process of FL is represented by 'in-FL' and 'out-FL'. Preprocessing details can be found in Note S6.

3.6. Training

Only the partial target set and its inverse set (background) are used to pretrain partial teacher models. Dice and BCE losses are used as default loss functions. We train all methods for 500 communication rounds and 1 local round for each global one. We conduct 10 warmup rounds to increase the minimal learning rate and accumulate uncertainty values for loss weight scheduler. Unless specially remarked, post-processing is not used. Post-processing includes filling up holes and deleting small connected components. We only

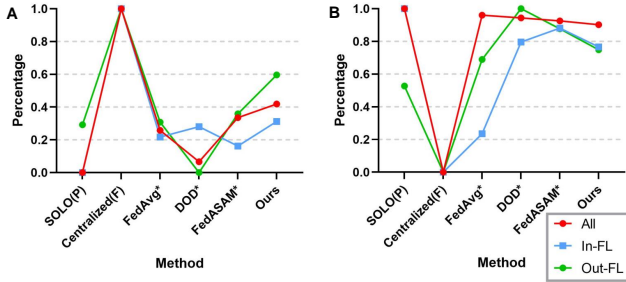


Figure 5: Client-wise comparison between SOTAs after post-processing.

- (A) Normalized Dice (↑).
- (B) Normalized HD (↓).

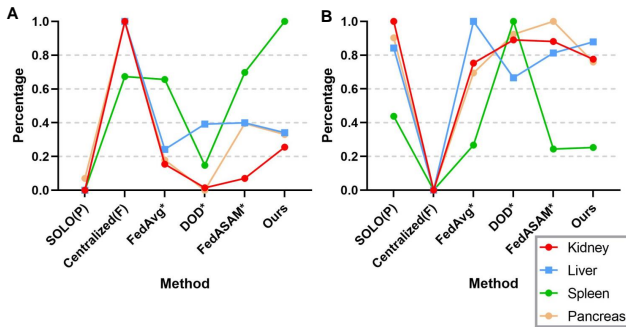


Figure 6: Organ-wise comparison between SOTAs after post-processing.

- (A) Normalized Dice (↑).
- (B) Normalized HD (↓).

show dice and HD for the mean of each dataset. Please refer to Note S6 for training details and complete results under more metrics.

3.7. Main results

3.7.1. Comparison with SOTAs

To show the lower and upper bounds of benchmarks, we first conduct experiments under local training (SOLO) and centralized training (Centralized) based on partially-annotated datasets and fully annotated ones, respectively. We use models pretrained in SOLO as organ-specific teachers to give pseudo labels. To demonstrate the effectiveness of UFPS, we compare UFPS with a variety of SOTA methods. FedAvg* is a simple combination of FedAvg and our proposed pseudo labeling procedure. Note that DOD is originally a partially-annotated method based on part model aggregation for centralized learning and we modify it into the personalized federated learning setting. Besides, FedASAM is a method designed for heterogeneous data for fully annotated federated learning. Here we embed FedASAM into the pseudo labeling framework for partially-annotated segmentation as FedASAM*. Details for all methods can be found in Note S6. Experimental results on in-FL and out-FL datasets for some representative methods are shown in Table 2, Figure 5 and Figure 6.

The benchmark, i.e., SOLO (partial), is based on

partially-annotated datasets within each client, thus incurring severe a domain gap for client 1 and client 3. For pFL based approaches, i.e., DOD* and FedCRLD, are essentially not compatible with FPSS since recognizing all classes largely depends on global universal features, as what is also demonstrated in⁵⁵ and that pFL models are likely to overfit to local biased distribution. Therefore, although DOD* is quite effective for client 2, owing to the largest aggregation weight based only on the amount of data, segmentation results for the rest are even worse than SOLO. The overall performance of FedCRLD is analogical to DOD* with only client 2 surviving the severe collapse. The over-fitting issue is exacerbated by the local momentum model. FedAvg*, FedASAM*, and UFPS (ours) are all based on the pseudo labeling framework, outperforming DOD*. Through unifying the class label space in FPSS, all these methods significantly benefit from class interactions, which proves the validity of using pseudo labels in FPSS for the first time.

Among all methods originally designed for PSS, i.e., CPS*, MS-KD*, and DOD*, CPS* achieves the best performance (73.80 in Dice). By co-training, the noise degree of pseudo labels from teacher models is somehow alleviated in a local perspective, which justifies our basic idea that the class heterogeneity problem can be translated to a noisy label learning issue.

Although the overall performance of MOON* is similar to FedAvg*, we notice that dice for client 4 is enhanced by 0.51 but in-FL results are not satisfying. We can conclude for the form of contrastive loss in²⁹ that forcing the local model to align with the global one and to keep away from its history version is potential to learn generalizable features for unseen domains, but feature extraction ability for native information may recede. Different from these contrastive learning based methods (FedCRLD and MOON*), UFPS not only justifies global distribution for all clients but it also takes some features which may be too hard to emphasize on for some clients but commonly stressed by others into account, leading to improvement for all clients compared with FedAvg*.

The tendency and principle of FedProx* are analogous to MOON* but with better out-FL performance and worse in-FL one. FedAlign refers to second-order calculation likewise. However, there is a large gap between it and sUSAM used alone, manifesting the significance of global distribution alignment under the highly non-iid setting. Since UFPS is universal for model type and regulation methods, appropriate combinations are probably beneficial.

As can be seen in Figure 5, thanks to ULL and sUSAM to denoise pseudo labels and to optimize towards the global direction, our method outperforms other methods (except upper bound Centralized Full) for both in-FL clients and out-FL clients. Specifically, our method increases by 5.35 for the baseline and 1.08 for FedASAM* in dice. Through simple post-processing, based on the accurate segmentation location and the intersection of teachers in GMT, HD of our method can also be reduced to a satisfying result, indicating its segmentation border is more refined than others. From Figure 6, it can be seen that our method even surpasses Cen-

Table 2. Comparison with SOTAs.

Method	Client 1	Client 2	Client 3	Client 4	Mean	Post
SOLO (partial, lower bound)	69.17 / 1.02	75.75 / 3.02	60.59 / 1.61	74.70 / 1.52	70.05 / 1.79	69.93 / 1.66
Centralized (full, upper bound)	78.76 / 1.10	88.33 / 1.72	79.18 / 1.33	80.78 / 1.41	81.76 / 1.39	82.25 / 1.23
FedCRLD	67.82 / 2.21	77.77 / 3.06	58.11 / 2.06	72.30 / 1.84	69.00 / 2.29	68.14 / 1.76
DOD*	61.95 / 1.15	81.76 / 2.59	60.57 / 1.69	53.52 / 1.14	70.62 / 1.72	70.77 / 1.63
CPS*	75.78 / 0.99	78.05 / 2.91	65.75 / 1.70	75.60 / 1.65	73.80 / 1.81	73.78 / 1.62
MS-KD*	74.35 / 1.00	76.68 / 2.96	63.33 / 1.66	73.10 / 1.64	71.86 / 1.81	71.77 / 1.82
FedAvg*	74.94 / 1.29	78.10 / 2.83	64.53 / 1.83	74.74 / 1.69	73.07 / 1.91	73.13 / 1.64
FedProx*	74.41 / 1.39	77.33 / 2.88	64.56 / 1.75	75.60 / 1.64	72.97 / 1.92	73.06 / 1.64
MOON*	75.00 / 1.22	77.89 / 2.88	64.10 / 1.83	75.25 / 1.69	73.06 / 1.90	73.12 / 1.61
FedAlign*	75.18 / 1.20	77.07 / 2.89	64.31 / 1.77	76.22 / 1.62	73.20 / 1.87	73.28 / 1.61
FedASAM*	77.02 / 1.39	78.15 / 2.91	65.60 / 1.75	75.14 / 1.71	73.97 / 1.94	74.20 / 1.63
UFPS (ours)	76.22 / 1.45	79.56 / 2.82	66.82 / 2.04	77.22 / 1.72	74.95 / 2.01	75.28 / 1.62

'Post' represents mean results after post-processing.

Here we only show Dice / HD (higher / lower numbers are better) for the mean of each dataset.

All methods marked asterisk are not FPSS methods originally and modified to fit the FPSS setting. DOD* is combined with the multi-decoder setting in empirical study. Others with asterisk are combined with the pseudo labeling procedure.

Please refer to Note S6 for modification details and Note S7 for complete results.

tralized Full on the class 'Spleen', which proves the strong generalization ability of our method and its potential to save labor for labeling full annotations. Besides, our approach also gains a large margin for the class 'Kidney' compared with methods except for the upper bound and achieves approximate performance for other organs.

3.7.2. Ablation study

In this subsection, we prove validity of each module proposed in our paper and provide main ablation studies for all of them.

Module validity. Table 3 shows module validity for UFPS. We can conclude that the order of module importance is $GMT > WS > sUSAM > UA > aRCE$. Since local teachers pretrained at client 1 and client 3 are not generalized enough for the global distribution, which is dominant by the dataset from client 2, predictions from local models trained in the FL process can be gradually less noisy than these pseudo labels. Therefore, using aRCE as an extra loss gets a reasonable promotion. When WS is employed to force these models to concentrate on hard classes, all classes can be fitted simultaneously with similar emphasis. What is more important, class interactions are fully explored by local models in this situation, resulting in enhancement for all clients by a large margin. UA is basically designed for these clients with high data quality and with head class annotations. By correctly rectifying the aggregation weight, the model performance gains. When all classes are denoised through previous modules, GMT is able to use the global model to give more reliable pseudo labels than locally pretrained teachers. Due to another favorable factor that the global model is indirectly trained on global distribution, the overall performance becomes even better. Benefitting from optimization towards the global steepest direction at each site and guidance for latent global directions from other clients, ULL additional

with sUSAM is profitable for most clients with few extra computational costs.

As for the relationship between modules, WS, as an essential part to ensure the training quality of the early training phase, mainly interacts with UA since a lot of uncertainty values are accumulated at this stage to model a reliable uncertainty distribution for each client. It also ensures that the noise degree of pseudo labels is not too large to affect basic parts in other modules implicitly. When GMT is invoked, it has mutual effects with sUSAM and UA considering the fact that sUSAM performs global alignment for the global model and UA rectifies the aggregation weights to guarantee the global model is dominated by local models trained with high quality data. Inversely, GMT offers more accurate pseudo labels for the two modules. Through analogy, aRCE relieves the influence of noisy labels as well, thus forming a virtuous cycle with GMT.

Ablation for ULL. Main ablations for ULL are all shown in Figure 7. In the subfigure of Figure 7A, it can be observed that the model performance of FedAvg* gets higher along with the training process and surpasses pretrained teachers, i.e., SOLO, at the 300-th epoch. Thus, it lays foundation to use RCE loss since predictions are better than pseudo labels due to organ interactions. The result in the bigger picture further proves our assumption that enlarging the coefficient for RCE loss, i.e., aRCE loss, is better than a fixed one for the increasing reliability of local models in the FL stage.

For the threshold of shifting in Figure 7B, when it is set to a moderate value, the local model is neither greatly affected by label noises nor easily neglects tail classes, thus enhancing performance for all clients. For our future work, we intend to solve this problem by determining this hyperparameter adaptively.

As demonstrated in Figure 7C, client 1 in this experi-

Table 3. Ablation study on module validity.

PL	aRCE	WS	UA	GMT	sUSAM	Client 1	Client 2	Client 3	Client 4	Mean
						69.17 / 1.02	75.75 / 3.02	60.59 / 1.61	74.70 / 1.52	70.05 / 1.79
✓						74.94 / 1.29	78.10 / 2.83	64.53 / 1.83	74.74 / 1.69	73.07 / 1.91
✓	✓					75.53 / 1.23	77.71 / 2.87	65.37 / 1.78	74.75 / 1.71	73.34 / 1.89
✓		✓				75.98 / 1.58	78.24 / 2.86	66.33 / 1.74	76.35 / 1.65	74.22 / 1.96
✓			✓			76.65 / 1.39	78.05 / 2.92	64.81 / 1.89	75.19 / 1.72	73.67 / 1.98
✓				✓		77.77 / 1.18	77.58 / 2.85	65.64 / 1.96	76.09 / 1.73	74.27 / 1.93
✓					✓	77.06 / 1.38	78.23 / 2.89	65.53 / 1.89	75.34 / 1.74	74.04 / 1.98
✓	✓	✓				75.99 / 1.44	78.22 / 2.86	66.89 / 1.92	76.48 / 1.70	74.39 / 1.98
✓	✓	✓	✓			76.93 / 1.37	78.08 / 2.89	66.56 / 1.95	76.22 / 1.62	74.44 / 1.98
✓	✓	✓	✓	✓		76.12 / 1.51	78.83 / 2.86	67.30 / 1.95	77.07 / 1.70	74.83 / 2.00
✓	✓	✓	✓	✓	✓	76.22 / 1.45	79.56 / 2.82	66.82 / 2.04	77.22 / 1.72	74.95 / 2.01

Pseudo label, adaptive RCE loss, weight scheduler, uncertainty-aware global aggregation, global main teacher, sparse Unified Sharpness Aware Minimization are denoted as PL, aRCE, WS, UA, GMT and sUSAM, respectively. Here we only show dice / HD (higher / lower numbers are better) for the mean of each dataset. Please refer to Note S8 for more results.

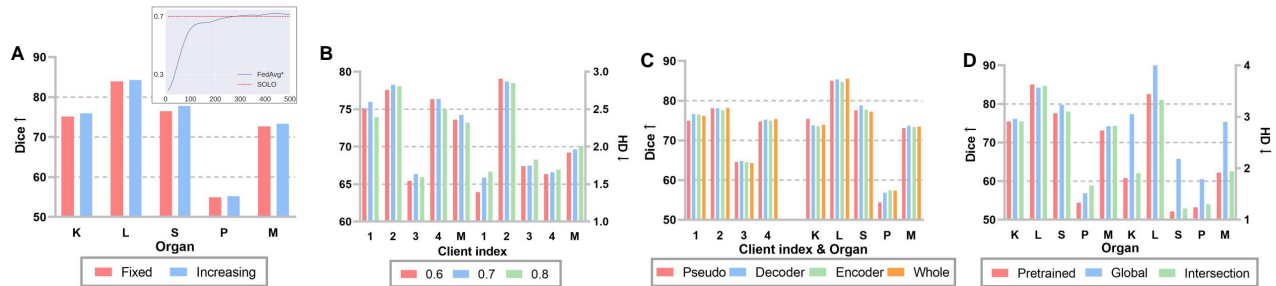


Figure 7: Ablation for ULL.

K, L, S, P, M represent kidney, liver, spleen, pancreas, mean, respectively.

(A) Organ-wise dice comparison for strategies of aRCE. The subfigure is a training dice curve for FedAvg*.

(B) Client-wise dice and HD comparison for the uncertainty threshold in WS.

(C) Client-wise and organ-wise dice comparison for module position of UA.

(D) Organ-wise dice and HD comparison for strategies of GMT.

mental setting only has the kidney class annotated before FL, whose aggregation weight is increased at most among all clients through UA. But the promotion is not from the class 'Kidney', which proves that the specific class(es) that a client has ground truth annotation is not necessarily related with the overall uncertainty of pseudo labels closely. What actually plays a key role is global model aggregation based on mean and variance of uncertainty. It rectifies model aggregation weights to those clients whose data is of high quality but of less amount. This operation sacrifices little or no fitting ability for others compared with the pseudo labeling baseline. Furthermore, conducting this module merely on the decoder is slightly better than on the whole model but much better than on the encoder plus deep supervision. The reason for this phenomenon is probably due to the closer relationship between prediction uncertainty and decoder.

It is obvious from Figure 7D that when the global model is taken as the main teacher after a certain point, i.e., the 300-th epoch in our experiment, owing to its better generalization ability than that of pretrained teacher models, it achieves a huge performance gain on the client who is of worse per-

formance. Furthermore, when we take intersection between global and pretrained teacher models, regions with high confidence are taken as our final prediction, so the ambiguity of border can be significantly alleviated, which is proven by HD.

Ablation for sUSAM. We first display Figure 8A to comprehensively validate our motivations for sUSAM. The data augmentation method that we use, i.e., CMIDG, whose distribution density is in direct proportion to the number of epochs. The comparison between (1) and (2) indicates its sensitivity to training rounds, thus resulting in heavy computational costs since the augmentation is generated from a network. Since the local sharpest direction is not necessarily the global steepest direction, simply performing the ascent step of ASAM on original data in (3) intensifies client drifts, and it is even worse than random perturbation in (4). USAM, i.e., (5), with comparison to (2) and (7), demonstrates our insight that local models can be free from performance degradation when optimized on strongly augmented datasets indirectly. That is, conducting CMIDG in the ascent step and descending on the original data benefit models from abun-

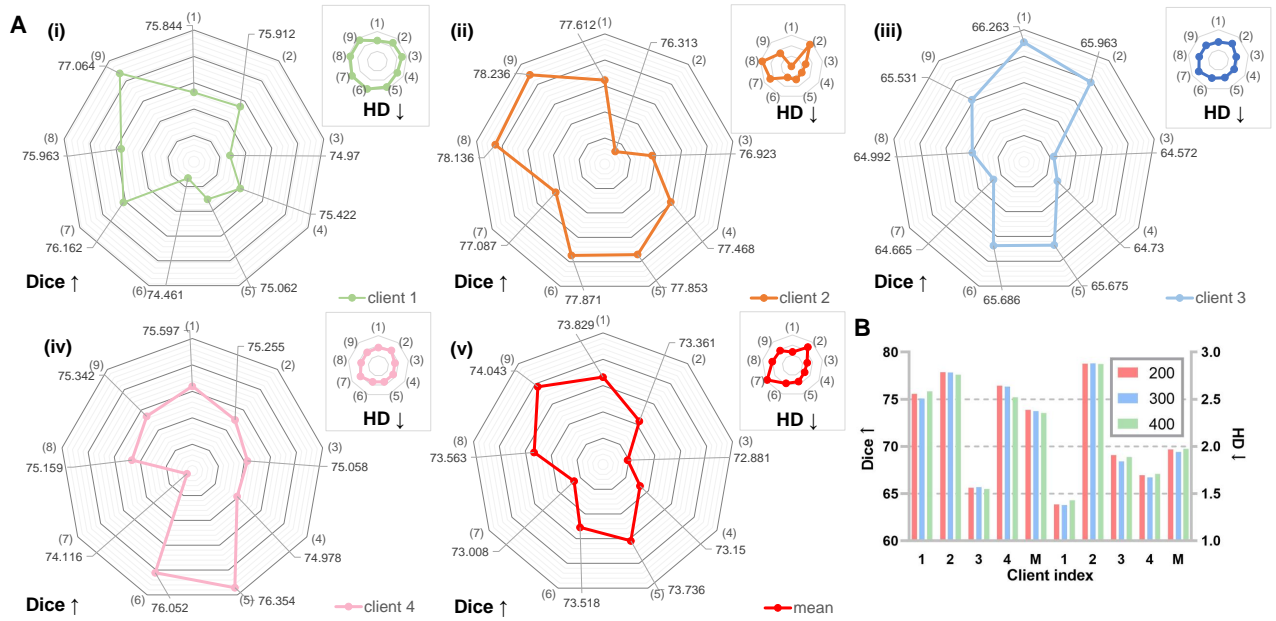


Figure 8: Strategy ablation for sUSAM.

(A) The larger radar map corresponds to dice and the smaller one corresponds to HD.

(1) CMIDG from beginning. (2) CMIDG from the 300th epoch. (3) Original data + ASAM. (4) Random perturbation + ASAM. (5) USAM. (6) USAM + (0.8 * original weight + 0.2 * perturbed weight for descent step). (7) CMIDG for both ascent and descent steps. (8) USAM + top k perturbation. (9) sUSAM.

(B) The start epoch of USAM.

dant data distribution while keeping their fitting ability on local distribution even under excessive augmentation. What should be paid most attention to is that the out-FL client BTCV achieves the best result in this setting, which shows the great potential of USAM to generalize better on unseen data distribution. If original parameters and perturbed ones are combined to calculate loss, i.e., (6), model performance slightly drops, proving necessity of the perturbation in the ascent step.

For partial gradient perturbation (8), it degrades the model performance for a little degree just as results in SSAM⁵³. Through the non-intersection global mask in sUSAM, underlying steep directions for global distribution are fully explored. Consequently, model performance for in-FL clients in (9) is greatly increased.

When modifying the start epoch of USAM from 300 to 200 in Figure 8B, we find the gain from data density is limited, so we choose 300 as the start epoch to balance training speed and accuracy. Besides, benefiting from most essential perturbation directions in a global perspective, our method mere with sUSAM for 200 epochs surpasses the SOTA method FedASAM with 500 epochs for ASAM.

To prove the generalization ability of sUSAM, we first plot loss landscape on the training set (Figure 9). Compared with FedAvg* achieving sharp minima for all clients, UFPS achieves lower loss for all clients. For client 1, the landscape under loss value 0.8 is overall flatter benefiting from the corrected model aggregation weights and gradient mask for the global descending direction. All statistics extracted from the Hessian for the global model (Table 4 and Figure 10) all

demonstrate the generalization ability can be improved by seeking to flatter minima explicitly in a heterogeneous setting.

3.7.3. Visual Evaluation

As the global model in our method is trained from multiple sites and organs, it is effective to reduce false negatives compared with other methods, e.g., spleen in client 1, kidney in client 2 and 3 in Figure 11. Besides, the overall contour predicted by our global model is obviously smoother, especially for pancreas and junctions between organs.

From the 3D segmentation results in Figure 12, DOD* generates more false positives for client 3 and client 4. It can explained by the facts that data distribution of client 3 is relatively biased from the global and that client 4 is not involved in training. This proves that personalized models do not have desirable generalization ability. By contrast, UFPS uses a single model to generalize well on all datasets and all classes. Furthermore, UFPS is also able to fix some unnatural segmentation in ground truth, e.g., spleen in client 1, which shows the great potential to apply our method in real-world applications.

4. Discussion

In this work, we analyze challenges in FPSS for direct combinations between PSS and FL methods. Our proposed UFPS is able to segment all classes based on several partially-annotated datasets by a single global model. Our training process integrates ULL and sUSAM. While ULL

UFPS

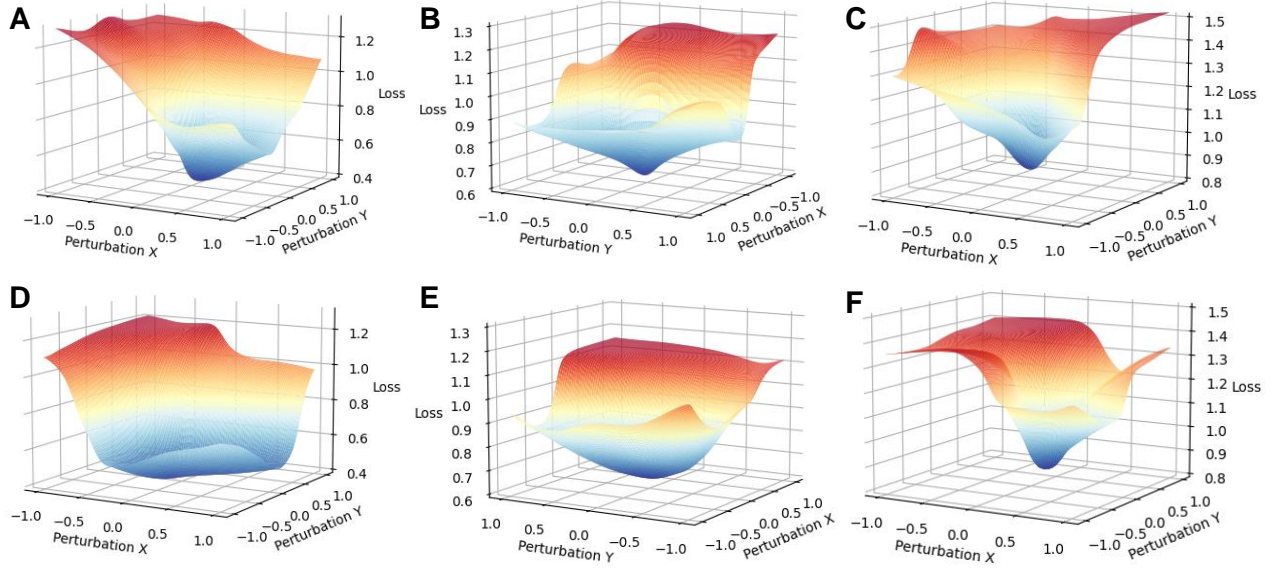


Figure 9: Loss landscape on the training set.

Model generalization is better when the overall loss landscape is flatter.

(A, B and C) Loss landscapes from FedAvg* for client 1, client 2 and client 3, respectively.

(D, E and F) Loss landscapes from UFPS (ours) for client 1, client 2 and client 3, respectively.

Table 4. Statistics related to model generalization.

Client	λ_{max} (pseudo)	λ_{max} (ours)	λ_{max}/λ_5 (pseudo)	λ_{max}/λ_5 (ours)	trace(pseudo)	trace(ours)
1	11.512	8.422	2.125	1.956	170.1	60.8
2	68.286	21.84	6.643	3.132	393.7	269.6
3	158.768	31.221	5.723	2.245	165.6	57.2

Model generalization is better when all of these statics are lower.

λ_{max} and λ_5 mean the top eigenvalue and the 5th top eigenvalue of the Hessian for the global model, respectively.

denoises pseudo labels and explores underlying values in hard classes, sUSAM unifies local training in FL to a global direction. The overall framework is of low demand for computational resources and time-saving during test time compared with pFL based methods.

Our experiments demonstrate the strong generalization ability of UFPS since it absorbs knowledge from multiple sites and organ interactions. Effectiveness and sensitivity of hyper-parameters for each module in ULL are also comprehensively investigated. Through detailed module ablation studies of sUSAM, we verify our key insights on how to en-

hance ASAM based framework to a more generalized and faster version in FL.

In terms of limitation, some key hyper-parameters, e.g. threshold in WS and perturbation radius of UFPS, rely on manual fine-tuning. This can be resolved by reinforced learning or other automatic parameter adjusting methods.

5. SUPPLEMENTAL INFORMATION

Supplemental information can be found at Supplemental information.pdf.

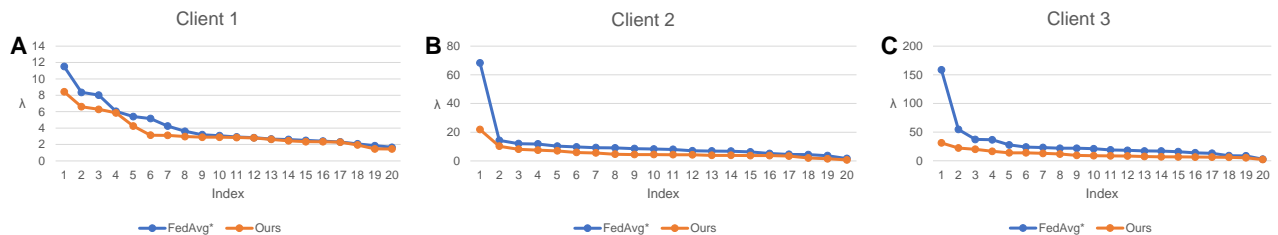


Figure 10: Hessian eigenspectra of the global model.

(A, B and C) Statistics of Hessian for client 1, client 2, client 3, respectively.

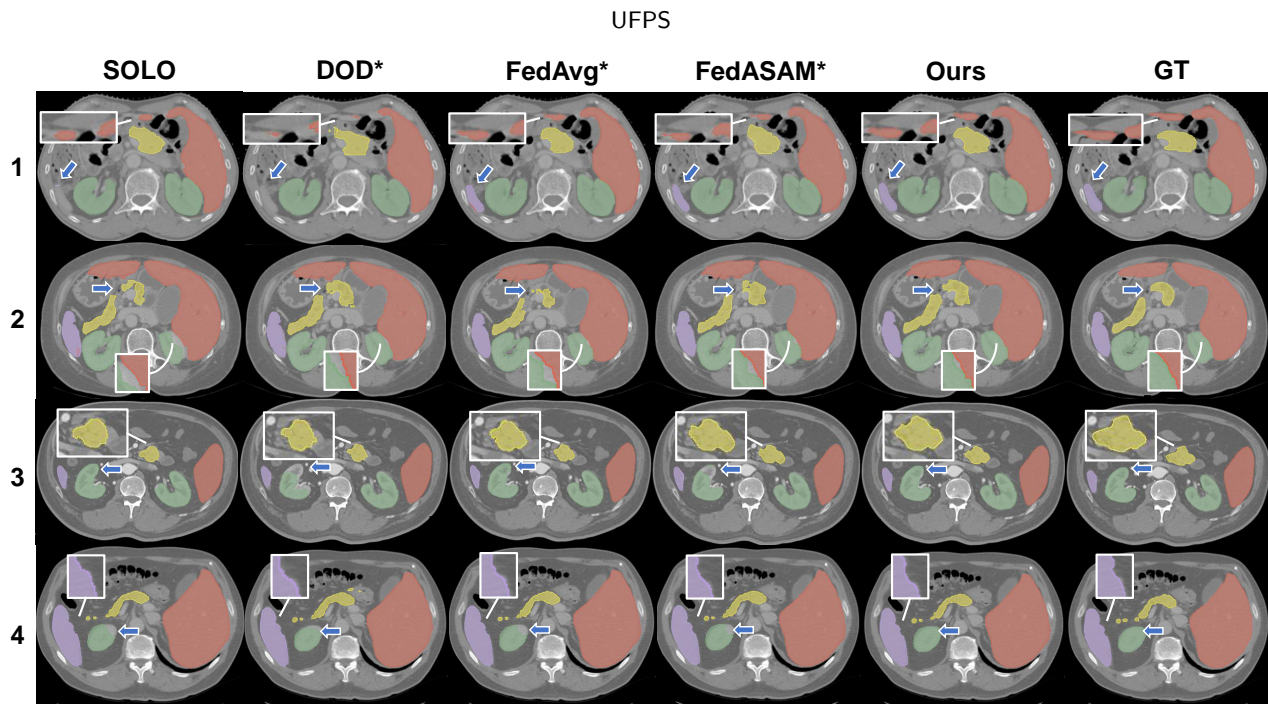


Figure 11: 2D segmentation result on the test set. Numbers on the left side of images refer to client index. Green, red, purple, yellow regions represent kidney, liver, spleen and pancreas, respectively.

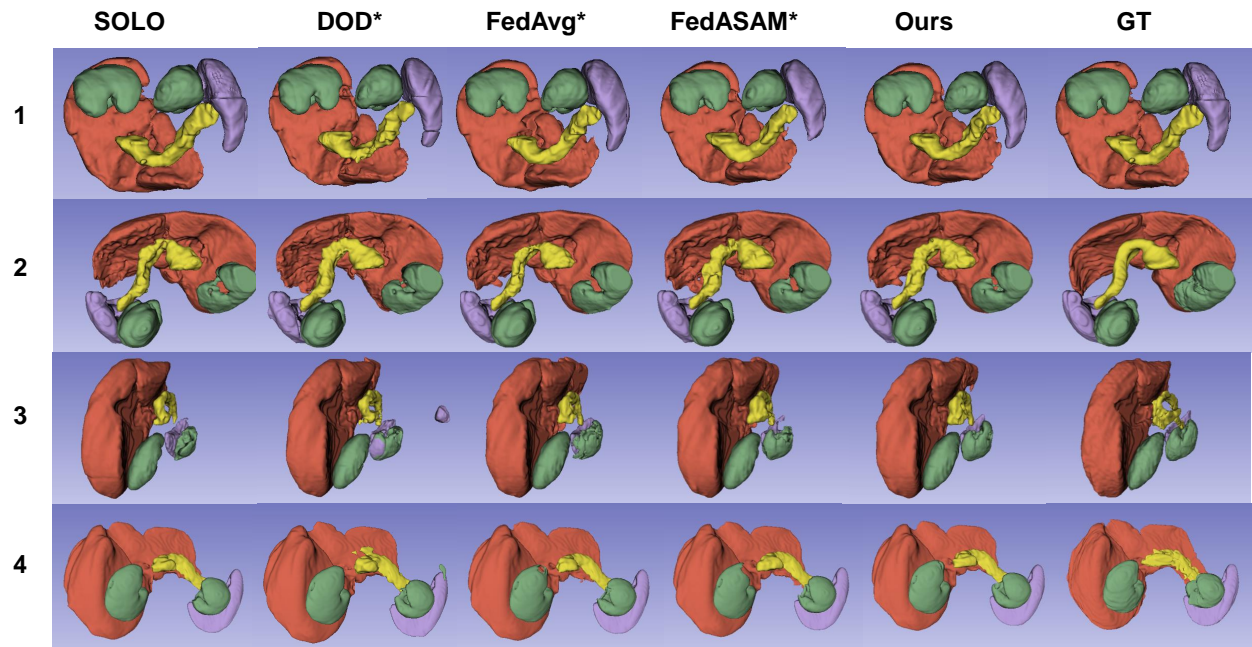


Figure 12: 3D segmentation result on the test set. Numbers on the left side of images refer to client index. Green, red, purple, yellow regions represent kidney, liver, spleen and pancreas, respectively.

6. ACKNOWLEDGMENTS

This work was supported in part by the National Key R&D Program of China (No. 2021YFA1003004), in part by the Shanghai Municipal Natural Science Foundation under Grant 21ZR1423300.

7. AUTHOR CONTRIBUTIONS

Conceptualization, Jiang, L.; methodology, Jiang, L.; formal analysis, Jiang, L. and Ma, L.-Y.; investigation, Jiang, L. and Ma, L.-Y.; writing – original draft, Jiang, L. and Ma, L.-Y.; writing – review & editing, all authors; visualization, Jiang, L.; funding acquisition, Ma, L.-Y., Zeng, T.-Y. and Ying, S.-

H.; resources, Ma, L.-Y. and Zeng, T.-Y.; supervision, Ma, L.-Y. and Zeng, T.-Y.

8. DECLARATION OF INTERESTS

The authors declare no competing interests.

9. Reference

References

- Yann LeCun, Yoshua Bengio, and Geoffrey Hinton. Deep learning. *nature*, 521(7553):436–444, 2015. <https://doi.org/10.1038/nature14539>.
- Kunio Doi, Heber MacMahon, Shigehiko Katsuragawa, Robert M Nishikawa, and Yulei Jiang. Computer-aided diagnosis in radiology: potential and pitfalls. *European Journal of Radiology*, 31(2):97–109, 1999. [https://doi.org/10.1016/S0720-048X\(99\)00016-9](https://doi.org/10.1016/S0720-048X(99)00016-9).
- Kunio Doi. Computer-aided diagnosis in medical imaging: Historical review, current status and future potential. *Computerized Medical Imaging and Graphics*, 31(4):198–211, 2007. <https://doi.org/10.1016/j.compmedimag.2007.02.002>.
- Noah F Greenwald, Geneva Miller, Erick Moen, Alex Kong, Adam Kagel, Thomas Dougherty, Christine Camacho Fullaway, Brianna J McIntosh, Ke Xuan Leow, Morgan Sarah Schwartz, et al. Whole-cell segmentation of tissue images with human-level performance using large-scale data annotation and deep learning. *Nature biotechnology*, 40(4):555–565, 2022. <https://doi.org/10.1038/s41587-021-01094-0>.
- Laurianne David, Josep Arús-Pous, Johan Karlsson, Ola Engkvist, Esben Jannik Bjerrum, Thierry Kogej, Jan M Kriegl, Bernd Beck, and Hongming Chen. Applications of deep-learning in exploiting large-scale and heterogeneous compound data in industrial pharmaceutical research. *Frontiers in pharmacology*, 10:1303, 2019. <https://www.frontiersin.org/articles/10.3389/fphar.2019.01303>.
- Yuyin Zhou, Zhe Li, Song Bai, Chong Wang, Xinlei Chen, Mei Han, Elliot Fishman, and Alan L Yuille. Prior-aware neural network for partially-supervised multi-organ segmentation. In *Proceedings of the IEEE/CVF international conference on computer vision*, pages 10672–10681, 2019. <https://doi.org/10.1109/ICCV.2019.01077>.
- Gonglei Shi, Li Xiao, Yang Chen, and S. Kevin Zhou. Marginal loss and exclusion loss for partially supervised multi-organ segmentation. *Medical Image Analysis*, 70:101979, 2021. <https://doi.org/10.1016/j.media.2021.101979>.
- Qi Fan, Lei Ke, Wenjie Pei, and Yu-Wing Tang, Chi-Keung and Tai. Commonality-parsing network across shape and appearance for partially supervised instance segmentation. In *Computer Vision – ECCV 2020*, pages 379–396. Springer International Publishing, 2020. https://doi.org/10.1007/978-3-030-58598-3_23.
- Xi Fang and Pingkun Yan. Multi-organ segmentation over partially labeled datasets with multi-scale feature abstraction. *IEEE Transactions on Medical Imaging*, 39(11):3619–3629, 2020. <https://doi.org/10.1109/TMI.2020.3001036>.
- George J Annas. Medical privacy and medical research: judging the new federal regulations. *New England Journal of Medicine*, 346:216, 2002. <https://www.nejm.org/doi/full/10.1056/NEJM200205233462118>.
- Brendan McMahan, Eider Moore, Daniel Ramage, Seth Hampson, and Blaise Aguerre y Arcas. Communication-efficient learning of deep networks from decentralized data. In *Artificial intelligence and statistics*, pages 1273–1282. PMLR, 2017. <https://www.nejm.org/doi/full/10.1056/NEJM200205233462118>.
- James M. Balter, Kwok L. Lam, Cornealeus J. McGinn, Theodore S. Lawrence, and Randall K. Ten Haken. Improvement of ct-based treatment-planning models of abdominal targets using static exhale imaging. *International Journal of Radiation Oncology*Biophysics*, 41(4):939–943, 1998. [https://doi.org/10.1016/S0360-3016\(98\)00130-8](https://doi.org/10.1016/S0360-3016(98)00130-8).
- Yefeng Zheng, David Liu, Bogdan Georgescu, Daguang Xu, and Dorin Comaniciu. *Deep Learning Based Automatic Segmentation of Pathological Kidney in CT: Local Versus Global Image Context*, pages 241–255. Springer International Publishing, 2017. https://doi.org/10.1007/978-3-319-42999-1_14.
- Duowen Chen, Yunhao Bai, Wei Shen, Qingli Li, Lequan Yu, and Yan Wang. Magicnet: Semi-supervised multi-organ segmentation via magic-cube partition and recovery. *arXiv preprint arXiv:2212.14310*, 2022. <https://arxiv.org/abs/2212.14310>.
- Yue Zhao, Meng Li, Liangzhen Lai, Naveen Suda, Damon Civin, and Vikas Chandra. Federated learning with non-iid data. *arXiv preprint arXiv:1806.00582*, 2018. <https://arxiv.org/abs/1806.00582>.
- Xiang Li, Kaixuan Huang, Wenhao Yang, Shusen Wang, and Zhihua Zhang. On the convergence of fedavg on non-iid data. *arXiv preprint arXiv:1907.02189*, 2019. <https://arxiv.org/abs/1907.02189>.
- F. van Ommen, H.W.A.M. de Jong, J.W. Dankbaar, E. Bennink, T. Leiner, and A.M.R. Schilham. Dose of ct protocols acquired in clinical routine using a dual-layer detector ct scanner: A preliminary report. *European Journal of Radiology*, 112:65–71, 2019. <https://doi.org/10.1016/j.ejrad.2019.01.011>.
- Oleg Tischenko, Yuan Xu, and Christoph Hoeschen. A new scanning device in ct with dose reduction potential. In *Medical Imaging 2006: Physics of Medical Imaging*, volume 6142, pages 893–899. SPIE, 2006. <https://doi.org/10.1117/12.654463>.
- Ashwarya Sharma and Latha Palaniappan. Improving diversity in medical research. *Nature Reviews Disease Primers*, 7(1):74, 2021. <https://doi.org/10.1038/s41572-021-00316-8>.
- Tian Li, Anit Kumar Sahu, Manzil Zaheer, Maziar Sanjabi, Ameet Talwalkar, and Virginia Smith. Federated optimization in heterogeneous networks. *Proceedings of Machine Learning and Systems*, 2:429–450, 2020. https://proceedings.mlsys.org/paper_files/paper/2020/file/38af86134b65d0f10fe33d30dd76442e-Paper.pdf.
- Sai Praneeth Karimireddy, Satyen Kale, Mehryar Mohri, Sashank Reddi, Sebastian Stich, and Ananda Theertha Suresh. Scaffold: Stochastic controlled averaging for federated learning. In *International Conference on Machine Learning*, pages 5132–5143. PMLR, 2020. <https://proceedings.mlr.press/v119/karimireddy20a.html>.
- Lin Zhang, Yong Luo, Yan Bai, Bo Du, and Ling-Yu Duan. Federated learning for non-iid data via unified feature learning and optimization objective alignment. In *Proceedings of the IEEE/CVF international conference on computer vision*, pages 4420–4428, 2021. <https://doi.org/10.1109/ICCV48922.2021.00438>.
- Meirui Jiang, Zirui Wang, and Qi Dou. Harmoff: Harmonizing local and global drifts in federated learning on heterogeneous medical images. In *Proceedings of the AAAI Conference on Artificial Intelligence*, volume 36, pages 1087–1095, 2022. <https://doi.org/10.1609/aaai.v36i1.19993>.
- Liang Gao, Huazhu Fu, Li Li, Yingwen Chen, Ming Xu, and Cheng-Zhong Xu. Feddc: Federated learning with non-iid data via local drift decoupling and correction. In *Proceedings of the IEEE/CVF Conference on Computer Vision and Pattern Recognition*, pages 10112–10121, 2022. <https://doi.org/10.1109/CVPR52688.2022.00987>.
- Matias Mendieta, Taojiannan Yang, Pu Wang, Minwoo Lee, Zhengming Ding, and Chen Chen. Local learning matters: Rethinking data heterogeneity in federated learning. In *Proceedings of the IEEE/CVF Conference on Computer Vision and Pattern Recognition*, pages 8397–8406, 2022. <https://doi.org/10.1109/CVPR52688.2022.00821>.
- Debora Caldarola, Barbara Caputo, and Marco Ciccone. Improving generalization in federated learning by seeking flat minima. In Shai Avidan, Gabriel Brostow, Moustapha Cissé, Giovanni Maria Farinella, and Tal Hassner, editors, *Computer Vision – ECCV 2022*, pages 654–672, Cham, 2022. Springer Nature Switzerland. https://doi.org/10.1007/978-3-031-20050-2_38.
- Ravikumar Balakrishnan, Tian Li, Tianyi Zhou, Nageen Himayat, Virginia Smith, and Jeff Bilmes. Diverse client selection for federated learning via submodular maximization. In *International Conference on Learning Representations*, 2022.

- <https://openreview.net/pdf?id=nwKXyFvaUm>.
28. Minxue Tang, Xuefei Ning, Yitu Wang, Jingwei Sun, Yu Wang, Hai Li, and Yiran Chen. Fedcor: Correlation-based active client selection strategy for heterogeneous federated learning. In *Proceedings of the IEEE/CVF Conference on Computer Vision and Pattern Recognition*, pages 10102–10111, 2022. <https://doi.org/10.1109/CVPR52688.2022.00986>.
 29. Qinbin Li, Bingsheng He, and Dawn Song. Model-contrastive federated learning. In *Proceedings of the IEEE/CVF Conference on Computer Vision and Pattern Recognition*, pages 10713–10722, 2021. <https://doi.org/10.1109/CVPR46437.2021.01057>.
 30. Sungwon Han, Sungwon Park, Fangzhao Wu, Sundong Kim, Chuhan Wu, Xing Xie, and Meeyoung Cha. Fedx: Unsupervised federated learning with cross knowledge distillation. In Shai Avidan, Gabriel Brostow, Moustapha Cissé, Giovanni Maria Farinella, and Tal Hassner, editors, *Computer Vision – ECCV 2022*, pages 691–707, Cham, 2022. Springer Nature Switzerland. https://doi.org/10.1007/978-3-031-20056-4_40.
 31. Xiaoming Qi, Guanyu Yang, Yuting He, Wangyan Liu, Ali Islam, and Shuo Li. Contrastive re-localization and history distillation in federated cmr segmentation. In Linwei Wang, Qi Dou, P. Thomas Fletcher, Stefanie Speidel, and Shuo Li, editors, *Medical Image Computing and Computer Assisted Intervention – MICCAI 2022*, pages 256–265, Cham, 2022. Springer Nature Switzerland. https://doi.org/10.1007/978-3-031-16443-9_25.
 32. Qiyang Yu, Yang Liu, Yimu Wang, Ke Xu, and Jingjing Liu. Multimodal federated learning via contrastive representation ensemble. *arXiv preprint arXiv:2302.08888*, 2023. <https://arxiv.org/html/2302.08888>.
 33. Xutong Mu, Yulong Shen, Ke Cheng, Xueli Geng, Jiaxuan Fu, Tao Zhang, and Zhiwei Zhang. Fedproc: Prototypical contrastive federated learning on non-iid data. *Future Generation Computer Systems*, 143:93–104, 2023. <https://doi.org/10.1016/j.future.2023.01.019>.
 34. Jason Posner, Lewis Tseng, Moayad Aloqaily, and Yaser Jararweh. Federated learning in vehicular networks: Opportunities and solutions. *IEEE Network*, 35(2):152–159, 2021. <https://doi.org/10.1109/MNET.011.2000430>.
 35. Jungmin Kwon, Jeongseop Kim, Hyunseo Park, and In Kwon Choi. Asam: Adaptive sharpness-aware minimization for scale-invariant learning of deep neural networks. In *International Conference on Machine Learning*, pages 5905–5914. PMLR, 2021. <https://proceedings.mlr.press/v139/kwon21b.html>.
 36. Sheng Lian, Lei Li, Zhiming Luo, Zhun Zhong, Beizhan Wang, and Shaozi Li. Learning multi-organ segmentation via partial- and mutual-prior from single-organ datasets. *Biomedical Signal Processing and Control*, 80:104339, 2023. <https://doi.org/10.1016/j.bspc.2022.104339>.
 37. Konstantin Dmitriev and Arie E Kaufman. Learning multi-class segmentations from single-class datasets. In *Proceedings of the IEEE/CVF Conference on Computer Vision and Pattern Recognition*, pages 9501–9511, 2019. <https://doi.org/10.1109/CVPR.2019.00973>.
 38. Jianpeng Zhang, Yutong Xie, Yong Xia, and Chunhua Shen. Dodnet: Learning to segment multi-organ and tumors from multiple partially labeled datasets. In *Proceedings of the IEEE/CVF conference on computer vision and pattern recognition*, pages 1195–1204, 2021. <https://doi.org/10.1109/CVPR46437.2021.00125>.
 39. Xiaokang Chen, Yuhui Yuan, Gang Zeng, and Jingdong Wang. Semi-supervised semantic segmentation with cross pseudo supervision. In *Proceedings of the IEEE/CVF Conference on Computer Vision and Pattern Recognition*, pages 2613–2622, 2021. <https://doi.org/10.1109/CVPR46437.2021.00264>.
 40. Shixiang Feng, Yuhang Zhou, Xiaoman Zhang, Ya Zhang, and Yanfeng Wang. Ms-kd: Multi-organ segmentation with multiple binary-labeled datasets. *arXiv preprint arXiv:2108.02559*, 2021. <https://arxiv.org/abs/2108.02559>.
 41. Peter Hall. On kullback-leibler loss and density estimation. *The Annals of Statistics*, pages 1491–1519, 1987. <https://doi.org/10.1214/aos/1176350606>.
 42. Pavel Izmailov, Dmitrii Podoprikin, Timur Garipov, Dmitry Vetrov, and Andrew Gordon Wilson. Averaging weights leads to wider optima and better generalization. *arXiv preprint arXiv:1803.05407*, 2018. <https://arxiv.org/abs/1803.05407>.
 43. Xuanang Xu and Pingkun Yan. Federated multi-organ segmentation with partially labeled data. *arXiv preprint arXiv:2206.07156*, 2022. <https://arxiv.org/abs/2206.07156>.
 44. Chen Shen, Pochuan Wang, Dong Yang, Daguang Xu, Masahiro Oda, Po-Ting Chen, Kao-Lang Liu, Wei-Chih Liao, Chiou-Shann Fuh, Kensaku Mori, Weichung Wang, and Holger R. Roth. Joint multi organ and tumor segmentation from partial labels using federated learning. In Shadi Albarqouni, Spyridon Bakas, Sophia Bano, M. Jorge Cardoso, Bishesh Khanal, Bennett Landman, Xiaoxiao Li, Chen Qin, Islem Rekik, Nicola Rieke, Holger Roth, Debodoot Sheet, and Daguang Xu, editors, *Distributed, Collaborative, and Federated Learning, and Affordable AI and Healthcare for Resource Diverse Global Health*, pages 58–67, Cham, 2022. Springer Nature Switzerland. https://doi.org/10.1007/978-3-031-18523-6_6.
 45. Paul Pu Liang, Terrance Liu, Liu Ziyin, Nicholas B Allen, Randy P Auerbach, David Brent, Ruslan Salakhutdinov, and Louis-Philippe Morency. Think locally, act globally: Federated learning with local and global representations. *arXiv preprint arXiv:2001.01523*, 2020. <https://arxiv.org/abs/2001.01523>.
 46. Liam Collins, Hamed Hassani, Aryan Mokhtari, and Sanjay Shakkottai. Exploiting shared representations for personalized federated learning. In *International Conference on Machine Learning*, pages 2089–2099. PMLR, 2021. <https://proceedings.mlr.press/v139/collins21a.html>.
 47. Alysa Ziyang Tan, Han Yu, Lizhen Cui, and Qiang Yang. Towards personalized federated learning. *IEEE Transactions on Neural Networks and Learning Systems*, 2022. <https://doi.org/10.1109/TNNLS.2022.3160699>.
 48. Enmao Diao, Jie Ding, and Vahid Tarokh. Semifi: Semi-supervised federated learning for unlabeled clients with alternate training. *Advances in Neural Information Processing Systems*, 35:17871–17884, 2022. https://proceedings.neurips.cc/paper_files/paper/2022/file/71c3451f6cd6a4f82bb822db25cea4fd-Paper-Conference.pdf.
 49. Zhedong Zheng and Yi Yang. Rectifying pseudo label learning via uncertainty estimation for domain adaptive semantic segmentation. *International Journal of Computer Vision*, 129(4):1106–1120, 2021. <https://doi.org/10.1007/s11263-020-01395-y>.
 50. Cheng Chen, Quande Liu, Yueming Jin, Qi Dou, and Pheng-Ann Heng. Source-free domain adaptive fundus image segmentation with denoised pseudo-labeling. In Marleen de Bruijne, Philippe C. Cattin, Stéphane Cotin, Nicolas Padoy, Stefanie Speidel, Yefeng Zheng, and Caroline Essert, editors, *Medical Image Computing and Computer Assisted Intervention – MICCAI 2021*, pages 225–235, Cham, 2021. Springer International Publishing. https://doi.org/10.1007/978-3-030-87240-3_22.
 51. Yisen Wang, Xingjun Ma, Zaiyi Chen, Yuan Luo, Jinfeng Yi, and James Bailey. Symmetric cross entropy for robust learning with noisy labels. In *Proceedings of the IEEE/CVF International Conference on Computer Vision*, pages 322–330, 2019. <https://doi.org/10.1109/ICCV.2019.00041>.
 52. Cheng Ouyang, Chen Chen, Surui Li, Zeru Li, Chen Qin, Wenjia Bai, and Daniel Rueckert. Causality-inspired single-source domain generalization for medical image segmentation. *IEEE Transactions on Medical Imaging*, 2022. <https://doi.org/10.1109/TMI.2022.3224067>.
 53. Peng Mi, Li Shen, Tianhe Ren, Yiyi Zhou, Xiaoshuai Sun, Rongrong Ji, and Dacheng Tao. Make sharpness-aware minimization stronger: A sparsified perturbation approach. *arXiv preprint arXiv:2210.05177*, 2022. https://proceedings.neurips.cc/paper_files/paper/2022/file/c859b99b5d717c9035e79d43dfd69435-Paper-Conference.pdf.
 54. Le Jiang, Liyan Ma, Tiejong Zeng, and Shi Hui Ying. Code, datasets, and results for the paper "ufps: A unified framework for partially-annotated federated segmentation in heterogeneous data distribution".

2023. <https://zenodo.org/doi/10.5281/zenodo.10140361>.
55. Liangze Jiang and Tao Lin. Test-time robust personalization for federated learning. *arXiv preprint arXiv:2205.10920*, 2022. <https://arxiv.org/abs/2205.10920>.

Supplementary Information

Supplementary Note 1: Notations

Table S1. Description for notations occurred in this paper.

Notation	Description
$(x, y/y^p)$	Image and corresponding fully-annotated / partially-annotated label.
$(X, Y/Y^p)$	Joint space for image and fully-annotated / partially-annotated label.
D_i^p/D^p	Partially-annotated dataset for i -th client. / Global partially-annotated dataset.
N_i/N	Number of data samples in D_i^p/D^p .
C	Label set for all classes occurring in Y .
$ C_i $	Number of classes in label space for i -th client.
N_c	Number of classes in Y .
$c_{i,j}$	Intersection between C_i and C_j .
R	Total number of communication round.
K	Total number of local rounds.
w_i^r/w_0^r	Local model for i -th client at communication round r . / Global model at communication round r .
$w^{G/L}$	Model part aggregated globally / kept local.
w_i^T/w^T	Teacher model pretrained by i -th client. / All pretrained teacher models.
$f(\cdot)$	Loss function.
PL	Operation to predict pseudo labels.
Y_i	Annotated ground-truth label within foreground classes.
$p(x)$	Ground truth.
$q(x)/\tilde{q}(x)$	Model prediction. / One-hot model prediction.
E	Information entropy.
\mathcal{T}	Hyper-parameter of uncertainty threshold.
$U/U_{\mathcal{T}}$	Data-wise uncertainty. / Uncertainty value at lowest \mathcal{T} percentage.
U_{bank}	Uncertainty bank.
$\mu/\sigma/U_{\text{max/min}}$	Mean / variance / maximal / minimal uncertainty value for the uncertainty bank.
α	Hyper-parameter to determine the minimal base in BD.
β	Hyper-parameter to balance terms in RG.
$\tau^{\mu/\sigma}$	Temperature hyper-parameter for mean / variance in uncertainty-based aggregation.
A^w	Aggregation weight only based on the number of local samples.
v	Hyper-parameter of volume threshold.
W	Joint model parameter space.
T_w^{-1}	Normalization operator.
η	Hyper-parameter to balance stability and universality in ASAM.
ρ	Hyper-parameter of searching radius for disturbance in ASAM.
$\nabla f_{\text{USAM}}/\nabla f_{\text{base}}$	Gradients of USAM / pseudo label baseline.
T_{sUSAM}	Hyper-parameter of local mask percentage threshold in sUSAM.
M_L/M_G	Local / Global mask in sUSAM.
T_L	Hyper-parameter of non-masking percentage of local mask in sUSAM.
T_G	Hyper-parameter of non-masking percentage of local mask according to the global mask in sUSAM.
$M_{L,mo}$	Momentum local mask.
α_{mo}	Hyper-parameter for the update of local momentum gradients.
G_N	Gradients not in top $T_L\%$ of M_L but in the nonintersecting part of M_G .
r_{warmup}	Number of warmup rounds.
r_{WS}	End global round for weight scheduler.
$r_{UA/GMT/sUSAM}$	Start global round for uncertainty-based aggregation / global mean teacher / sUSAM.
r_{fre}	Hyper-parameter of the updating frequency for local mask in sUSAM.

Notations are described in Table S1.

Supplementary Note 2: Proof of Theorem 1

Definition 1. Given a bounded loss satisfying $|f(x, w)| \leq f_{upper}$, the Wasserstein distance between two data distribution A, B is:

$$\mathbb{W}_{f_c}(A, B) = \inf_{f_{upper} \in \Pi(A, B)} \mathbb{E}_{f_{upper}} [f_c(X, X')],$$

where $\Pi(A, B)$ represents couplings of A, B , f_c denotes nonnegative, lower semi-continuous cost function.

Here we cite the lemma from Sinha et.al¹, which demonstrates the result on any distribution A and B .

Lemma 2.1. Let $f : X \times W \rightarrow \mathbb{R}$ and $f_c : X \times X \rightarrow \mathbb{R}_+$ be continuous. Let $\varphi_\gamma(x', w) = \sup_{x \in X} [f(x, w) - \gamma c(x, x')]$ be the surrogate objective function. For any distribution B and any $g > 0, \gamma > 0$

$$\sup_{\mathbb{W}_{f_c}(A, B) \leq g} \mathbb{E}_A[f(X, w)] = \inf_{\gamma \geq 0} \gamma g + \mathbb{E}_B[\varphi_\gamma(x', w)],$$

and for any $\gamma \geq 0$, we have

$$\sup_A \left\{ \mathbb{E}_A[f(X, w)] - \gamma \mathbb{W}_{f_c}(A, B) \right\} = \mathbb{E}_B[\varphi_\gamma(X, w)].$$

Theorem 1. For any constant $t > 0, g > 0, \gamma > 0, w \in W$, expected error of risk function on the global data distribution satisfies the following inequality at the probability of $1 - e^{-t}$:

$$\sup_{\mathbb{W}_{f_c}(D_{global}, D_{aug}) \leq g} \mathbb{E}_{D_{global}} [f(X, w)] \leq \mathbb{E}_{\hat{D}_{aug}} [\varphi_\gamma(X, w)] + \gamma g + \epsilon_n(t),$$

$$\text{where } \epsilon_n(t) = \gamma b_1 \sqrt{\frac{f_{upper}}{n}} \cdot \int_0^1 \sqrt{\log N(\mathcal{F}, f_{upper} \epsilon, \|\cdot\|_{L^\infty(X)})} d\epsilon + b_2 f_{upper} \sqrt{\frac{t}{n}},$$

$D_{global}, D_{aug}, \hat{D}_{aug}$ corresponds to global data distribution, augmented local data distribution and empirical augmented local data distribution, respectively, $\varphi_\gamma(x, w) = \sup_{x' \in X} [f(x', w) - \gamma f_c(x', x)]$ is a surrogate objective function with penalty γ and augmentation x' of x , n is number of samples of D_{aug} , \mathcal{F} is the hypothesis class, $N(\cdot)$ is covering numbers of \mathcal{F} , b_1, b_2 are both constants.

Proof.

Leveraging Lemma 2.1 to our problem, for all $g > 0, \gamma > 0$, distribution D_{aug} , we have the deterministic result

$$\sup_{\mathbb{W}_{f_c}(D_{global}, D_{aug}) \leq g} \mathbb{E}_{D_{global}} [f(X, w)] \leq \mathbb{E}_{D_{aug}} [\varphi_\gamma(X, w)] + \gamma g.$$

To get the complete form of Theorem 1, we first show that for the empirical augmented local data distribution \hat{D}_{aug} , $\mathbb{E}_{\hat{D}_{aug}} [\varphi_\gamma(X, w)]$ concentrates around its population counterpart at the usual rate. Since $-f_{upper} \leq f(x, w) \leq \varphi_\gamma(X, w) \leq \sup_x f(x, w) \leq f_{upper}$, the functional $w \rightarrow F_n(w)$ satisfies bounded difference. Substituting standard result on Rademacher complexity² and entropy integrals³ gives the result.

Supplementary Note 3: Assumption

Assumption 1 (Smoothness). $\forall i \in [N], w_a, w_b \in W$, f_i is L -smooth:

$$\|\nabla f_i(w_a) - \nabla f_i(w_b)\| \leq L \|w_a - w_b\|.$$

Assumption 2 (Bounded variance of global gradient). $\forall i \in [N], r \in [R]$, the variance between global and local gradient for the global model is bounded by σ_g :

$$\|\nabla f_i(w^r) - \nabla f(w^r)\|^2 \leq \sigma_g^2.$$

Assumption 3 (Bounded variance of stochastic gradient). $\forall i \in [N]$, the stochastic gradient $\nabla f_i(w, \xi_i)$, computed by the i -th client of w using mini-batch ξ_i , is an unbiased estimator $\nabla f_i(w)$ with variance bounded by σ_l^2 :

$$\mathbb{E}_{\xi_i} \left\| \frac{\nabla f_i(w, \xi_i)}{\|\nabla f_i(w, \xi_i)\|} - \frac{\nabla f_i(w)}{\|\nabla f_i(w)\|} \right\|^2 \leq \sigma_l^2,$$

where the expectation is over all local datasets.

Assumption 4 (Upper bound of stochastic gradient with sparse mask). $\forall i \in [N]$, the arbitrary stochastic gradient with sparse mask m is bounded by G_s :

$$\mathbb{E}_{\xi_i} \left\| \frac{\nabla f_i(w, \xi_i)}{\|\nabla f_i(w, \xi_i)\|} \odot (1 - m) \right\|^2 \leq G_s^2,$$

where G_s and m depend on hyper-parameters T_L, T_G .

Supplementary Note 4: Proof of Theorem 2 and 3

Description of sUSAM Algorithm and Key Lemmas. We list flow of sUSAM in Algorithm 2. For the part client participating circumstance, we randomly choose $S^r \subseteq [N]$ clients with $|S^r| = S$ in global round r and conduct following updates: the server first sends the global model for local initialization $w_{i,0}^r = w^r$. Then each client updates the local model in K local rounds:

$$\begin{aligned} \tilde{w}_{i,k+\frac{1}{2}}^r &= w_{i,k-1}^r + \rho \frac{g_{i,k-1}^r}{\|g_{i,k-1}^r\|} \odot m, \\ w_{i,k}^r &= w_{i,k-1}^r + \eta_l \tilde{g}_{i,k+\frac{1}{2}}^r, \\ \Delta_i^r &= w_{i,k}^r - w^r, \\ \Delta^r &= \frac{1}{N} \sum_{i=1}^N \Delta_i^{r-1}, \\ w^{r+1} &= w^r + \eta_g \Delta^r, \end{aligned}$$

where $g_{i,k-1}^r$ is the gradient at the r -th global round and $(k-1)$ -th local round for client i , the fractional part and tilde signal in $\tilde{g}_{i,k+\frac{1}{2}}^r$ denotes 'already perturbed' and 'sparsely perturbed', respectively. η_g means the global learning rate.

Lemma 4.1. (Relaxed triangle inequality). Let $\{v_1, \dots, v_n\}$ be n vectors in \mathbb{R}^d . The following folds: (1) $\forall a > 0$, $\|v_i + v_j\|^2 \leq (1+a)\|v_i\|^2 + \left(1 + \frac{1}{a}\right)\|v_j\|^2$, and (2) $\|\sum_{i=1}^n v_i\|^2 \leq n \sum_{i=1}^n \|v_i\|^2$.

Lemma 4.2. For random variables x_1, \dots, x_n , the following holds:

$$\mathbb{E} \left[\left\| x_1 + \dots + x_n \right\|^2 \right] \leq n \mathbb{E} \left[\|x_1\|^2 + \dots + \|x_n\|^2 \right].$$

Lemma 4.3. For independent, mean 0 variables x_1, \dots, x_n , the following holds:

$$\mathbb{E} \left[\left\| x_1 + \dots + x_n \right\|^2 \right] \leq \mathbb{E} \left[\|x_1\|^2 + \dots + \|x_n\|^2 \right].$$

Lemma 4.4. (Separating mean and variance for sUSAM). The accumulated sparse gradient for the i -th client at the k -th local round and the r -th global round in sUSAM is bounded by:

$$\mathbb{E} \left[\left\| \sum_{k=0}^{K-1} \tilde{g}_{i,k}^r \right\|^2 \right] \leq K \sum_{k=0}^{K-1} \mathbb{E} \left[\left\| \tilde{g}_{i,k+\frac{1}{2}}^r \right\|^2 \right] + \frac{KL^2\rho^2}{N} (\sigma_l^2 + G_s^2).$$

Proof.

$$\begin{aligned} & \mathbb{E} \left[\left\| \sum_{k=0}^{K-1} \tilde{g}_{i,k+\frac{1}{2}}^r \right\|^2 \right] \\ & \stackrel{(1)}{=} \mathbb{E} \left[\left\| \sum_{k=0}^{K-1} \tilde{g}_{i,k+\frac{1}{2}}^r \right\|^2 \right] + \mathbb{E} \left[\left\| \sum_{k=0}^{K-1} \left(\tilde{g}_{i,k+\frac{1}{2}}^r - \nabla f \left(w_{i,k+\frac{1}{2}}^r \right) \right) \right\|^2 \right] \end{aligned}$$

$$\begin{aligned}
&\stackrel{(2)}{\leq} \sum_{k=0}^{K-1} \mathbb{E} \left[\left\| \tilde{g}_{i,k+\frac{1}{2}}^r \right\|^2 \right] + L^2 \sum_{k=0}^{K-1} \mathbb{E} \left[\left\| \frac{1}{N} \sum_{i \in [N]} \left(w_{i,k+\frac{1}{2}}^r - \hat{w}_{i,k+\frac{1}{2}}^r + \tilde{w}_{i,k+\frac{1}{2}}^r - w_{i,k+\frac{1}{2}}^r \right) \right\|^2 \right] \\
&\stackrel{(3)}{\leq} K \sum_{k=0}^{K-1} \mathbb{E} \left[\left\| \tilde{g}_{i,k+\frac{1}{2}}^r \right\|^2 \right] + L^2 K \mathbb{E} \left[\frac{1}{N^2} \cdot N \cdot 2 \left(\left\| w_{i,k+\frac{1}{2}}^r - \hat{w}_{i,k+\frac{1}{2}}^r \right\|^2 + \left\| \tilde{w}_{i,k+\frac{1}{2}}^r - w_{i,k+\frac{1}{2}}^r \right\|^2 \right) \right] \\
&\stackrel{(4)}{\leq} \sum_{k=0}^{K-1} \mathbb{E} \left[\left\| \tilde{g}_{i,k+\frac{1}{2}}^r \right\|^2 \right] + \frac{2L^2 K}{N} \mathbb{E} \left[\left\| w_{i,k-1}^r + \delta_{i,k}^r \left(w_{i,k-1}^r, \xi_{i,k-1}^r \right) - w_{i,k-1}^r + \delta_{i,k}^r \left(w_{i,k-1}^r \right) \right\|^2 + \left\| \tilde{w}_{i,k}^r - w_{i,k}^r \right\|^2 \right] \\
&\stackrel{(5)}{\leq} K \sum_{k=0}^{K-1} \mathbb{E} \left[\left\| \tilde{g}_{i,k+\frac{1}{2}}^r \right\|^2 \right] + \frac{2L^2 K}{N} \mathbb{E} \left[\left\| \rho \frac{\nabla f_i \left(w_{i,k-1}^r, \xi_i \right)}{\left\| \nabla f_i \left(w_{i,k-1}^r, \xi_i \right) \right\|} - \rho \frac{\nabla f_i \left(w_{i,k-1}^r \right)}{\left\| \nabla f_i \left(w_{i,k-1}^r \right) \right\|} \right\|^2 + \left\| \tilde{w}_{i,k}^r - w_{i,k}^r \right\|^2 \right] \\
&\stackrel{(6)}{\leq} K \sum_{k=0}^{K-1} \mathbb{E} \left[\left\| \tilde{g}_{i,k+\frac{1}{2}}^r \right\|^2 \right] + \frac{2L^2 K \rho^2 \sigma_i^2}{N} + \frac{2L^2 K}{N} \mathbb{E} \left[\left\| \rho \frac{\nabla f_i \left(w_{i,k-1}^r, \xi_i \right)}{\left\| \nabla f_i \left(w_{i,k-1}^r, \xi_i \right) \right\|} \odot (1-m) \right\|^2 \right] \\
&\stackrel{(7)}{\leq} K \sum_{k=0}^{K-1} \mathbb{E} \left[\left\| \tilde{g}_{i,k+\frac{1}{2}}^r \right\|^2 \right] + \frac{2L^2 K \rho^2}{N} \left(\sigma_i^2 + G_s^2 \right)
\end{aligned}$$

where $\hat{w}_{i,k}^r$ denotes unbiased perturbed weight without mask, $w_{i,k}^r$ denotes perturbed weight without mask, $\tilde{w}_{i,k}^r$ denotes perturbed weight with mask. (1) is from the assumption that the stochastic gradient $\nabla f_i(\tilde{w}, \xi_i)$ computed by the i -th client of w using mini-batch ξ_i is an unbiased estimator $\nabla f_i(w)$ with variance bounded by σ_i . (2) is from Assumption 1. (3) is from Lemma 4.1 with $a = 1$ and Lemma 4.2. (4) is from the definition of perturbed weight. (5) extends the formulation of perturbation. (6) is similar to (4) and (5). (7) is from Assumption 4.

Lemma 4.5. (Bounded variance of global perturbed gradient). *The variance of local and global gradients with sparse perturbation $\tilde{\delta}$ can be bounded as:*

$$\left\| \nabla f_i \left(\tilde{w}_{+\frac{1}{2}} \right) - \nabla f \left(\tilde{w}_{+\frac{1}{2}} \right) \right\|^2 \leq 3\sigma_g^2 + 6L^2 \rho^2.$$

Proof.

$$\begin{aligned}
&\left\| \nabla f_i \left(\tilde{w}_{+\frac{1}{2}} \right) - \nabla f \left(\tilde{w}_{+\frac{1}{2}} \right) \right\|^2 \\
&\stackrel{(1)}{=} \left\| \nabla f_i \left(w + \tilde{\delta}_i \right) - \nabla f \left(w + \tilde{\delta} \right) \right\|^2 \\
&= \left\| \left(\nabla f_i \left(w + \tilde{\delta}_i \right) - \nabla f_i \left(w \right) \right) + \left(\nabla f_i \left(w \right) - \nabla f \left(w \right) \right) + \left(\nabla f \left(w \right) - \nabla f \left(w + \tilde{\delta} \right) \right) \right\|^2 \\
&\stackrel{(2)}{\leq} 3 \left\| \nabla f_i \left(w + \tilde{\delta}_i \right) - \nabla f_i \left(w \right) \right\|^2 + 3 \left\| \nabla f_i \left(w \right) - \nabla f \left(w \right) \right\|^2 + 3 \left\| \nabla f \left(w \right) - \nabla f \left(w + \tilde{\delta} \right) \right\|^2 \\
&\stackrel{(3)}{\leq} 3\sigma_g^2 + 3L^2 \left\| w + \rho \cdot \text{sign} \left(\nabla f_i \left(w \right) \right) \frac{\nabla f_i \left(w \right)}{\left\| \nabla f_i \left(w \right) \right\|} \odot m - w \right\|^2 + 3L^2 \left\| w + \rho \cdot \text{sign} \left(\nabla f \left(w \right) \right) \frac{\nabla f \left(w \right)}{\left\| \nabla f \left(w \right) \right\|} \odot m - w \right\|^2 \\
&\stackrel{(4)}{\leq} 3\sigma_g^2 + 6L^2 \rho^2
\end{aligned}$$

(1) is from the definition of perturbed weight. (2) is from Lemma 4.2. (3) is from Assumption 1, Assumption 2 and formulation of perturbation. (4) is from the fact that $\left\| \frac{\nabla f(w)}{\left\| \nabla f(w) \right\|} \odot m \right\|^2 < 1$.

Lemma 4.6. (Bounded ε_δ of sUSAM). *Suppose $\exists \alpha_{g_s}$, s.t. $\frac{\left\| f_i \left(\tilde{w}_{i,k+\frac{1}{2}} \right) \odot m \right\|^2}{\left\| \nabla f_i \left(w_{i,0} \right) \right\|^2} \leq \alpha_{g_s}$, and local learning rates satisfy $\eta_l \leq \frac{1}{4KL}$.*

Denote $\tilde{\delta}_{i,k} = \rho \frac{\nabla f_i \left(w_{i,k}, \xi_i \right)}{\left\| \nabla f_i \left(w_{i,k}, \xi_i \right) \right\|}$, $\tilde{\delta} = \rho \frac{\nabla f \left(w \right)}{\left\| \nabla f \left(w \right) \right\|} \odot m$, $\tilde{\delta}_{i,k} = \rho \frac{\nabla f_i \left(w_{i,k}, \xi_i \right)}{\left\| \nabla f_i \left(w_{i,k}, \xi_i \right) \right\|} \odot m$. Under Assumption 1, 2, 3, 4, the shift of perturbation of sUSAM can be bounded as follows:

$$\varepsilon_\delta = \frac{1}{N} \sum_i \mathbb{E} \left[\left\| \tilde{\delta}_{i,k} - \tilde{\delta} \right\|^2 \right] \leq 2\rho^2 K^2 L^2 \eta_l^2 \alpha_{g_s}.$$

Proof.

When the local learning rate is small, the gradient $\nabla f_i(w_{i,k}, \xi_i)$ is small too. Based on the first order Hessian approximation, the optimal gradient is:

$$\begin{aligned}\nabla f_i(w_{i,k}) &= \nabla f_i\left(w_{i,k-1} - \eta_l \tilde{g}_{i,k+\frac{1}{2}}\right) \\ &= \nabla f_i(w_{i,k-1}) - H\eta_l \tilde{g}_{i,k+\frac{1}{2}} - O\left(\left\|\eta_l \tilde{g}_{i,k+\frac{1}{2}}\right\|^2\right),\end{aligned}$$

where H is the Hessian matrix at $w_{i,k-1}$. The shift of perturbation is then:

$$\begin{aligned}\varepsilon_\delta &= \mathbb{E}\left[\left\|\tilde{\delta}_{i,k} - \tilde{\delta}\right\|^2\right] \\ &= \rho^2 \mathbb{E}\left[\left\|\left(\frac{\nabla f_i(w_{i,k})}{\left\|\nabla f_i(w_{i,k})\right\|} - \frac{\nabla f(w)}{\left\|\nabla f(w)\right\|}\right) \odot m\right\|^2\right] \\ &\stackrel{(1)}{\leq} \rho^2 \frac{\left\|\left(\nabla f_i(w_{i,k}) - \nabla f_i(w_{i,0})\right) \odot m\right\|^2}{\left\|\nabla f_i(w_{i,0})\right\|^2} \\ &\stackrel{(2)}{\leq} \rho^2 \left(\left(1 + \frac{1}{k-1}\right) \cdot \frac{\left\|\left(\nabla f_i(w_{i,k-1}) - \nabla f_i(w_{i,0})\right) \odot m\right\|^2}{\left\|\nabla f_i(w_{i,0})\right\|^2} + K \frac{\left\|\left(H\eta_l \tilde{g}_{i,k+\frac{1}{2}} + \left(\left\|\eta_l \tilde{g}_{i,k+\frac{1}{2}}\right\|^2\right)\right) \odot m\right\|^2}{\left\|\nabla f_i(w_{i,0})\right\|^2} \right) \\ &\stackrel{(3)}{\leq} \rho^2 \left(\left(1 + \frac{1}{k-1}\right) \cdot \frac{\left\|\left(\nabla f_i(w_{i,k-1}) - \nabla f_i(w_{i,0})\right) \odot m\right\|^2}{\left\|\nabla f_i(w_{i,0})\right\|^2} + KL^2\eta_l^2\alpha_{g_s} \right) \\ &= \frac{1}{N} \sum_{i \in [N]} \mathbb{E}\left[\left\|\tilde{\delta}_{i,k} - \tilde{\delta}\right\|^2\right] \\ &\stackrel{(4)}{\leq} \rho^2 \left(\sum_{\tau=0}^{k-1} \left(1 + \frac{1}{k-1}\right)^\tau KL^2\eta_l^2\alpha_{g_s} \right) \\ &\leq 2\rho^2 K^2 L^2 \eta_l^2 \alpha_{g_s}\end{aligned}$$

(1) can be explained through spherical coordinate system (Please refer to FedSAM⁴ for more details). (2) is from the first order Hessian approximation and Lemma 4.1 with $a = \frac{1}{K-1}$. (3) is due to top eigenvalue of H is bounded by L under Assumption 1. Expanding the recursion between (1) and (3) results in (4).

Lemma 4.7. (Bounded ε_w of sUSAM). Suppose local learning rates satisfy $\eta_l \leq \frac{1}{10KL}$. Under Assumption 1, 2, 3, 4, the shift of model parameters can of sUSAM can be bounded as follows:

$$\varepsilon_w = \frac{1}{N} \sum_i \mathbb{E}\left[\left\|w_{i,k} - w\right\|^2\right] \leq 5K^2\eta_l^2 \left(2L^2\rho^2\sigma_l^2 + 6K \left(3\sigma_g^2 + 6L^2\rho^2\right) + 6K \left\|\nabla f(\tilde{w})\right\|^2 + 24K^3\eta_l^4 L^4 \rho^2\right).$$

Proof of this Lemma is same as the one in FedSAM⁴.

Lemma 4.8.

$$\begin{aligned}&\left\langle \nabla f\left(\tilde{w}_{+\frac{1}{2}}^r\right), \mathbb{E}_r\left[\Delta^r + \eta_l K \nabla f\left(\tilde{w}_{+\frac{1}{2}}^r\right)\right] \right\rangle \\ &\leq \frac{\eta_l K}{2} \left\|\nabla f\left(\tilde{w}_{+\frac{1}{2}}^r\right)\right\|^2 + K\eta_l L^2 \varepsilon_w + K\eta_l L^2 \varepsilon_\delta - \frac{\eta_l}{2KN^2} \mathbb{E}_r \left\|\sum_{i,k} \nabla f_i\left(\tilde{w}_{i,k+\frac{1}{2}}^r\right)\right\|^2.\end{aligned}$$

Proof.

$$\left\langle \nabla f\left(\tilde{w}_{+\frac{1}{2}}^r\right), \mathbb{E}_r\left[\Delta^r + \eta_l K \nabla f\left(\tilde{w}_{+\frac{1}{2}}^r\right)\right] \right\rangle$$

$$\begin{aligned}
&\stackrel{(1)}{=} \sqrt{K} \frac{1}{\sqrt{K}} \left\langle \nabla f \left(\tilde{w}_{+\frac{1}{2}}^r \right), \mathbb{E}_r \left[-\frac{\eta_l}{N} \sum_{i,k} \tilde{g}_{i,k-1}^{r-1} + \frac{\eta_l}{N} \sum_{i,k} \nabla f_i \left(\tilde{w}_{+\frac{1}{2}}^r \right) \right] \right\rangle \\
&\stackrel{(2)}{=} \frac{\eta_l K}{2} \left\| \nabla f \left(\tilde{w}_{+\frac{1}{2}}^r \right) \right\|^2 + \frac{\eta_l}{2KN^2} \mathbb{E}_r \left\| \sum_{i,k} \left(\nabla f_i \left(\tilde{w}_{i,k+\frac{1}{2}}^r \right) - \nabla f_i \left(\tilde{w}_{+\frac{1}{2}}^r \right) \right) \right\|^2 - \frac{\eta_l}{2KN^2} \mathbb{E}_r \left\| \sum_{i,k} \nabla f_i \left(\tilde{w}_{i,k+\frac{1}{2}}^r \right) \right\|^2 \\
&\stackrel{(3)}{\leq} \frac{\eta_l K}{2} \left\| \nabla f \left(\tilde{w}_{+\frac{1}{2}}^r \right) \right\|^2 + \frac{\eta_l}{2N} \sum_{i,k} \mathbb{E}_r \left\| \nabla f_i \left(\tilde{w}_{i,k+\frac{1}{2}}^r \right) - \nabla f_i \left(\tilde{w}_{+\frac{1}{2}}^r \right) \right\|^2 - \frac{\eta_l}{2KN^2} \mathbb{E}_r \left\| \sum_{i,k} \nabla f_i \left(\tilde{w}_{i,k+\frac{1}{2}}^r \right) \right\|^2 \\
&\stackrel{(4)}{\leq} \frac{\eta_l K}{2} \left\| \nabla f \left(\tilde{w}_{+\frac{1}{2}}^r \right) \right\|^2 + \frac{\eta_l L^2}{2N} \sum_{i,k} \mathbb{E}_r \left\| \tilde{w}_{i,k+\frac{1}{2}}^r - \tilde{w}_{+\frac{1}{2}}^r \right\|^2 - \frac{\eta_l}{2KN^2} \mathbb{E}_r \left\| \sum_{i,k} \nabla f_i \left(\tilde{w}_{i,k+\frac{1}{2}}^r \right) \right\|^2 \\
&\stackrel{(5)}{\leq} \frac{\eta_l K}{2} \left\| \nabla f \left(\tilde{w}_{+\frac{1}{2}}^r \right) \right\|^2 + \frac{\eta_l L^2}{N} \sum_{i,k} \mathbb{E}_r \left\| w_{i,k}^r - w^r \right\|^2 + \frac{\eta_l L^2}{N} \sum_{i,k} \mathbb{E}_r \left\| \tilde{\delta}_{i,k}^r - \tilde{\delta}^r \right\|^2 - \frac{\eta_l}{2KN^2} \mathbb{E}_r \left\| \sum_{i,k} \nabla f_i \left(\tilde{w}_{i,k+\frac{1}{2}}^r \right) \right\|^2 \\
&\stackrel{(6)}{\leq} \frac{\eta_l K}{2} \left\| \nabla f \left(\tilde{w}_{+\frac{1}{2}}^r \right) \right\|^2 + K\eta_l L^2 \varepsilon_w + K\eta_l L^2 \varepsilon_\delta - \frac{\eta_l}{2KN^2} \mathbb{E}_r \left\| \sum_{i,k} \nabla f_i \left(\tilde{w}_{i,k+\frac{1}{2}}^r \right) \right\|^2
\end{aligned}$$

(1) can be derived from:

$$\begin{aligned}
&\eta_l K \nabla f \left(\tilde{w}_{+\frac{1}{2}}^r \right) \\
&= \eta_l K \frac{1}{N} \sum_{i \in [N]} \nabla f_i \left(\tilde{w}_{+\frac{1}{2}}^r \right) \\
&= \eta_l K \frac{1}{N} \sum_{i \in [N]} \frac{1}{K} \sum_{k \in [K]} \nabla f_i \left(\tilde{w}_{+\frac{1}{2}}^r \right) \\
&= \frac{\eta_l}{N} \sum_{i,k} \nabla f_i \left(\tilde{w}_{+\frac{1}{2}}^r \right) \\
\Delta^r &= \frac{1}{N} \sum_{i=1}^N \Delta_i^{r-1} \\
&= \frac{1}{N} \sum_{i=1}^N \left(w_{i,0}^{r-1} - \sum_k \eta_l \tilde{g}_{i,k-1}^{r-1} - w_i^{r-1} \right) \\
&= -\frac{\eta_l}{N} \sum_{i,k} \tilde{g}_{i,k-1}^{r-1}
\end{aligned}$$

(2) is from the lemma that $\langle a, b \rangle = \frac{1}{2} (\|a\|^2 + \|b\|^2 - \|a-b\|^2)$ with $a = \sqrt{\eta_l K} \nabla f \left(\tilde{w}_{+\frac{1}{2}}^r \right)$ and $b = -\frac{\sqrt{\eta_l}}{N\sqrt{K}} \sum_{i,k} \left(\nabla f_i \left(\tilde{w}_{i,k+\frac{1}{2}}^r \right) - \nabla f_i \left(\tilde{w}_{+\frac{1}{2}}^r \right) \right)$. (3) is from Lemma 4.2. (4) is from Assumption 1. (5) is from definition of sparse perturbation and Lemma 4.2. (6) is from Lemma 4.6 and Lemma 4.7.

Lemma 4.9. For the full client participating scheme, the bound of $\mathbb{E}_r [\|\Delta^r\|^2]$ is:

$$\mathbb{E}_r \left[\|\Delta^r\|^2 \right] \leq \frac{2K\eta_l^2 L^2 \rho^2}{N} (\sigma_l^2 + G_s^2) + \frac{\eta_l^2}{N^2} \left\| \sum_{i,k} \nabla f_i \left(\tilde{w}_{i,k+\frac{1}{2}}^r \right) \right\|^2.$$

Proof.

$$\begin{aligned}
&\mathbb{E}_r \left[\|\Delta^r\|^2 \right] \\
&\stackrel{(1)}{\leq} \frac{\eta_l^2}{N^2} \mathbb{E}_r \left\| \sum_{i,k} \tilde{g}_{i,k+\frac{1}{2}}^r \right\|^2
\end{aligned}$$

$$\begin{aligned}
&\stackrel{(2)}{=} \frac{\eta_l^2}{N^2} \mathbb{E}_r \left\| \sum_{i,k} \left(\tilde{g}_{i,k+\frac{1}{2}}^r - \nabla f_i \left(\tilde{w}_{i,k+\frac{1}{2}}^r \right) \right) \right\|^2 + \frac{\eta_l^2}{N^2} \mathbb{E}_r \left\| \sum_{i,k} \nabla f_i \left(\tilde{w}_{i,k+\frac{1}{2}}^r \right) \right\|^2 \\
&\stackrel{(3)}{\leq} \frac{2K\eta_l^2 L^2 \rho^2}{N} (\sigma_l^2 + G_s^2) + \frac{\eta_l^2}{N^2} \mathbb{E}_r \left\| \sum_{i,k} \nabla f_i \left(\tilde{w}_{i,k+\frac{1}{2}}^r \right) \right\|^2
\end{aligned}$$

(1) is from Lemma 4.2 and the fact that the optimal gradient is smaller than the empirical one. (2) is from Lemma 4.3 since the gradient is merely within one local epoch k and the mean for r is 0 in this situation. (3) is scaled from the second term in Lemma 4.4.(1).

Lemma 4.10. For all $r \in [R-1]$, with proper choices of local and global learning rates, the iterates from sUSAM satisfy:

$$\begin{aligned}
\mathbb{E}_r \left[f \left(\tilde{w}_{+\frac{1}{2}}^{r+1} \right) \right] &\leq f \left(\tilde{w}_{+\frac{1}{2}}^r \right) - K\eta_g \eta_L \left(\frac{1}{2} - 30K^2 L^2 \eta_L^2 \right) \left\| \nabla f \left(\tilde{w}_{+\frac{1}{2}}^r \right) \right\|^2 + K\eta_g \eta_L (10KL^4 \eta_L^2 \rho^2 \sigma_l^2 \\
&+ 90K^2 L^2 \eta_L^2 \sigma_g^2 + 180K^2 L^4 \eta_L^2 \rho^2 + 24K^4 L^6 \eta_L^6 \rho^2 \alpha_{g_s} + \frac{\eta_g \eta_L L^3 \rho^2}{N} (\sigma_l^2 + G_s^2)).
\end{aligned}$$

Proof.

$$\begin{aligned}
&\mathbb{E}_r \left[f \left(\tilde{w}_{+\frac{1}{2}}^{r+1} \right) \right] \\
&\stackrel{(1)}{\leq} f \left(\tilde{w}_{+\frac{1}{2}}^r \right) + \mathbb{E}_r \left\langle \nabla f \left(\tilde{w}_{+\frac{1}{2}}^r \right), \tilde{w}_{+\frac{1}{2}}^{r+1} - \tilde{w}_{+\frac{1}{2}}^r \right\rangle + \frac{L}{2} \mathbb{E}_r \left\| \tilde{w}_{+\frac{1}{2}}^{r+1} - \tilde{w}_{+\frac{1}{2}}^r \right\|^2 \\
&\stackrel{(2)}{=} f \left(\tilde{w}_{+\frac{1}{2}}^r \right) + \mathbb{E}_r \left\langle \nabla f \left(\tilde{w}_{+\frac{1}{2}}^r \right), -\eta_g \Delta^r + K\eta_g \eta_L \nabla f \left(\tilde{w}_{+\frac{1}{2}}^r \right) - K\eta_g \eta_L \nabla f \left(\tilde{w}_{+\frac{1}{2}}^r \right) \right\rangle + \frac{L\eta_g^2}{2} \mathbb{E}_r \|\Delta^r\|^2 \\
&\stackrel{(3)}{=} f \left(\tilde{w}_{+\frac{1}{2}}^r \right) - K\eta_g \eta_L \left\| \nabla f \left(\tilde{w}_{+\frac{1}{2}}^r \right) \right\|^2 + \eta_g \left\langle \nabla f \left(\tilde{w}_{+\frac{1}{2}}^r \right), \mathbb{E}_r [-\Delta^r + K\eta_L \nabla f \left(\tilde{w}_{+\frac{1}{2}}^r \right)] \right\rangle \\
&+ \frac{L\eta_g^2}{2} \mathbb{E}_r \|\Delta^r\|^2 \\
&\stackrel{(4)}{\leq} f \left(\tilde{w}_{+\frac{1}{2}}^r \right) - \frac{K\eta_g \eta_L}{2} \left\| \nabla f \left(\tilde{w}_{+\frac{1}{2}}^r \right) \right\|^2 + K\eta_g \eta_L L^2 \varepsilon_\omega + K\eta_g \eta_L L^2 \varepsilon_\delta - \frac{\eta_g \eta_L}{2KN} \mathbb{E}_r \left\| \sum_{i,k} \nabla f_i \left(\tilde{w}_{i,k+\frac{1}{2}}^r \right) \right\|^2 \\
&+ \frac{L}{2} \eta_g^2 \mathbb{E}_r \|\Delta^r\|^2 \\
&\stackrel{(5)}{\leq} f \left(\tilde{w}_{+\frac{1}{2}}^r \right) - \frac{K\eta_g \eta_L}{2} \left\| \nabla f \left(\tilde{w}_{+\frac{1}{2}}^r \right) \right\|^2 + K\eta_g \eta_L L^2 \varepsilon_\omega + K\eta_g \eta_L L^2 \varepsilon_\delta + \frac{K\eta_g^2 \eta_l^2 L^3 \rho^2}{N} (\sigma_l^2 + G_s^2) \\
&\stackrel{(6)}{\leq} f \left(\tilde{w}_{+\frac{1}{2}}^r \right) - K\eta_g \eta_L \left(\frac{1}{2} - 30K^2 L^2 \eta_L^2 \right) \left\| \nabla f \left(\tilde{w}_{+\frac{1}{2}}^r \right) \right\|^2 + K\eta_g \eta_L (10KL^4 \eta_L^2 \rho^2 \sigma_l^2 + 90K^2 L^2 \eta_L^2 \sigma_g^2 \\
&+ 180K^2 L^4 \eta_L^2 \rho^2 + 24K^4 L^6 \eta_L^6 \rho^2 \alpha_{g_s} + \frac{\eta_g \eta_L L^3 \rho^2}{N} (\sigma_l^2 + G_s^2))
\end{aligned}$$

(1) is from the lemma of L-smooth that $f(a) \leq f(b) + \nabla f(b)(a-b) + \frac{L}{2} \|a-b\|^2$. (2) is from the description of sUSAM. (3) is from the unbiased estimators. (4) is from Lemma 4.3. (5) is from Lemma 4.9 and neglection of the negative term. (6) is from Lemma 4.6, Lemma 4.7 and the assumption that $\eta_l \leq \frac{1}{10KL}$.

Theorem 2. Let local and global learning rates be set as $\eta_l \leq \frac{1}{10KL}$, $\eta_l \eta_G \leq \frac{1}{KL}$. Under Assumption 1, 2, 3, 4 and full client participation, the sequence of iterates generated by sUSAM satisfies:

$$\min_{r \in [R]} \mathbb{E} \left[\|\nabla f(w^r)\|^2 \right] \leq \frac{f^0 - f^*}{CK\eta_g \eta_L} + \Phi,$$

where $\Phi = \frac{1}{C} \left(10KL^4\eta_L^2\rho^2\sigma_l^2 + 90K^2L^2\eta_L^2\sigma_g^2 + 180K^2L^4\eta_L^2\rho^2 + 24K^4L^6\eta_L^6\rho^2\alpha_{g_s} + 16K^3L^6\eta_L^4\rho^2\alpha_{g_s} + \frac{\eta_g\eta_LL^3\rho^2}{N} (\sigma_l^2 + G_s^2) \right)$. If local and global learning rates are chosen as $\eta_l = \frac{1}{\sqrt{RKL}}$ and $\eta_g = \sqrt{KN}$, and perturbation radius is chosen as $\rho = \frac{1}{\sqrt{R}}$, the convergence rates can be expressed as:

$$\frac{1}{R} \sum_{r=1}^R \mathbb{E} \left[\left\| f(w^{r+1}) \right\|^2 \right] = O \left(\frac{FL}{\sqrt{RKN}} + \frac{\sigma_g^2}{R} + \frac{L^2(\sigma_l^2 + G_s^2)}{R^{\frac{3}{2}}\sqrt{KN}} + \frac{L^2}{R^2} + \frac{L^2\sigma_l^2}{R^2K} \right).$$

Proof.

$$\begin{aligned} & \frac{1}{R} \sum_{r=1}^R \mathbb{E} \left[\left\| f(w^{r+1}) \right\|^2 \right] \\ & \stackrel{(1)}{=} \frac{1}{R} \sum_{r=1}^R \mathbb{E} \left[\left\| f\left(\tilde{w}_{+\frac{1}{2}}^{r+1}\right) \right\|^2 \right] \\ & \stackrel{(2)}{\leq} \frac{f\left(\tilde{w}_{+\frac{1}{2}}^r\right) - f\left(\tilde{w}_{+\frac{1}{2}}^{r+1}\right)}{CK\eta_g\eta_LR} + \frac{1}{C} \left(10KL^4\eta_L^2\rho^2\sigma_l^2 + 90K^2L^2\eta_L^2\sigma_g^2 + 180K^2L^4\eta_L^2\rho^2 + 24K^4L^6\eta_L^6\rho^2\alpha_{g_s} \right. \\ & \quad \left. + 16K^3L^6\eta_L^4\rho^2\alpha_{g_s} + \frac{\eta_g\eta_LL^3\rho^2}{N} (\sigma_l^2 + G_s^2) \right) \\ & \stackrel{(3)}{\leq} \frac{f\left(\tilde{w}_{+\frac{1}{2}}^0\right) - f^*}{CK\eta_g\eta_LR} + \frac{1}{C} \left(10KL^4\eta_L^2\rho^2\sigma_l^2 + 90K^2L^2\eta_L^2\sigma_g^2 + 180K^2L^4\eta_L^2\rho^2 + 24K^4L^6\eta_L^6\rho^2\alpha_{g_s} \right. \\ & \quad \left. + 16K^3L^6\eta_L^4\rho^2\alpha_{g_s} + \frac{\eta_g\eta_LL^3\rho^2}{N} (\sigma_l^2 + G_s^2) \right) \end{aligned}$$

(1) is due to Assumption 1 and taking expectation of $f\left(\tilde{w}_{+\frac{1}{2}}^{r+1}\right)$ over randomness at global round r . (2) is from transposition of Lemma 4.10, summing it for $r = [R]$, and multiplying both sides by $\frac{1}{CK\eta_g\eta_LR}$ with $0 < C < \frac{1}{2} - 30K^2L^2\eta_L^2$ if $\eta_L < \frac{1}{\sqrt{30KL}}$. (3) is from the relationship between current loss and optimal loss $f\left(\tilde{w}_{+\frac{1}{2}}^{r+1}\right) \geq f^*$, and the one between current loss and initial loss $f\left(\tilde{w}_{+\frac{1}{2}}^0\right) \geq f\left(\tilde{w}_{+\frac{1}{2}}^r\right)$. If we choose local and global learning rates as $\eta_l = \frac{1}{\sqrt{RKL}}$ and $\eta_g = \sqrt{KN}$, and choose perturbation radius as $\rho = \frac{1}{\sqrt{R}}$, we have:

$$\frac{1}{R} \sum_{r=1}^R \mathbb{E} \left[\left\| f(w^{r+1}) \right\|^2 \right] = O \left(\frac{FL}{\sqrt{RKN}} + \frac{\sigma_g^2}{R} + \frac{L^2(\sigma_l^2 + G_s^2)}{R^{\frac{3}{2}}\sqrt{KN}} + \frac{L^2}{R^2} + \frac{L^2\sigma_l^2}{R^2K} + \frac{L^2\alpha_{g_s}}{R^3K} + \frac{\alpha_{g_s}}{R^4K^2} \right).$$

After neglecting high order terms, we have:

$$\frac{1}{R} \sum_{r=1}^R \mathbb{E} \left[\left\| f(w^{r+1}) \right\|^2 \right] = O \left(\frac{FL}{\sqrt{RKN}} + \frac{\sigma_g^2}{R} + \frac{L^2(\sigma_l^2 + G_s^2)}{R^{\frac{3}{2}}\sqrt{KN}} + \frac{L^2}{R^2} + \frac{L^2\sigma_l^2}{R^2K} \right).$$

Lemma 4.11. For the circumstance of partial client participation without replacement, the upper bound of $\mathbb{E}_r \left[\left\| \Delta^r \right\|^2 \right]$ is:

$$\mathbb{E}_r \left[\left\| \Delta^r \right\|^2 \right] \leq \frac{2K\eta_l^2L^2\rho^2}{N} (\sigma_l^2 + G_s^2) + \frac{\eta_l^2}{NS} \sum_i \left\| \sum_{j=1}^{K-1} \nabla f_i \left(\tilde{w}_{i,j+\frac{1}{2}}^r \right) \right\|^2 + \frac{(S-1)\eta_L^2}{SN^2} \left\| \sum_{j=0}^{K-1} \nabla f_i \left(\tilde{w}_{i,j+\frac{1}{2}}^r \right) \right\|^2.$$

Proof.

$$\mathbb{E}_r \left[\left\| \Delta^r \right\|^2 \right]$$

$$\begin{aligned}
&\stackrel{(1)}{\leq} \frac{\eta_l^2}{S^2} \mathbb{E}_r \left[\left\| \sum_{i \in S^r} \sum_k \tilde{g}_{i,k+\frac{1}{2}} \right\|^2 \right] \\
&= \frac{\eta_l^2}{S^2} \mathbb{E}_r \left[\left\| \sum_i \mathbb{1}\{i \in S^r\} \sum_k \tilde{g}_{i,k+\frac{1}{2}} \right\|^2 \right] \\
&\stackrel{(2)}{\leq} \frac{\eta_l^2}{NS} \mathbb{E}_r \left[\left\| \sum_i \sum_{j=0}^{K-1} \left(\tilde{g}_{i,j+\frac{1}{2}} - \nabla f_i \left(\tilde{w}_{i,j+\frac{1}{2}}^r \right) \right) \right\|^2 \right] + \frac{\eta_l^2}{S^2} \mathbb{E}_r \left[\left\| \sum_i \mathbb{1}\{i \in S^r\} \sum_{j=0}^{K-1} \nabla f_i \left(\tilde{w}_{i,j+\frac{1}{2}}^r \right) \right\|^2 \right] \\
&\stackrel{(3)}{\leq} \frac{2K\eta_l^2 L^2 \rho^2}{N} (\sigma_l^2 + G_s^2) + \frac{\eta_l^2}{S^2} \mathbb{E}_r \left[\left\| \sum_{i=1}^s \sum_{j=0}^{K-1} \nabla f_i \left(\tilde{w}_{i,j+\frac{1}{2}}^r \right) \right\|^2 \right] \\
&\stackrel{(4)}{\leq} \frac{2K\eta_l^2 L^2 \rho^2}{N} (\sigma_l^2 + G_s^2) + \frac{\eta_l^2}{NS} \sum_i \left\| \sum_{j=1}^{K-1} \nabla f_i \left(\tilde{w}_{i,j+\frac{1}{2}}^r \right) \right\|^2 + \frac{(S-1)\eta_l^2}{SN^2} \left\| \sum_{j=0}^{K-1} \nabla f_i \left(\tilde{w}_{i,j+\frac{1}{2}}^r \right) \right\|^2
\end{aligned}$$

(1) is from Lemma 4.2. (2) is from Lemma 4.3. (3) is from Lemma 4.4. (4) is from Yang's proof⁵ in 'For strategy 1' of their Theorem 2.

Lemma 4.12. *If we choose all $k \in [K]$ and $i \in [N]$ for sUSAM, the upper bound of $\sum_i \mathbb{E} \left[\left\| \sum_k \nabla f_i \left(\tilde{w}_{i,k+\frac{1}{2}} \right) \right\|^2 \right]$ is then:*

$$\begin{aligned}
\sum_i \mathbb{E} \left[\left\| \sum_k \nabla f_i \left(\tilde{w}_{i,k+\frac{1}{2}} \right) \right\|^2 \right] &\leq 30NK^2 L^2 \eta_L^2 \left(2L^2 \rho^2 \sigma_l^2 + 6K (3\sigma_g^2 + 6L^2 \rho^2) + 6K \left\| \nabla f \left(\tilde{w}_{+\frac{1}{2}} \right) \right\|^2 \right. \\
&\quad \left. + 144K^4 L^6 \eta_L^4 \rho^2 + 12NK^4 L^2 \eta_L^2 \rho^2 \alpha_{g_s} + 3NK^2 (3\sigma_g^2 + 6L^2 \rho^2) + 3NK^2 \left\| \nabla f \left(\tilde{w}_{+\frac{1}{2}} \right) \right\|^2 \right).
\end{aligned}$$

Proof.

$$\begin{aligned}
&\sum_i \mathbb{E} \left[\left\| \sum_k \nabla f_i \left(\tilde{w}_{i,k+\frac{1}{2}} \right) \right\|^2 \right] \\
&= \sum_i \mathbb{E} \left[\left\| \sum_k \nabla f_i \left(\tilde{w}_{i,k+\frac{1}{2}} \right) - \nabla f_i \left(\tilde{w}_{+\frac{1}{2}} \right) + \nabla f_i \left(\tilde{w}_{i,k+\frac{1}{2}} \right) - \nabla f \left(\tilde{w}_{+\frac{1}{2}} \right) + \nabla f \left(\tilde{w}_{+\frac{1}{2}} \right) \right\|^2 \right] \\
&\stackrel{(1)}{\leq} 6KL^2 \sum_{i,k} \mathbb{E} \left[\left\| w_{i,k} - w \right\|^2 \right] + 6KL^2 \sum_{i,k} \mathbb{E} \left[\left\| \tilde{\delta}_{i,k} - \tilde{\delta} \right\|^2 \right] + 3NK^2 (3\sigma_g^2 + 6L^2 \rho^2) + 3NK^2 \left\| \nabla f \left(\tilde{w}_{+\frac{1}{2}} \right) \right\|^2 \\
&\stackrel{(2)}{\leq} 30NK^2 L^2 \eta_L^2 \left(2L^2 \rho^2 \sigma_l^2 + 6K (3\sigma_g^2 + 6L^2 \rho^2) + 6K \left\| \nabla f \left(\tilde{w}_{+\frac{1}{2}} \right) \right\|^2 + 144K^4 L^6 \eta_L^4 \rho^2 + 12NK^4 L^2 \eta_L^2 \rho^2 \alpha_{g_s} \right. \\
&\quad \left. + 3NK^2 (3\sigma_g^2 + 6L^2 \rho^2) + 3NK^2 \left\| \nabla f \left(\tilde{w}_{+\frac{1}{2}} \right) \right\|^2 \right)
\end{aligned}$$

(1) is from Lemma 4.2, Assumption 1, definition of perturbed model parameter, and Lemma 4.5. (2) is from Lemma 4.6 and Lemma 4.7.

Theorem 3. *Let local and global learning rates be set as $\eta_l \leq \frac{1}{10KL}$, $\eta_l \eta_G \leq \frac{1}{KL}$. Under Assumption 1, 2, 3, 4 and part client participation, the sequence of iterates generated by sUSAM satisfies:*

$$\min_{r \in [R]} \mathbb{E} \left[\left\| \nabla f \left(w^r \right) \right\|^2 \right] \leq \frac{f^0 - f^*}{CK\eta_g\eta_L} + \Phi,$$

where $\Phi = \frac{1}{C} \left(10KL^4 \eta_L^2 \rho^2 \sigma_l^2 + 90K^2 L^2 \eta_L^2 \sigma_g^2 + 180K^2 L^4 \eta_L^2 \rho^2 + 24K^4 L^6 \eta_L^6 \rho^2 + 2K^2 L^4 \eta_L^2 \rho^2 \alpha_{g_s} + 16K^3 L^6 \eta_L^4 \rho^2 + \frac{\eta_g \eta_L L^3 \rho^2}{2S} (\sigma_l^2 + G_s^2) + \frac{\eta_g \eta_L}{S} \left(30KL^5 \eta_L^2 \rho^2 \sigma_l^2 + 270K^2 L^3 \eta_L^2 \sigma_g^2 + 540K^2 L^5 \eta_L^2 \rho^2 + 72K^3 L^7 \eta_L^4 \rho^2 + 6K^3 L^3 \eta_L^2 \rho^2 \alpha_{g_s} + \frac{9}{2} KL \sigma_g^2 + 9KL^3 \rho^2 \right) \right)$. If local and global learning rates are chosen as $\eta_l = \frac{1}{\sqrt{RKL}}$ and

$\eta_G = \sqrt{KS}$, and perturbation radius is chosen as $\rho = \frac{1}{\sqrt{R}}$, the convergence rate can be expressed as:

$$\frac{1}{R} \sum_{r=1}^R \mathbb{E} \left[\left\| f(w^{r+1}) \right\|^2 \right] = O \left(\frac{FL}{\sqrt{RKS}} + \frac{\sqrt{K}\sigma_g^2}{\sqrt{RS}} + \frac{\sigma_g^2}{R} + \frac{L^2(\sigma_l^2 + G_s^2) + \sigma_g^2}{R^{\frac{3}{2}}\sqrt{KS}} + \frac{\sqrt{KL}L^2}{R^{\frac{3}{2}}} + \frac{L^2}{R^2} (1 + \alpha_{g_s}) \right).$$

Proof.

$$\begin{aligned} & \mathbb{E} \left\| f \left(\tilde{w}_{+\frac{1}{2}}^{r+1} \right) \right\|^2 \\ & \stackrel{(1)}{\leq} \left\| f \left(\tilde{w}_{+\frac{1}{2}}^r \right) - \frac{K\eta_g\eta_L}{2} \left\| \nabla f \left(\tilde{w}_{+\frac{1}{2}}^r \right) \right\|^2 + K\eta_g\eta_L L^2 \varepsilon_w + K\eta_g\eta_L L^2 \varepsilon_\delta - \frac{K\eta_g\eta_L}{2} \mathbb{E}_r \left\| \sum_{i,k} \nabla f_i \left(\tilde{w}_{i,k+\frac{1}{2}}^r \right) \right\|^2 \right. \\ & \quad \left. + \frac{L}{2} \eta_g^2 \mathbb{E}_r \left[\|\Delta^r\|^2 \right] \right. \\ & \stackrel{(2)}{\leq} \left\| f \left(\tilde{w}_{+\frac{1}{2}}^r \right) - \frac{K\eta_g\eta_L}{2} \left\| \nabla f \left(\tilde{w}_{+\frac{1}{2}}^r \right) \right\|^2 + K\eta_g\eta_L L^2 \varepsilon_w + K\eta_g\eta_L L^2 \varepsilon_\delta - \frac{K\eta_g\eta_L}{2} \mathbb{E}_r \left\| \sum_{i,k} \nabla f_i \left(\tilde{w}_{i,k+\frac{1}{2}}^r \right) \right\|^2 \right. \\ & \quad \left. + \frac{K\eta_g^2\eta_l^2 L^3 \rho^2}{2S} (\sigma_l^2 + G_s^2) + \frac{\eta_g^2 LS}{2N} \sum_i \left\| \sum_{j=1}^{K-1} \nabla f_i \left(\tilde{w}_{i,j+\frac{1}{2}}^r \right) \right\|^2 + \frac{\eta_g^2 LS(S-1)}{2N^2} \left\| \sum_{j=0}^{K-1} \nabla f_i \left(\tilde{w}_{i,j+\frac{1}{2}}^r \right) \right\|^2 \right. \\ & \stackrel{(3)}{\leq} \left\| f \left(\tilde{w}_{+\frac{1}{2}}^r \right) - \frac{K\eta_g\eta_L}{2} \left\| \nabla f \left(\tilde{w}_{+\frac{1}{2}}^r \right) \right\|^2 + K\eta_g\eta_L L^2 \varepsilon_w + K\eta_g\eta_L L^2 \varepsilon_\delta + \frac{K\eta_g^2\eta_l^2 L^3 \rho^2}{2S} (\sigma_l^2 + G_s^2) \right. \\ & \quad \left. + \frac{L\eta_g^2\eta_l^2}{2NS} \sum_i \left\| \sum_k \nabla f_i \left(\tilde{w}_{i,k+\frac{1}{2}}^r \right) \right\|^2 \right. \\ & \stackrel{(4)}{\leq} \left\| f \left(\tilde{w}_{+\frac{1}{2}}^r \right) - K\eta_g\eta_L \left(\frac{1}{2} - 30K^2 L^2 \eta_L^2 - \frac{K\eta_g\eta_L}{2S} (3K + 180K^2 L^4 \eta_L^2 \rho^2) \right) \left\| \nabla f \left(\tilde{w}_{+\frac{1}{2}}^r \right) \right\|^2 \right. \\ & \quad \left. + K\eta_g\eta_L \left(10KL^4 \eta_L^2 \rho^2 \sigma_l^2 + 90K^2 L^2 \eta_L^2 \sigma_g^2 + 180K^2 L^4 \eta_L^2 \rho^2 + 24K^4 L^6 \eta_L^6 \rho^2 + 2K^2 L^4 \eta_L^2 \rho^2 \alpha_{g_s} + 16K^3 L^6 \eta_L^4 \rho^2 \right. \right. \\ & \quad \left. \left. + \frac{\eta_g\eta_L L^3 \rho^2}{2S} (\sigma_l^2 + G_s^2) \right) + \frac{K\eta_g^2\eta_l^2}{S} \left(30KL^5 \eta_L^2 \rho^2 \sigma_l^2 + 270K^2 L^3 \eta_L^2 \sigma_g^2 + 540K^2 L^5 \eta_L^2 \rho^2 + 72K^3 L^7 \eta_L^4 \rho^2 \right. \right. \\ & \quad \left. \left. + 6K^3 L^3 \eta_L^2 \rho^2 \alpha_{g_s} + \frac{9}{2} KL \sigma_g^2 + 9KL^3 \rho^2 \right) \right. \\ & \stackrel{(5)}{\leq} \left\| f \left(\tilde{w}_{+\frac{1}{2}}^r \right) - CK\eta_g\eta_L \left\| \nabla f \left(\tilde{w}_{+\frac{1}{2}}^r \right) \right\|^2 + K\eta_g\eta_L \left(10KL^4 \eta_L^2 \rho^2 \sigma_l^2 + 90K^2 L^2 \eta_L^2 \sigma_g^2 + 180K^2 L^4 \eta_L^2 \rho^2 \right. \right. \\ & \quad \left. \left. + 24K^4 L^6 \eta_L^6 \rho^2 + 2K^2 L^4 \eta_L^2 \rho^2 \alpha_{g_s} + 16K^3 L^6 \eta_L^4 \rho^2 + \frac{\eta_g\eta_L L^3 \rho^2}{2S} (\sigma_l^2 + G_s^2) \right) + \frac{K\eta_g^2\eta_l^2}{S} \left(30KL^5 \eta_L^2 \rho^2 \sigma_l^2 \right. \right. \\ & \quad \left. \left. + 270K^2 L^3 \eta_L^2 \sigma_g^2 + 540K^2 L^5 \eta_L^2 \rho^2 + 72K^3 L^7 \eta_L^4 \rho^2 + 6K^3 L^3 \eta_L^2 \rho^2 \alpha_{g_s} + \frac{9}{2} KL \sigma_g^2 + 9KL^3 \rho^2 \right) \right. \end{aligned}$$

(1) is from Lemma 4.10.(4). (2) is from Lemma 4.11. (3) is due to taking the expectation of r -th round and under the assumption that learning rates satisfy $KL\eta_g\eta_L \leq \frac{S-1}{S}$. (4) is from Lemma 4.6, Lemma 4.7, Lemma 4.12. (5) is because there exists $C > 0$, s.t. $0 < C < \left(\frac{1}{2} - 30K^2 L^2 \eta_L^2 - \frac{K\eta_g\eta_L}{2S} (3K + 180K^2 L^4 \eta_L^2 \rho^2) \right)$.

After Lemma 4.10.(6) for $r = [R]$ is summed and both sides are multiplied by $\frac{1}{CK\eta_g\eta_LR}$, the following holds:

$$\begin{aligned} & \frac{1}{R} \sum_{r=1}^R \mathbb{E} \left[\left\| f(w^{r+1}) \right\|^2 \right] \\ & \stackrel{(6)}{\leq} \frac{f \left(\tilde{w}_{+\frac{1}{2}}^0 \right) - f^*}{CK\eta_g\eta_LR} + \frac{1}{C} \left(10KL^4 \eta_L^2 \rho^2 \sigma_l^2 + 90K^2 L^2 \eta_L^2 \sigma_g^2 + 180K^2 L^4 \eta_L^2 \rho^2 + 24K^4 L^6 \eta_L^6 \rho^2 + 2K^2 L^4 \eta_L^2 \rho^2 \alpha_{g_s} \right. \end{aligned}$$

$$\begin{aligned}
& + 16K^3L^6\eta_L^4\rho^2 + \frac{\eta_g\eta_L L^3\rho^2}{2S}(\sigma_l^2 + G_s^2) + \frac{\eta_g\eta_L}{S}\left(30KL^5\eta_L^2\rho^2\sigma_l^2 + 270K^2L^3\eta_L^2\sigma_g^2 + 540K^2L^5\eta_L^2\rho^2 + 72K^3L^7\eta_L^4\rho^2\right. \\
& \left. + 6K^3L^3\eta_L^2\rho^2\alpha_{g_s} + \frac{9}{2}KL\sigma_g^2 + 9KL^3\rho^2\right).
\end{aligned}$$

(6) is from the relationship between current loss and optimal loss $f\left(\tilde{w}_{+\frac{1}{2}}^{r+1}\right) \geq f^*$, and the one between current loss and initial loss $f\left(\tilde{w}_{+\frac{1}{2}}^0\right) \geq f\left(\tilde{w}_{+\frac{1}{2}}^r\right)$. If we choose local and global learning rates as $\eta_l = \frac{1}{\sqrt{RKL}}$ and $\eta_g = \sqrt{KS}$, and choose perturbation radius as $\rho = \frac{1}{\sqrt{R}}$ and $F = f\left(\tilde{w}_{+\frac{1}{2}}^0\right) - f^*$, we have:

$$\begin{aligned}
& \frac{1}{R} \sum_{r=1}^R \mathbb{E} \left[\left\| f(w^{r+1}) \right\|^2 \right] \\
& \leq \frac{FL}{CK\eta_g\eta_LR} + \frac{1}{C} \left(10 \frac{KL^2\sigma_l^2}{R} + 90 \frac{\sigma_g^2}{R} + 180 \frac{L^2}{R^2} + 24 \frac{1}{R^4K^2} + 2 \frac{L^2}{R^2} \alpha_{g_s} + 16 \frac{L^2}{R^3K} + \frac{L^2}{2R^{\frac{3}{2}}\sqrt{KS}} (\sigma_l^2 + G_s^2) \right. \\
& \left. + 30 \frac{L^2\sigma_l^2}{R^{\frac{5}{2}}K^{\frac{3}{2}}\sqrt{S}} + 270 \frac{\sigma_g^2}{R^{\frac{3}{2}}\sqrt{SK}} + 540 \frac{L^2}{R^{\frac{5}{2}}\sqrt{KS}} + 72 \frac{L^2}{R^{\frac{7}{2}}K^{\frac{3}{2}}\sqrt{S}} + 6 \frac{\sqrt{K}\alpha_{g_s}}{R^{\frac{5}{2}}\sqrt{S}} + \frac{9\sqrt{K}\sigma_g^2}{2\sqrt{SR}} + 9 \frac{\sqrt{KL}^2}{R^{\frac{3}{2}}} \right).
\end{aligned}$$

If the number of sampled clients is larger than the one of epochs and high order terms are neglected, the convergence rate of part client participation for sUSAM is:

$$\frac{1}{R} \sum_{r=1}^R \mathbb{E} \left[\left\| f(w^{r+1}) \right\|^2 \right] = O \left(\frac{FL}{\sqrt{RKS}} + \frac{\sqrt{K}\sigma_g^2}{\sqrt{RS}} + \frac{\sigma_g^2}{R} + \frac{L^2(\sigma_l^2 + G_s^2) + \sigma_g^2}{R^{\frac{3}{2}}\sqrt{KS}} + \frac{\sqrt{KL}^2}{R^{\frac{3}{2}}} + \frac{L^2}{R^2} (1 + \alpha_{g_s}) \right).$$

Discussion. It can be concluded for Theorem 2 and Theorem 3 that $\frac{\sigma_g^2}{R}$ and $\frac{\sqrt{K}\sigma_g^2}{\sqrt{RS}}$ are caused by heterogeneity between clients; $\frac{L^2\sigma_l^2}{R^{\frac{3}{2}}\sqrt{KN}}$, $\frac{L^2\sigma_l^2}{R^{\frac{3}{2}}\sqrt{KS}}$, $\frac{\sqrt{KL}^2}{R^{\frac{3}{2}}}$, $\frac{L^2}{R^2}$, $\frac{L^2\sigma_l^2}{R^2K}$ are relevant to local SGD; $\frac{L^2G_s^2}{R^{\frac{3}{2}}\sqrt{KN}}$, $\frac{L^2G_s^2}{R^{\frac{3}{2}}\sqrt{KS}}$, $\frac{L^2\alpha_{g_s}}{R^2}$ depend on hyper-parameters of the sparse ratio. $\frac{FL}{\sqrt{RKN}}$, $\frac{FL}{\sqrt{RKS}}$ and $\frac{\sqrt{K}\sigma_g^2}{\sqrt{RS}}$ represent main terms for the convergence rate. If learning rates are set properly, the convergence rate for sUSAM can be compatible with existing non-convex FL works. Since the mask in sUSAM constrains sparse gradients, additional square and two-thirds terms are also negligible. Besides, sUSAM is potential to generalize better by the dynamic mask, thus alleviating weight shifts in $\frac{\sigma_g^2}{R}$ and $\frac{\sqrt{K}\sigma_g^2}{\sqrt{RS}}$.

Supplementary Note 5: Complete Algorithms

Algorithm 1 describes the local pretraining process, which can be conducted at any time before the federated training stage. Each client pretrains an organ(s)-specific teacher model based on the partially-annotated dataset. After that, all clients send locally pretrained teacher models to the server for the future pseudo labeling stage.

Algorithm 1 UFPS(pretraining)

Require: Number of clients N ; number of local epochs K ; initial local models w^1, \dots, w^N ; partially-annotated local datasets

D_1^p, \dots, D_N^p .

- 1: **for** each client $i \in \{1, \dots, N\}$ in parallel **do**
 - 2: **for** $k \in 1, \dots, K$ **do**
 - 3: $w_i^T = \text{MiniBatchUpdate}(D_i^p, w_i^T)$
 - 4: **end for**
 - 5: **end for**
 - 6: **return** $\{w_i^T\}_{i=1}^N$
-

Algorithm 2 introduces the federated learning flow. Gradient masks and statistics for uncertainty are communicated according to r_{sUSAM} and r_{UA} , respectively. r_{UA} is used to ensure statistics of uncertainty banks are sufficient to modify the aggregation weight. After uncertainty-aware global aggregation and calculation of the nonintersecting global gradient mask, the global mask is sent to clients along with the global model.

Algorithm 2 UFPS(federated training)

Require: Number of local and global rounds K and R ; number of clients N ; partially-annotated local datasets D_1^p, \dots, D_N^p ; pretrained teacher models w_1^T, \dots, w_N^T ; initial global model w_0^0 ; uncertainty banks $U_{bank}^1, \dots, U_{bank}^N$; global mask M_G ; local masks M_L^1, \dots, M_L^N ; local momentum gradients $G_{mo}^1, \dots, G_{mo}^N$; start epoch for global mean teacher, uncertainty-aware aggregation, sUSAM $r_{GMT}, r_{UA}, r_{sUSAM}$.

```

1: server sends all teacher models  $w^T$  to all clients
2: for each global round  $r \in \{1, \dots, R\}$  do
3:   for each client  $i \in \{1, \dots, N\}$  in parallel do
4:      $w_{i,0}^r = w_0^r$ 
5:     for each local round  $k \in \{1, \dots, K\}$  do
6:       if  $r < r_{sUSAM}$  then
7:          $w_{i,k}^r = \text{LocalTraining}(D_i^{PL}, w^T)$ 
8:         client  $i$  sends  $w_{i,k}^r$  to server
9:       else if  $r \geq r_{sUSAM}$  and  $r < r_{UA}$  then
10:         $w_{i,k}^r, M_L^i = \text{LocalTraining}(D_i^{PL}, w^T)$ 
11:        client  $i$  sends  $w_{i,k}^r, M_L^i$  to server
12:      else
13:         $w_{i,k}^r, \mu^i, \sigma^i, M_L^i = \text{LocalTraining}(D_i^{PL}, w^T)$ 
14:        client  $i$  sends  $w_{i,k}^r, \mu^i, \sigma^i, M_L^i$  to server
15:      end if
16:    end for
17:  end for
18:  if  $r < r_{UA}$  then
19:     $w_0^r = \sum_{i \in [N]} A_i^w w_i^r$ 
20:  else
21:     $\hat{A}^w \leftarrow$  server calculates aggregation weights based on  $\mu^i, \sigma^i$  according to Equation 7
22:     $w_0^r = \sum_{i \in [N]} \hat{A}_i^w w_i^r$ 
23:  end if
24:  server sends  $w_0^r$  to all clients
25:  if  $r \geq r_{sUSAM}$  then
26:     $M_G \leftarrow$  server updates global mask according to Equation 12
27:    server sends global mask  $M_G$  to all clients
28:  end if
29: end for
30: return  $w_0^*$ 

```

Algorithm 3 is about the local training stage in FL. At each local round, each client first uses pretrained local teacher models to get the pseudo label and replaces classes with ground truth at hand. During this process, the uncertainty value is also calculated with logits from teachers. When local training converges, one can decide whether to use the global model to get the pseudo label and refine it by pretrained teachers. With data and pseudo labels, each client updates the local model either through vanilla SGD or sUSAM depending on the current training stage. After local training, each client uploads information according to the current global epoch.

Algorithm 4 mainly discriminates the calculation of losses. In the warmup global epochs, only basic losses are used. Later, the weight scheduler is used to enforce the local model to concentrate on classes with specific uncertainty values. When the local model converges, aRCE loss is then adopted to help escape from local minima caused by noisy pseudo labels. Note that RCE loss only works when predictions from local models are confirming, so we use it after the end epoch of WS.

Algorithm 3 UFPS(LocalTraining)

Require: Current local round r ; batch size B ; partially-annotated dataset D^P ; local model w ; random initialized blender node and image transform node for CMIDG; warmup epoch r_{warmup} ; end epoch for weight scheduler r_{WS} ; start epoch for global mean teacher, uncertainty-aware aggregation, sUSAM $r_{GMT}, r_{UA}, r_{sUSAM}$; updating frequency for sUSAM r_{fre} ; global mask M_G .

```
1:  $\mu = 0, \sigma = 0$ 
2: for each batch  $\{x, y\}_{i=1}^B \in D^P$  do
3:    $q^T \leftarrow$  forward all teacher models  $w_1^T, \dots, w_N^T$  on  $\{x\}_{i=1}^B$ 
4:    $U \leftarrow$  calculate Equation 6 through  $q^T$ 
5:    $\tilde{q}^T \leftarrow$  merge foreground classes and post-processing background class for  $\hat{q}^T$ 
6:   if  $r \geq r_{GMT}$  then
7:      $\tilde{q}^G \leftarrow$  forward global model on  $\{x\}_{i=1}^B$ 
8:      $\tilde{q} \leftarrow$  refine  $\tilde{q}^G$  through  $\tilde{q}^T$  according to Equation 5
9:      $y' \leftarrow$  merge foreground class in ground truth  $y$  into  $\tilde{q}$ 
10:  end if
11:  if  $r < r_{sUSAM}$  then
12:     $\hat{q} \leftarrow$  forward  $w$  on  $\{x\}_{i=1}^B$ 
13:     $f = \text{CalculateLoss}(\hat{q}, y', w(U))$ 
14:     $w = w - \eta \nabla f$ 
15:  else
16:     $\{x_{aug}\}_{i=1}^B \leftarrow$  perform CMIDG on  $\{x\}_{i=1}^B$ 
17:     $\hat{q}_{aug} \leftarrow$  forward  $w$  on  $\{x_{aug}\}_{i=1}^B$ 
18:     $f = \text{CalculateLoss}(\hat{q}_{aug}, y', w(U))$ 
19:    if  $r = r_{sUSAM}$  then
20:       $M_L \leftarrow \text{TopKSort}_{T_L} |\nabla f|$ 
21:       $G_{mo} \leftarrow$  initialize local momentum gradient
22:    else if  $r > r_{sUSAM}$  and  $r \% r_{fre} = 1$  then
23:       $M_L \leftarrow \text{TopKSort}_{T_L} |\nabla f|$ 
24:       $G_{mo} \leftarrow$  update local momentum gradient according to Equation 11
25:    else
26:      take history mask  $M_E$  as current local mask
27:    end if
28:     $\tilde{w}_{+\frac{1}{2}} \leftarrow$  perturb model parameters with sparse mask
29:     $\hat{q} \leftarrow$  forward  $\tilde{w}_{+\frac{1}{2}}$  on  $\{x\}_{i=1}^B$ 
30:     $\tilde{f}_{+\frac{1}{2}} = \text{CalculateLoss}(\hat{q}, y', w(U))$ 
31:     $w = w - \eta \nabla \tilde{f}_{+\frac{1}{2}}$ 
32:  end if
33: end for
34: if  $r \geq r_{UA}$  then
35:    $\mu = \frac{1}{|U_{bank}|} \sum_{i=1}^{|U_{bank}|} U_{bank}^i$ 
36:    $\sigma = \frac{1}{|U_{bank}|} \sum_{i=1}^{|U_{bank}|} (U_{bank}^i - \mu)^2$ 
37: end if
38: if  $r \geq r_{sUSAM}$  then
39:    $M_L \leftarrow \text{argmax}_{T_L} G_{mo}$ 
40: end if
41: if  $r < r_{sUSAM}$  then
42:   return  $w$ 
43: else if  $r \geq r_{sUSAM}$  and  $r < r_{UA}$  then
44:   return  $w, M_L$ 
45: else
46:   return  $w, \mu, \sigma, M_L$ 
47: end if
```

Algorithm 4 CalculateLoss

Require: Model prediction \hat{q} ; pseudo label y' ; model parameter w ; uncertainty based weight scheduler $w(U)$.

```
1: if  $r < r_{warmup}$  then  
2:    $w = w - \eta \nabla f_{Dice+BCE}(\hat{q}, y')$   
3: else if  $r \geq r_{warmup}$  and  $r < r_{WS}$  then  
4:    $w = w - \eta \nabla (w(U) f_{Dice+BCE}(\hat{q}, y'))$   
5: else  
6:    $w = w - \eta \nabla f_{Dice+BCE+RCE}(\hat{q}, y')$   
7: end if  
8: return  $f$ 
```

Supplementary Note 6: Detailed Experimental Setups

6.1. Datasets

We conduct our experiments with four originally fully-annotated (labels for liver, kidney (left + right), spleen, pancreas) CT image datasets: WORD, AbdomenCT-1K, AMOS (AMOS2022), and BTCV. In the preprocessing stage, we first crop the foreground region with Hounsfield units (HU) more than 0 with a bounding box. Image intensities are then truncated into $[-500, 500]$ to filtrate non-organ volumes. We divide each dataset with a ratio of 7:1:2 for training, validation, and testing sets.

WORD. Whole abdominal ORgan Dataset (WORD) totally contains 150 abdominal CT volumes (30495 slices) from 150 patients before the radiation therapy. Each volume consists of 159 to 330 slices of 512×512 pixels with an in-plane resolution of $0.976 \text{ mm} \times 0.976 \text{ mm}$ and slice spacing of 2.5-3.0 mm, indicating that the WORD is a very high-resolution dataset. The whole dataset has 16 organs with fine pixel-level annotations and scribble-based sparse annotation, including the liver, spleen, kidney (L), kidney (R), stomach, gallbladder, esophagus, duodenum, colon, intestine, adrenal, rectum, bladder, head of the femur (L), and head of the femur (R). For large and small organs, pixel distribution is extremely unbalanced (as shown in Fig2 in the paper of WORD). 120 volumes with annotation and 30 without annotation are published.

AbdomenCT-1K. AbdomenCT-1K totally contains 1112 abdominal CT volumes from 12 medical centers. Since the information about which center each data belongs to is privacy concerned, we do not further split this dataset into more datasets. Organs in this dataset are liver, kidney, spleen, and pancreas. Resolution of all CT scans is 512×512 pixels with varying pixel sizes and slice thickness between 1.25-5 mm. 1000 volumes with annotation and 63 without annotation are published. We pick 266 samples from 1000 labeled volumes with the smallest file size to accelerate the training process.

AMOS. AMOS consists of 500 CT and 100 MRI with 15 organs, including spleen, right kidney, left kidney, gallbladder, esophagus, liver, stomach, aorta, inferior vena cava, pancreas, right adrenal gland, left adrenal gland, duodenum, bladder, prostate/uterus. The dataset is from five domains, whereas we do not split it since no domain information is provided. 200 annotated CT images and 40 annotated MRI images are published and we only use CT images.

BTCV. BTCV provides 50 CT volumes captured during portal venous contrast phase with variable volume sizes $512 \times 512 \times (85-198)$ and field of views $280 \times 280 \times 280 \text{ mm}^3$ - $500 \times 500 \times 650 \text{ mm}^3$. The in-plane resolution varies from $0.54 \times 0.54 \text{ mm}^2$ to $0.98 \times 0.98 \text{ mm}^2$, while the slice thickness ranges from 2.5-5.0 mm. 13 organs are in BTCV, i.e., spleen, right kidney, left kidney, gallbladder, esophagus, liver, stomach, aorta, inferior vena cava, portal vein and splenic vein, pancreas, right adrenal gland, left adrenal gland. We merge left kidney and right kidney when testing. We choose 30 training samples in divided BTCV as our out-FL client.

6.2. Training

All methods are based on generic modular UNet from nnUNet⁶ with auto mixed precision to save GPU memory and accelerate training. We modify deep supervision brunches after decoder to ones after encoder to extract more informative features. The attribute 'tracking_running_states' of batch normalization layers is set to False, which is same as FedAvg⁷. The output channel number of the segmentation head is set according to the specific method.

The best global model evaluated on validation sets of clients is used to perform testing for the final result. Only the partial target set and its inverse set (background) are used to train local teacher models. Training transform is conducted by MONAI⁸, including normalize to $[-1,1]$, spatial pad, random crop patch (pos:neg=1:1, pos=HU>0) with size (80,192,192), random rotate and flip in x and y axis, affine, grid distortion, cutout, random scale and shift intensity. Dice and BCE losses are used as default loss functions. Transformations for validation and testing only include normalization and spatial pad. Sliding window inference from MONAI is used with ROI size (80,192,192), sw batch size 2 and overlap 0.5. We train all methods for 500 communication rounds. In each communication round, all clients in FL are selected for one epoch of local training. We choose AdamW⁹ as our optimizer with weight decay 10^{-6} . We conduct 10 warmup rounds from minimal learning rate

10^{-6} to the initiate learning rate 10^{-4} and change the learning rate by warmup restart scheduler in rest rounds. All methods are implemented in PyTorch on two Nvidia GeForce RTX 3090s.

6.3. Metric

Here, we use TP, TN, FP, FN as abbreviation for true positive, true negative, false positive and false negative. Besides, x_{GT}, x_{pred} represent ground truth and model prediction.

Dice. The ratio between the intersection part of two objects and the total area:

$$\text{Dice} = \frac{2 |x_{GT} \cap x_{pred}|}{|x_{GT}| + |x_{pred}|} = \frac{2TP}{2TP + FP + FN}$$

Hausdorff Distance (HD). HD measures the similarity between the point sets $\{X, Y\}$ for segmentation border:

$$\begin{aligned} HD &= \max \{d_{XY}, d_{YX}\} \\ &= \max \left\{ \max_{x \in X} \min_{y \in Y} d(x, y), \min_{y \in Y} \max_{x \in X} d(x, y) \right\} \end{aligned}$$

Jaccard Coefficient (JC). The ratio between intersection and union:

$$JC = \frac{|x_{GT} \cap x_{pred}|}{|x_{GT} \cup x_{pred}|} = \frac{TP}{TP + FP + FN}$$

Sensitivity (Sen). Sensitivity is also called recall, which measures the model ability to segment interested regions:

$$Sen = \frac{|x_{GT} \cap x_{pred}|}{|x_{GT}|} = \frac{TP}{TP + FN}$$

Specificity (Spe). Specificity measures the model ability to judge uninterested regions correctly:

$$Spe = \frac{TN}{TN + FP}$$

Relative Volume Error (RVE). Ratio between absolute error and measurement being taken:

$$RVE = \frac{abs(|x_{GT}| - |x_{pred}|)}{|x_{GT}|}$$

6.4. Complete model aggregation

Datasets, i.e., WORD, AbdomenCT-1K, AMOS, with partially-annotated labels are used to train the model(s) by Dice loss and binary cross entropy (BCE) loss only for annotated foreground class(es). Except for Multi-head, Multi-encoder, and Multi-decoder, we only use foreground label(s) to calculate dice and BCE losses.

FedAvg. Above three datasets are used to train three local models. The aggregated global model is used for evaluation.

Cond-dec. Above three datasets are used to train three local models. Client index is additionally input into the decoder after each BN layer as a hash value matching magnitude for BN output. Other procedures are same with FedAvg. During validation, same operation as the one in training is performed to get foreground classes corresponding to client indexes. For the background class, three logits for corresponding indexes are averaged in the 0-th channel.

FedBN. Above three datasets are used to train three local models. All procedures are same as FedAvg except that batch normalization layers are personalized. During validation, same operations as ones in Cond-dec are performed for foreground classes and the background class.

FedASAM. Above three datasets are used to train three local models. All procedures are same as FedAvg except methods in FedASAM are additionally used.

MENU-Net. Above three datasets are used to train local models with multi-encoders by ME loss. The total number of encoders is equal to the organ amount in our experiment, i.e., four encoders. During the forward pass of training, all features from the last layer of four encoders are concatenated as input to the decoder and all features from each layer of four encoders are concatenated as input to deep supervision layers. Moreover, only the encoder corresponding to the specific organ, which is the current training target, is updated (thus we update Abdomen-1K twice). It should be noted that the whole patch training strategy in MENU-Net is changed to one random patch chosen by the percentage of pos:neg = 1:1 since the time gap can be tens of times in our experiment. When the server aggregates local models, for the multi-encoder part(s), only the encoder(s) from the client owning the annotated organ label is(are) used to update the part(s) in the global model. When testing, all clients forward all encoders to get four features of the bottleneck layer as the input to the decoder.

6.5. Part model aggregation

Datasets, i.e., WORD, AbdomenCT-1K, AMOS, with partially-annotated labels are used to train models by dice and BCE losses only for annotated foreground class(es). Validation in this category is performed before model aggregation. For Multi-encoder and Multi-decoder, the same operation is performed for foreground classes and the background class as in Cond-dec since the output channel of the segmentation head is five (four for the foreground and one for the background).

Multi-head. All procedures are same with FedAvg except for what is mentioned above and that segmentation heads (the final convolution layer) are personalized.

Multi-encoder. All procedures are same with FedAvg except for what is mentioned above and that encoders are personalized.

Multi-decoder. All procedures are same with FedAvg except for what is mentioned above and that decoders are personalized.

6.6. Baseline and SOTAs

We modify existing methods to better suit our experiment and tune hyper-parameters under each method. For all methods except SOLO, Centralized, FedCRLD, and DOD*, model aggregation is conduct before validation and we evaluate on test sets only by the global model. Unless specified, dice and BCE losses are used to train the model(s).

SOLO (partial). Each client trains a model on the partially-annotated local dataset by dice and BCE losses. During test time, we use three models to get three predictions and merge metrics from all of them. Result models for this method are used as pretrained teacher models for all SOTAs except FedCRLD and DOD*.

Centralized (full). Only a centralized model is trained on WORD, AbdomenCT-1K, and AMOS with fully annotated labels.

FedCRLD. FedCRLD is a pFL method with encoders personalized so we perform evaluation before aggregation. This method is based on contrastive learning like BYOL¹⁰. Cross-attention and self-attention of features are added to the network. Besides segmentation loss, there are three additional losses: MSE loss for predictions between the current local model and the momentum local model; MSE loss for features between the current local model and the momentum local model, and between the global model and the momentum local model; knowledge distillation (KD) loss between the current local model and the global model.

DOD*. DOD is originally a PSS method designed for centralized learning. A controller is proposed to generate dynamic weights for the segmentation head. The input of the controller is the organ index and the bottleneck feature. The encoder and deep supervision are globally aggregated and the rest remains local. We perform evaluation before model aggregation for this method just as other pFL methods.

CPS*. CPS is originally a PSS method designed for centralized learning. A co-training method in which two local models with different initializations offer extra pseudo labels for cooperative learning. We modify it into our pseudo labeling framework.

MS-KD*. MS-KD is originally a PSS method designed for centralized learning. Several losses are added: multi-scale knowledge distillation loss for original logits between local model and teacher models, and the one for features between local model and teacher models. Both of them use one-hot pseudo labels predicted from teacher models to serve as foreground masks.

FedAvg*. FedAvg is originally an FL method for datasets with all class annotated. We modify it into our pseudo labeling framework. After all clients send their pretrained teacher models to the server, the server sends all of them and the initialized global model to clients. Other procedures are same with FedAvg except that each client uses pretrained teacher models to get pseudo labels in each round.

FedProx*. FedProx is originally an FL method for datasets with all classes annotated. We modify it into our pseudo labeling framework. MSE loss for model parameters between local and global models is added.

MOON*. MOON is originally an FL method for datasets with all classes annotated. We modify it into our pseudo labeling framework. The contrastive loss of MOON includes features between current local and global models as positive pairs and ones between the current local model and the local model in the last round as negative pairs.

FedAlign*. FedAlign is originally an FL method for datasets with all classes annotated. A regulation loss of Lipschitz constant for features between the complete local model and the slimmed local model is added.

FedASAM*. The two-step minimization method of FedASAM is most similar with the one in our work. Original data are used in the ascent step. Stochastic weight averaging (SWA) is used on the server-side after model aggregation. FedASAM is modified into the pseudo label framework as FedASAM*. For ASAM, we set the start epoch as 0, perturbation radius ρ as 0.7, and balancing coefficient η as 0.001. For SWA, we tune the start epoch percentage from 0.25, 0.5, 0.75 and choose 0.75 as the best one, we also tune the cycle from 2,4,6 and choose 2 as the best one.

UFPS. Here we list all hyper-parameters for all modules in our method. The coefficient for aRCE loss is set to 0.01 and the start epoch is set to 200. For weight scheduler based on uncertainty score, we choose tail shift with 0.7 as the tail percentage threshold and set the end epoch for weight scheduler as 200. For uncertainty-aware global aggregation, we choose decoder as the target part and set τ^m, τ^v as 0.05, 0.001, respectively. The corresponding start epoch r_{UA} is set as 300 to accumulate enough statistics in the uncertainty bank. For global mean teacher, we choose 300 as the start epoch for this module and the intersection percentage is set to 0.8. For sUSAM, we set the start epoch r_{sUSAM} as 300, perturbation radius ρ as 0.7,

balancing coefficient η as 0.001, non-masked percentage for local mask T_L as 0.4, non-masked percentage for global mask T_L as 0.1, gradient momentum coefficient α_{mo} as 0.9, local mask update frequency r_{fre} as 5.

Supplementary Note 7: Complete comparison between SOTAs

Unless 'Post' is written as the header of a table or post-processing is marked in the title of the table, the default setting does not include any post-processing. Post-processing methods consist of filling up binary holes and removing small connected components which are below 20% percentage of the largest non-background connected component.

Original results and ones with post-processing are demonstrated in Table S2 and Table S3, separately. Dice is considered as the most important metric in our experiment as it directly reflects the overlap between ground truth and prediction. No matter whether post-processing is used, our model is able to predict accurate results for whole organs, thus getting a great result for dice and other supplementary metrics, i.e., JC and Sen. Just getting a large overlap is not enough since medical diagnosis requires an elaborate segmentation. The ability to refine segmentation border is closely related to HD and RVE. We note that FL based methods all suffer from the excess of smoothness, thus directly not satisfying for the two metrics. However, they can be significantly reduced by simple post-processing in practice. For Specificity, all methods achieve a great score close to 1, meaning all methods are capable of filtering out the most uninterested regions, so the lowest percentage of our method makes little difference compared with other methods in real medical applications.

Supplementary Note 8: More ablation study

Ablation for adaptive RCE. From Table S4, it can be seen that model performance is better when the coefficient for aRCE loss is set to a moderate value. When it is set too large, model prediction can be dominant when it is not reliable enough compared to pseudo labels. Otherwise, noises in pseudo labels are not sufficiently alleviated.

Ablation for Weight schedulers. Here we propose three schedulers focusing on different ranges of uncertainty for various situations as shown in Figure S1.

Tail shift (TS).

$$w(U_j) = \begin{cases} 2 - e^{\text{norm}(U_j) - \frac{r}{R}}, & U_j > U_{\mathcal{T}} \\ 2 - e^{\text{norm}(U_j)}, & \text{else} \end{cases}, \text{ where } \text{norm}(U_j) = \frac{U_j - \mu}{U_{\max} - U_{\min}}$$

where $U_{\mathcal{T}}$ corresponds to the uncertainty value at the lowest \mathcal{T} percentage. μ, U_{\max}, U_{\min} represent mean, maximal, minimal uncertainty in the uncertainty bank, respectively.

Base Decrement (BD).

$$w(U_j) = 2 - \left(\frac{\alpha - e}{R} r + e \right)^{\text{norm}(U_j)}, \text{ where } \text{norm}(U_j) = \frac{U_j - \mu}{U_{\max} - U_{\min}}$$

α is a hyper-parameter determining the minimal base, and we empirically set it to 1.

Round-trip Gaussian (RG)

$$w(U_j) = (1 - \beta) \cdot G(U_j) + \beta \cdot (2 - e^{\text{norm}(U_j)}),$$

$$\text{where } G(U_j) = \frac{1}{\sqrt{2\pi}\rho} \cdot e^{-\frac{(\text{norm}(U_j) - \text{norm}(\mu) - \text{Range}(r))^2}{2\rho^2}},$$

$$\text{Range}(r) = \begin{cases} \frac{U_{\text{range}} \cdot r}{\lfloor \frac{R}{2} \rfloor}, & r \leq \lfloor \frac{R}{2} \rfloor \\ U_{\text{range}} - \frac{U_{\text{range}} \cdot (r - \lfloor \frac{R}{2} \rfloor)}{\lfloor \frac{R}{2} \rfloor}, & \text{else} \end{cases},$$

$$U_{\text{range}} = \text{norm}(U_{\mathcal{T}}) - \text{norm}(U_{\min}),$$

$$\text{norm}(x) = \frac{x - \mu}{U_{\max} - U_{\min}},$$

where β is a balancing factor, ρ is used to calibrate amplitude with other schedulers, $\lfloor \cdot \rfloor$ is a rounding operator.

At the beginning of training, less uncertain samples are endowed with higher loss weight compared to dubious ones under any weight scheduler. Afterwards, TS puts more emphasis on least confident patches, which mainly consist of noisy pseudo labels and ones for hard classes. BD equally treats each part, which is equivalent to weight decrease for the head part and increase for the middle and tail parts. RG pays less attention to the tail part since the shift in the uncertainty axis is

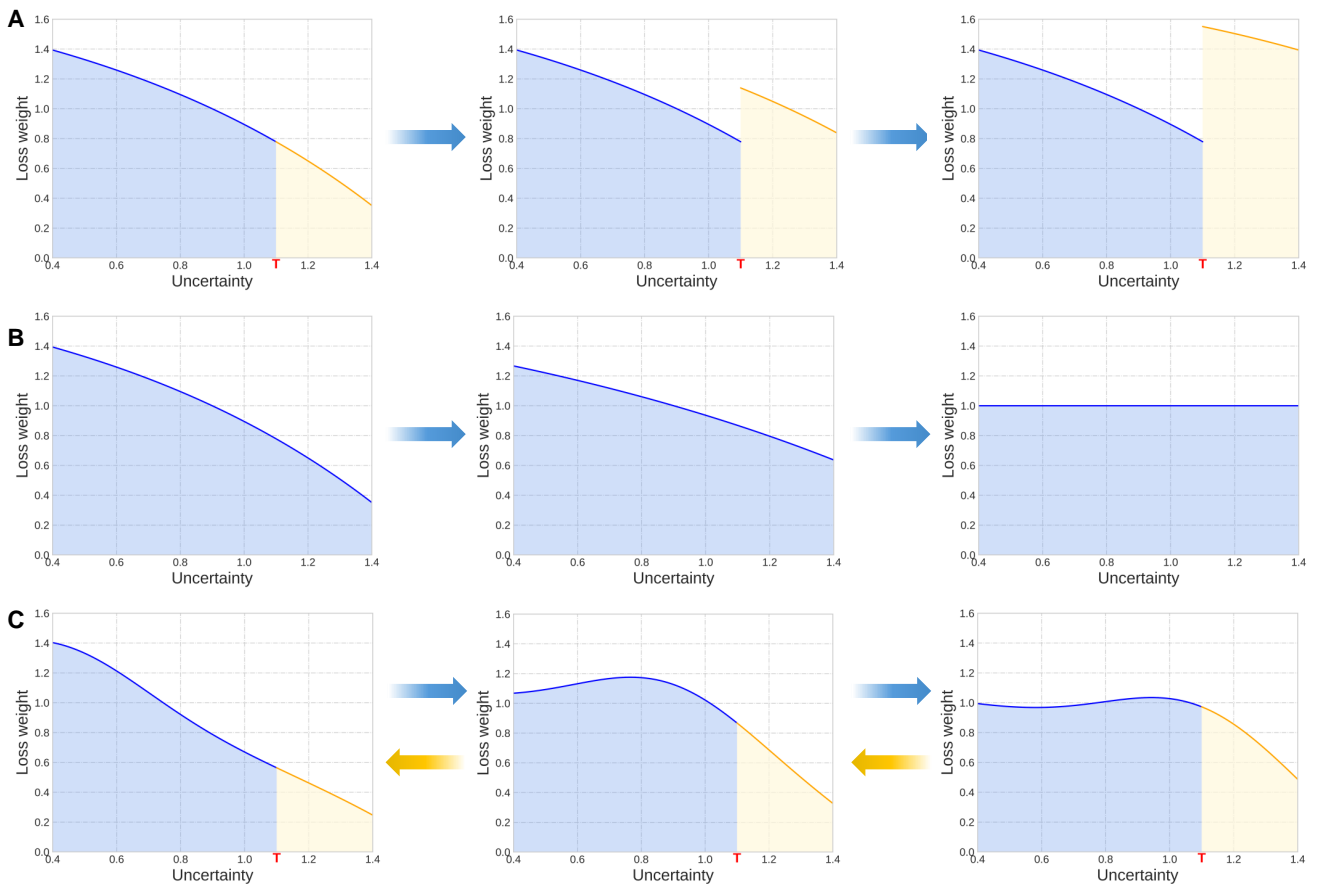


Figure S 1: Explanatory chart for three schedulers.

- (A) Tail shift.
- (B) Base decrement.
- (C) Round-trip gaussian.

blocked before the threshold. In our experiment, the loss weight scheduler for any client is disabled during warm-up epochs r_{warmup} until distribution for uncertainty can be approximately estimated.

From Table S5, it can be seen that TS, focusing on head and tail, achieves the best result in our experimental setting. The final epoch for weight scheduler should be decided depending on the fitting degree for different classes, which can be implicitly reflected from model performance for each class. Let us take TS as an example. As shown in Figure S2, model performance on the tail class, i.e., pancreas, is relatively stable after 150 epochs. Then, the larger weight on the tail class than head and middle classes should be controlled after this point. Through the results, we can find that prolonging the final epoch makes little difference as long as the noisy degree of tail classes is low. By using any one of these loss weight schedulers, the convergence speed is obviously accelerated due to concentration on uncertainty samples in previous rounds in Figure S2 and exploration of hard but valuable ones later.

Ablation for UA. Table S6 demonstrates a complete result for each organ and each client under more metrics. The conclusion for the usage of different model parts is basically same as what is discussed in our main paper.

To investigate the effect of changing aggregation weights on different parts of models, we use linear centralized kernel alignment¹¹ (Figure S3) as a measurement for the layer-wise similarity of network parameters. It can be observed that when global aggregation weights are linked up with uncertainty, similarity between deep layers of the network is greatly changed, indicating the high level information related to noise level may be learned. When UA is performed on different layers, the main difference falls around the bottleneck layer, which is related to the deepest global context.

Ablation for GMT. Table S7 demonstrates a complete result for each organ and each client under more metrics. The conclusion for the strategies is basically same as what is discussed in our main paper.

At the first row of Figure S4, the intersectant percentage is over 80%, so the intersection of predictions between pretrained teachers and the global one is taken. Although the global model over-segments some scraps and part of segmentation borders, the over-segmented result is offset with assistance from pretrained teacher models. In the third row, the circumstances happen to reverse. Thus, two kinds of main teachers give mutual aid when their segmentations are similar by eliminating noisy points.

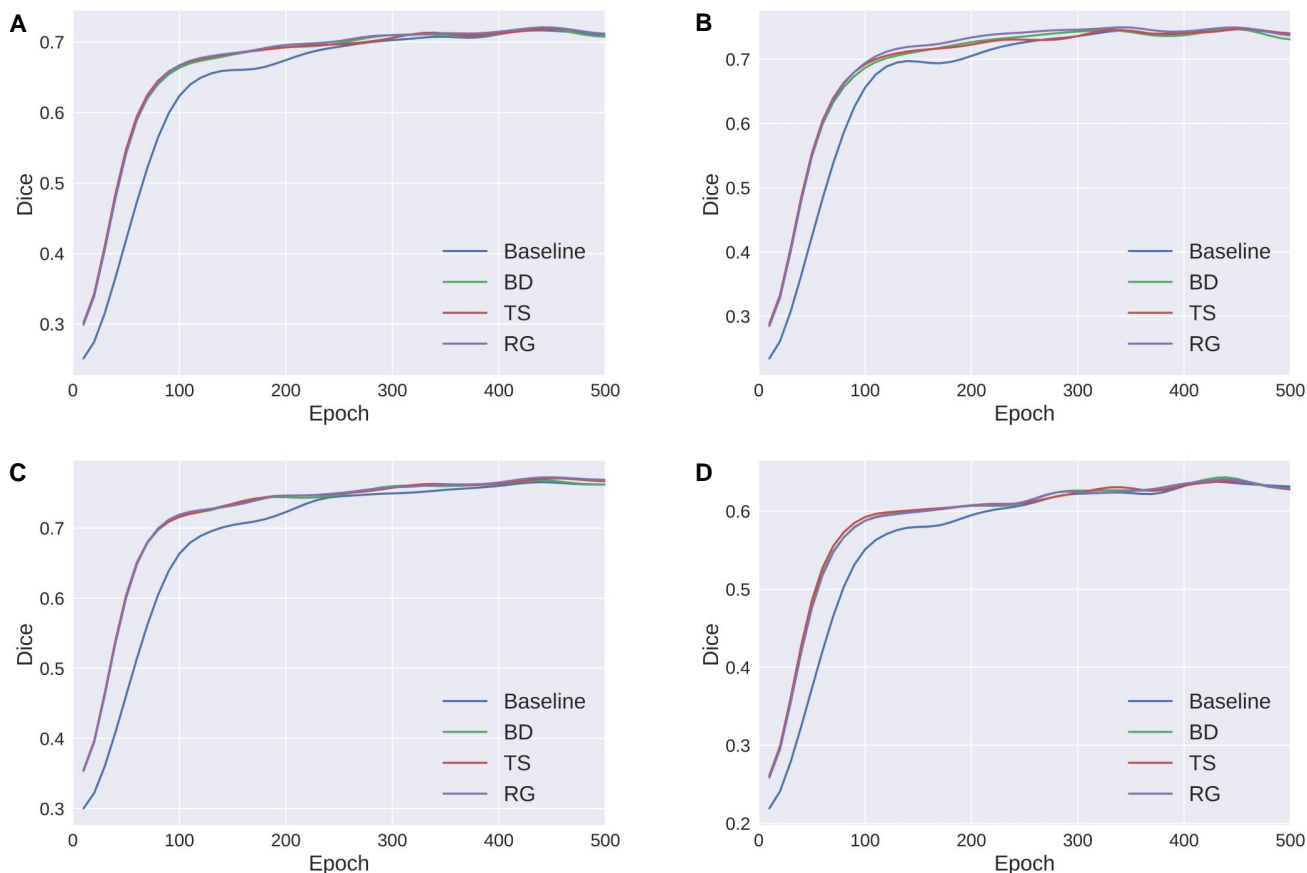


Figure S 2: Training curves for loss weight schedulers.
 (A) Testing dice during training for the mean of all clients.
 (B) Testing dice during training for the mean of client 1.
 (C) Testing dice during training for the mean of client 2.
 (D) Testing dice during training for the mean of client 3.

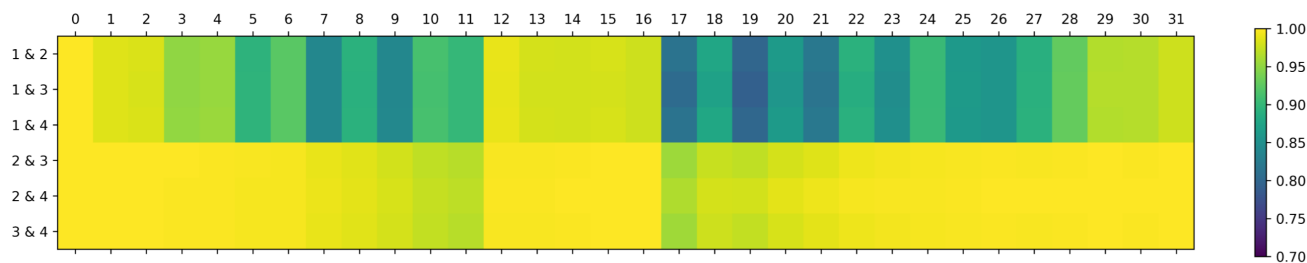


Figure S 3: Linear centered kernel alignment.
 Numbers on the left side of the bar refer to method index, where FedAvg*, Whole, Encoder, Decoder are in the number sequence. Numbers above the bar are layer indexes, where encoder corresponds to 0 to 11, transpose convolution layers in decoder are from 12 to 16, vanilla convolution layers in decoder are from 17 to 26, deep supervision layers are from 27 to 30, The last one is segmentation head.

As to the second row, the intersectant percentage is below 80%, so the accurate result from the global teacher is kept. This suggests that even when locally pretrained teachers may be hindered by domain gaps sometimes, the pseudo label from the GMT module can still be convincing owing to the generalization ability of the global model.

Complete results for sUSAM. Table S8 shows a complete result for each organ and each client under more metrics. (1) is 'CMIDG from 0 epoch'. We apply CMIDG to the data of the pseudo label baseline in the whole training process, i.e., 500 epochs, in which only descent steps are performed. (2) is 'CMIDG from 300 epoch', the mere difference between (1) and (2) is the start epoch, which is closely related to the generated data distribution. (3) is 'Original data + ASAM' in which ascent and descend steps are all performed on the original data without CMIDG. (4) is 'Random perturbation + ASAM' in

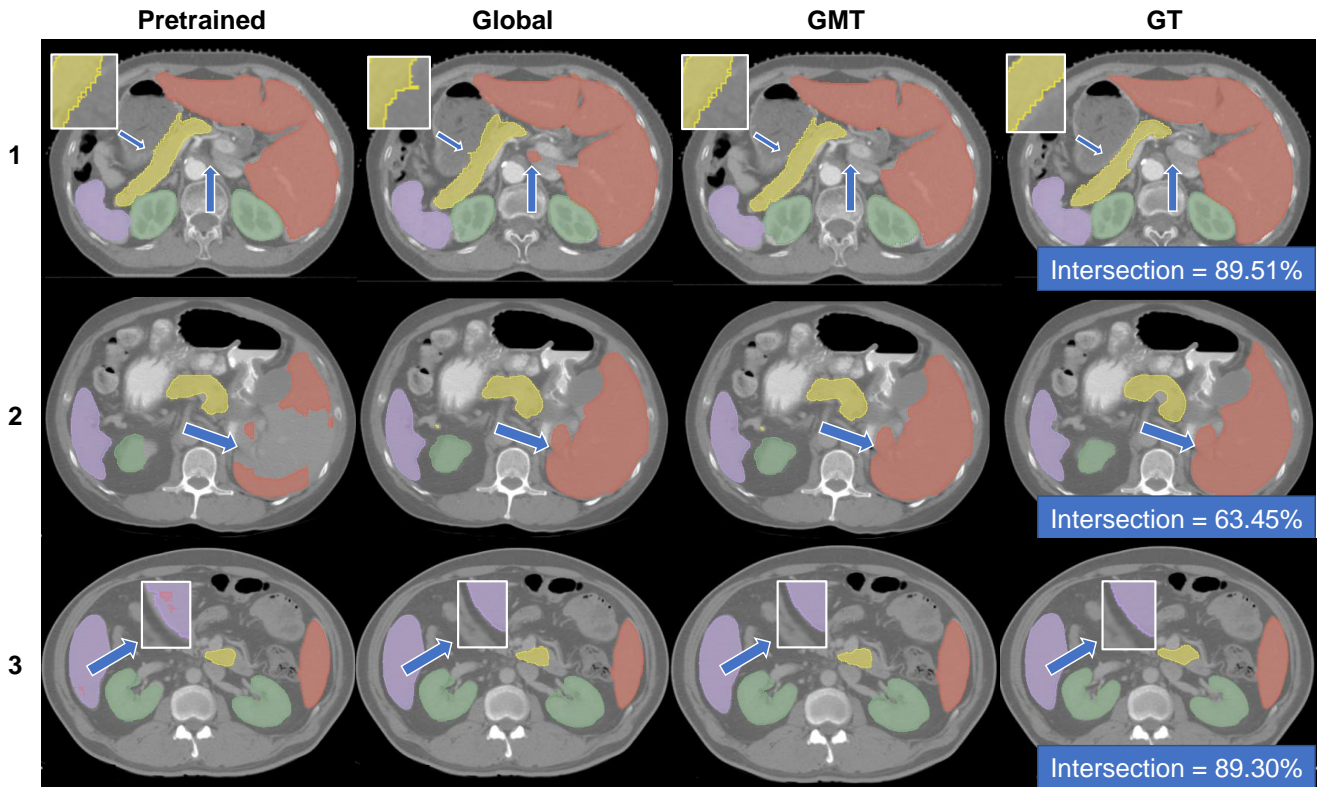


Figure S 4: Effect of global main teacher.

Numbers on the left side of images refer to client index. Green, red, purple, yellow regions represent kidney, liver, spleen and pancreas, respectively. Numbers in the blue box denotes intersection percentage between pretrained teachers and the global one.

which ascent steps are only performed to get a reference about perturbation amplitude and the perturbation follows a normal distribution. (5) is our proposed USAM in which CMIDG is only applied to the data in the ascent step. (6) is 'USAM + $(0.8 * \text{original weight} + 0.2 * \text{perturbed weight})$ for descent step' in which original gradients without perturbation and perturbed gradients by CMIDG are fused according to weights to update the model in the descent step. (7) is 'CMIDG for both ascent and descent step', in which CMIDG is applied to data in both steps. (8) is 'USAM + top k perturbation' based on (5) in which local perturbation is set to 50% up to sorted gradients and the global gradient mask is not used. (9) is our proposed sUSAM. Except (1), we use these modules only from the 300-th epoch to the 500-th epoch. For 'ASAM for 500 epochs', please refer to FedASAM in our experiment for SOTA comparison, in which extra modules are used in the same way as what is mentioned in the original paper. The ablation of perturbation radius hints that a moderate perturbation is better for the trade-off between generalization and stability. The conclusion for the strategies is basically same as discussed in our main paper.

Table S9 displays hyper-parameter ablation for sUSAM. The conclusion for the start epoch is basically same as what is discussed in our main paper. For the perturbation radius, USAM is sensitive to this hyper-parameter and 0.7 is the best suiting one for this experimental setting.

Supplementary Note 9: Generalization for different class division

Experiments in the main paper are based on one kind of setting for the class division. To prove that UFPS is universal under different class divisions, we conduct more experiments on the non-IID benchmark. As in our main paper, intersection between annotated classes is still null so the demand for labels is reduced to the lowest.

Setting 2. In setting 2, client 1 is only annotated for spleen, client 2 is only annotated for liver, and client 3 is annotated for kidney and pancreas. From Table S10, it can be seen that although the class division has changed, our proposed method is still solid for its universal design for the class division and strong generalization ability to different degrees of data heterogeneity.

Setting 3. In setting 3, client 1 is annotated for liver and pancreas, client 2 is only annotated for kidney, and client 3 is only annotated for spleen. Noise in this setting is the largest among three settings. From Table S11, it can be concluded that model performance is mainly affected by pancreas, which obviously is due to the domain gap. Even though the noise for pancreas is quite large, our method is capable of denoising this hard class for all clients by WS compared with other methods.

Supplementary Note 10: Privacy Analysis

Due to extra communication compared with FedAvg, i.e., the data package and teacher models, it is crucial to discuss the underlying privacy leakage. First of all, uncertainty values in the data package are merely two numbers, so the information revealed is negligible. Local masks in data packages leak no more privacy than the local model because of its generation process.

However, these pretrained teacher models are sent to all clients, which means either the server or other clients may leverage them to perform an attack, like membership inference attack¹². On account of the fact that local models are uploaded to the server for model aggregation, it makes little difference in the result of the server's attack whether teacher models are distributed or not. Besides, local models can reflect more information relevant to membership because its prediction is available considering all classes. Therefore, we only concentrate on the circumstance for MIA from client sides.

As we have mentioned in the experimental setting, we use a patch cropping strategy for training. It can drastically alleviate the risk of data leakage, as proven in¹³. Another factor influencing the vulnerability to MIA is data augmentation. To give an analysis, we start from the key assumption of MIA, that is, the target model suffers a large generalization gap between training and unseen datasets. Data in the training set of a teacher model are regarded as members while these in the validation set, testing set, and other clients' datasets are marked as 'not member'. Figure S5 demonstrates uncertainty for three teacher models with or without data augmentation. As can be seen, when data augmentation is added to train a teacher model, the overall uncertainty is reduced. Besides, no matter whether data augmentation is added, in our experimental setting, the overall shape of uncertainty distribution between membership and non-membership is approximate, which can be adverse for MIA. We owe the main reason to the patch cropping training strategy.

Attributed to the above difficulty for MIA, we assume that there is an honest but curious client who is able to get half of the training dataset from the target model to train the shadow model, and that all ground-truth labels are accessible as extra input to the attack model. Note that it is a rather strong assumption, which is hard to satisfy in practice. Here we only use it as a rough upper bound of the privacy risk for our method.

10.1. Experimental setup for MIA

For the shadow model, the training set is composed of half of the training dataset from the target model, 60% data with the lowest uncertainty in the 75% rest data from the global dataset union, and pseudo labels from the target (teacher) model. The testing set is composed of 40% data with the highest uncertainty in the 75% rest data from the global dataset union. Whether data augmentation is used identifies with the setting of the target model. The training loss is Dice and BCE and the metric is Dice and HD between predictions from the shadow model and pseudo labels from the target model.

For the attack model, the training set is composed of all data for the shadow model, predictions from the shadow model, ground-truth segmentation labels, and binary membership labels. Whether data augmentation is used identifies with the setting of the target model. The training loss is CE and metric is class-wise accuracy and F1 score. The testing set consists of another half of the training dataset from the target model, remaining 25% data from the global dataset union, predictions from the shadow model, and ground-truth segmentation labels.

10.2. Performance comparison between teacher models

The uncertainty comparison only reflects prediction distribution, so we supplement experiments on the performance for in-distribution and out-distribution datasets in Table S12, where DP is shorthand for differential privacy¹⁴ discussed in later analysis. It can be concluded that the domain gap for the global dataset union is extremely large but is significantly alleviated through abundant data augmentation. Besides, DP's protection comes with performance degradation.

10.3. MIA attack on teacher models

The imitation performance and attack performance under the strong attacking assumption are shown in Table S13. The stimulation performance of shadow models is in positive correlation with performance of teacher model except for client 2, which proves the reasonability of predictions from teacher models. Note that when data augmentation is not added to the teacher model from client 2, it completely fails to generalize on other clients. When segmentation results are meaningless, like fixed simple patterns, the mode is likely to be easier to imitate as a consequence.

As for the attack performance, when data augmentation is employed, the accuracy for class 1 is sharply reduced by 24.09, indicating the attacker cannot correctly distinguish these data in the training set from others and all clients get privacy protection considering this metric. However, the F1 score for class 1 increases by 5.93, meaning the attack model considers a bit more positive predictions into consideration. On the other hand, two metrics in the row 'Attack class mean' is elevated for 'Aug' and 'Aug + DP', suggesting the prediction for the background class is precise due to the better stimulation ability. When DP is used for privacy protection, metrics except for the accuracy of class 1 significantly decline. It demonstrates that with a slight increase in the accuracy of class 1 (1.07), the attack model is restricted in distinguishing both classes due to ambiguity of prediction distribution.

In conclusion, even under a strong assumption for the MIA attack, data augmentation is helpful to safeguard the membership privacy for these training data. With DP, the overall protection effect can be promoted for all data. Other methods, like knowledge distillation mentioned in ¹³, may also have a great impact and can be thoroughly analyzed in future studies.

Table S2. Complete comparison between SOTAs.

Method & Metric		Client index (the next line) & Organ index (after name of method)																				Mean
		1					2					3					4					
		1	2	3	4	mean	1	2	3	4	mean	1	2	3	4	mean	1	2	3	4	mean	
SOLO partial		1	2	3	4	mean	1	2	3	4	mean	1	2	3	4	mean	1	2	3	4	mean	
Dice		91.480	85.928	53.943	45.359	69.178	68.785	72.387	91.847	70.010	75.757	53.098	90.202	64.664	34.435	60.600	77.485	86.167	75.398	59.763	74.703	70.059
HD		0.803	1.219	1.229	0.852	1.026	3.204	6.348	1.050	1.530	3.033	2.113	1.745	1.270	1.352	1.620	1.575	2.282	1.129	1.116	1.526	1.801
JC		0.168	0.205	0.070	0.047	0.123	0.275	0.405	0.282	0.181	0.286	0.107	0.250	0.100	0.042	0.125	0.193	0.327	0.159	0.094	0.193	0.182
RVE		0.061	0.095	0.398	0.351	0.226	0.345	2.045	0.092	0.220	0.676	0.471	0.063	0.265	0.421	0.305	0.210	0.080	0.120	0.226	0.159	0.341
Sen		0.910	0.824	0.472	0.404	0.653	0.648	0.719	0.897	0.699	0.741	0.513	0.887	0.604	0.307	0.578	0.774	0.863	0.729	0.604	0.743	0.678
Spe		1.000	0.999	1.000	1.000	1.000	0.999	0.929	1.000	0.999	0.982	1.000	0.999	1.000	1.000	1.000	0.999	0.997	1.000	1.000	0.999	0.995
Centralized full		1	2	3	4	mean	1	2	3	4	mean	1	2	3	4	mean	1	2	3	4	mean	
Dice		87.979	83.599	70.348	73.130	78.764	94.994	95.440	91.348	71.520	88.325	88.422	89.558	72.715	66.019	79.179	88.684	89.583	77.146	67.706	80.780	
HD		0.825	2.238	0.684	0.678	1.106	1.681	2.733	1.055	1.428	1.724	1.211	2.314	0.838	0.958	1.330	1.383	2.286	1.011	0.985	1.416	1.394
JC		0.159	0.196	0.097	0.086	0.134	0.415	0.557	0.279	0.187	0.360	0.194	0.246	0.116	0.089	0.161	0.232	0.343	0.164	0.109	0.212	0.217
RVE		0.090	0.222	0.278	0.120	0.178	0.044	0.032	0.076	0.216	0.092	0.078	0.114	0.166	0.186	0.136	0.416	0.085	0.114	0.167	0.196	0.151
Sen		0.850	0.889	0.642	0.719	0.775	0.957	0.969	0.896	0.700	0.880	0.892	0.919	0.697	0.641	0.787	0.921	0.913	0.762	0.672	0.817	0.815
Spe		1.000	0.996	1.000	1.000	0.999	0.999	0.969	1.000	1.000	0.999	1.000	0.997	1.000	1.000	0.999	0.999	0.996	1.000	1.000	0.999	0.999
FedCRLD		1	2	3	4	mean	1	2	3	4	mean	1	2	3	4	mean	1	2	3	4	mean	
Dice		89.638	79.277	62.261	40.113	67.822	71.392	79.237	93.171	67.283	77.771	56.759	84.789	61.519	29.407	58.119	74.840	84.667	71.439	58.277	72.306	
HD		1.155	5.394	1.283	1.020	2.213	3.402	6.175	1.092	1.580	3.062	2.560	2.795	1.645	1.253	2.063	2.021	2.721	1.448	1.201	1.848	2.297
JC		0.162	0.182	0.084	0.042	0.118	0.284	0.441	0.288	0.172	0.296	0.111	0.228	0.095	0.035	0.117	0.181	0.317	0.149	0.091	0.185	0.179
RVE		0.090	0.302	0.287	0.344	0.256	0.340	1.634	0.067	0.268	0.577	0.345	0.182	0.345	0.520	0.348	0.188	0.088	0.166	0.242	0.171	0.338
Sen		0.893	0.852	0.575	0.359	0.670	0.681	0.784	0.933	0.688	0.772	0.529	0.874	0.589	0.259	0.563	0.746	0.846	0.700	0.596	0.722	0.682
Spe		1.000	0.995	1.000	1.000	0.999	0.998	0.945	1.000	0.999	0.986	0.999	0.995	1.000	1.000	0.999	0.999	0.999	0.996	1.000	0.999	0.995
DOD*		1	2	3	4	mean	1	2	3	4	mean	1	2	3	4	mean	1	2	3	4	mean	
Dice		86.762	83.903	54.178	22.977	61.955	79.231	89.113	92.128	66.570	81.760	51.877	89.853	64.434	36.129	60.573	73.214	85.997	69.744	53.529	70.621	
HD		0.996	1.328	1.454	0.829	1.152	3.117	4.607	1.117	1.534	2.594	2.005	1.789	1.673	1.315	1.695	1.916	2.423	1.437	1.142	1.729	1.857
JC		0.154	0.199	0.067	0.023	0.111	0.320	0.503	0.281	0.171	0.319	0.104	0.247	0.096	0.044	0.123	0.176	0.325	0.142	0.083	0.182	0.186
RVE		0.101	0.097	0.653	0.713	0.391	0.214	0.433	0.080	0.242	0.242	0.472	0.066	0.333	0.451	0.331	0.287	0.083	0.193	0.289	0.213	0.271
Sen		0.831	0.799	0.551	0.179	0.590	0.759	0.890	0.902	0.645	0.799	0.481	0.880	0.612	0.348	0.580	0.710	0.851	0.677	0.522	0.690	0.693
Spe		1.000	0.999	0.999	1.000	0.999	0.999	0.987	1.000	1.000	0.996	1.000	0.999	0.999	1.000	0.999	0.999	0.997	0.999	1.000	0.999	0.997
CPS*		1	2	3	4	mean	1	2	3	4	mean	1	2	3	4	mean	1	2	3	4	mean	
Dice		89.739	89.348	75.950	48.116	75.788	73.501	77.192	93.272	68.266	78.058	59.186	89.972	74.797	39.061	65.754	80.089	87.951	75.219	59.170	75.607	
HD		1.008	1.193	0.966	0.806	0.993	3.028	6.065	1.050	1.525	2.917	2.185	1.931	1.376	1.317	1.702	1.849	2.293	1.336	1.146	1.656	1.817
JC		0.163	0.217	0.060	0.051	0.134	0.302	0.437	0.288	0.176	0.301	0.122	0.249	0.117	0.048	0.134	0.200	0.335	0.158	0.092	0.196	0.191
RVE		0.068	0.055	0.174	0.293	0.147	0.290	2.112	0.089	0.221	0.678	0.411	0.098	0.246	0.391	0.287	0.270	0.075	0.153	0.197	0.174	0.322
Sen		0.884	0.883	0.698	0.432	0.724	0.702	0.779	0.933	0.677	0.773	0.578	0.901	0.711	0.359	0.637	0.820	0.891	0.734	0.595	0.760	0.724
Spe		1.000	0.999	1.000	1.000	0.999	0.999	0.927	1.000	0.999	0.981	0.999	0.997	1.000	1.000	0.999	0.999	0.999	0.996	1.000	0.999	0.995
MS-KD*		1	2	3	4	mean	1	2	3	4	mean	1	2	3	4	mean	1	2	3	4	mean	
Dice		89.920	88.511	71.978	46.995	74.351	72.861	75.769	90.539	66.100	76.317	55.820	89.298	69.066	39.118	63.326	77.914	86.683	71.644	56.173	73.104	
HD		0.899	1.282	1.020	0.813	1.004	2.978	6.159	1.209	1.585	2.983	2.088	1.880	1.360	1.336	1.666	1.777	2.332	1.323	1.132	1.641	1.824
JC		0.163	0.214	0.098	0.050	0.131	0.298	0.428	0.277	0.168	0.293	0.114	0.246	0.106	0.048	0.128	0.193	0.328	0.149	0.086	0.189	0.185
RVE		0.067	0.071	0.191	0.268	0.149	0.319	1.955	0.141	0.240	0.664	0.462	0.094	0.239	0.396	0.298	0.210	0.081	0.145	0.236	0.168	0.320
Sen		0.895	0.860	0.656	0.442	0.713	0.690	0.748	0.903	0.665	0.752	0.543	0.877	0.645	0.374	0.610	0.783	0.858	0.698	0.580	0.730	0.701
Spe		1.000	0.999	1.000	1.000	0.999	0.999	0.932	0.999	0.999	0.983	1.000	0.998	1.000	1.000	0.999	0.999	0.997	0.997	1.000	0.999	0.995
FedAvg*		1	2	3	4	mean	1	2	3	4	mean	1	2	3	4	mean	1	2	3	4	mean	
Dice		90.114	84.690	72.959	51.983	74.937	72.890	79.384	93.662	66.448	78.096	59.062	88.036	68.126	42.890	64.528	79.517	87.911	75.399	56.123	74.738	
HD		0.857	2.593	0.810	0.910	1.292	2.770	6.033	0.993	1.527	2.831	1.869	2.590	1.552	1.310	1.830	1.730	2.548	1.921	1.206	1.694	1.912
JC		0.164	0.200	0.101	0.056	0.130	0.296	0.449	0.290	0.169	0.301	0.119	0.239	0.107	0.054	0.130	0.197	0.333	0.158	0.086	0.194	0.189
RVE		0.065	0.176	0.223	0.196	0.165	0.310	2.211	0.063	0.240	0.706	0.409	0.221	0.343	0.348	0.330	0.249	0.093	0.125	0.210	0.169	0.343
Sen		0.897	0.892	0.677	0.485	0.738	0.692	0.803	0.926	0.645	0.766	0.571	0.920	0.640	0.402	0.633	0.807	0.904	0.734	0.561	0.752	0.722
Spe		1.000	0.997	1.000	1.000	0.999	0.999	0.925	1.000	0.999	0.981	1.000	0.994	0.999	1.000	0.998	0.999	0.995	1.000	1.000	0.998	0.994
FedProx*		1	2	3	4	mean	1	2	3	4	mean	1	2	3	4	mean	1	2	3	4	mean	
Dice		89.394	83.151	73.447	51.684	74.419	70.491	76.653	94.049	68.145	77.334	55.708	88.826	72.188	41.519	64.560	79.392	86.664	76.453	59.897	75.601	
HD		0.915	2.924	0.917	0.816	1.393	2.880	6.108	1.051	1.509	2.887	1.906	2.284	1.663	1.183	1.759	1.699	2.416	1.327	1.151	1.648	1.922
JC		0.162	0.194	0.101	0.056	0.128	0.285	0.433	0.291	0.175	0.296	0.113	0.243	0.112	0.052	0.130	0.198	0.328	0.161	0.094	0.195	0.187
RVE		0.076	0.233	0.220	0.247	0.194	0.363	2.060	0.057	0.239	0.680	0.459	0.148	0.276	0.378	0.315	0.228	0.075	0.129	0.214	0.162	0.338
Sen		0.876	0.885	0.673	0																	

Table S4. Ablation study on aRCE loss.

Strategy & Metric	Client index (the next line) & Organ index (after name of method)																				Mean
	1					2					3					4					
Fixed	1	2	3	4	mean	1	2	3	4	mean	1	2	3	4	mean	1	2	3	4	mean	
Dice	89.303	87.873	73.221	50.823	75.305	71.233	74.049	91.461	66.335	75.769	59.378	88.175	66.823	42.846	64.306	80.671	85.775	74.408	59.726	75.145	72.631
HD	0.998	1.610	0.874	0.782	1.066	2.928	6.232	1.001	1.556	2.929	2.082	2.217	1.272	1.190	1.690	1.714	2.413	1.196	1.161	1.621	1.827
JC	0.162	0.211	0.100	0.054	0.132	0.289	0.416	0.281	0.169	0.289	0.120	0.241	0.104	0.054	0.130	0.202	0.324	0.157	0.093	0.194	0.186
RVE	0.090	0.075	0.224	0.257	0.161	0.396	1.999	0.118	0.265	0.694	0.404	0.148	0.266	0.360	0.294	0.242	0.082	0.130	0.198	0.163	0.328
Sen	0.887	0.878	0.666	0.470	0.725	0.670	0.732	0.888	0.642	0.733	0.575	0.884	0.620	0.403	0.620	0.816	0.857	0.714	0.613	0.750	0.707
Spe	1.000	0.998	1.000	1.000	0.999	0.999	0.930	1.000	1.000	0.982	0.999	0.996	1.000	1.000	0.999	0.999	0.996	1.000	1.000	0.999	0.995
Increasing	1	2	3	4	mean	1	2	3	4	mean	1	2	3	4	mean	1	2	3	4	mean	
Dice	90.001	84.213	75.411	52.485	75.527	73.361	78.513	93.009	65.937	77.705	59.755	87.164	69.408	45.136	65.366	80.774	87.242	73.534	57.458	74.752	73.338
HD	0.893	2.347	0.786	0.895	1.230	2.839	6.107	0.994	1.559	2.875	1.974	2.504	1.400	1.261	1.785	1.782	2.536	1.330	1.224	1.718	1.902
JC	0.164	0.200	0.104	0.057	0.131	0.299	0.443	0.287	0.168	0.299	0.122	0.238	0.109	0.057	0.131	0.202	0.330	0.154	0.089	0.194	0.189
RVE	0.070	0.146	0.201	0.194	0.153	0.291	2.238	0.076	0.238	0.711	0.395	0.193	0.277	0.311	0.294	0.286	0.088	0.154	0.205	0.183	0.335
Sen	0.898	0.874	0.691	0.494	0.739	0.697	0.791	0.910	0.642	0.760	0.580	0.904	0.652	0.428	0.641	0.822	0.889	0.709	0.586	0.752	0.723
Spe	1.000	0.997	1.000	1.000	0.999	0.999	0.924	1.000	0.999	0.981	1.000	0.995	1.000	1.000	0.998	0.999	0.995	1.000	1.000	0.998	0.994
Coefficient & Metric	Client index (the next line) & Organ index (after name of method)																				Mean
	1					2					3					4					
0.1	1	2	3	4	mean	1	2	3	4	mean	1	2	3	4	mean	1	2	3	4	mean	
Dice	88.956	87.513	73.106	47.670	74.311	70.003	77.757	91.819	64.715	76.074	55.920	88.767	73.197	36.014	63.474	79.886	87.630	75.264	57.077	74.964	72.206
HD	0.925	2.081	0.912	0.757	1.169	2.885	6.096	1.054	1.549	2.896	1.946	2.575	1.737	1.114	1.843	1.724	2.447	1.334	1.118	1.656	1.891
JC	0.161	0.210	0.100	0.051	0.130	0.282	0.438	0.282	0.164	0.292	0.113	0.243	0.114	0.044	0.128	0.200	0.332	0.157	0.088	0.194	0.186
RVE	0.076	0.093	0.223	0.360	0.188	0.376	2.047	0.093	0.290	0.702	0.452	0.153	0.331	0.460	0.349	0.237	0.082	0.159	0.226	0.176	0.354
Sen	0.872	0.890	0.660	0.421	0.711	0.649	0.777	0.891	0.617	0.733	0.533	0.903	0.683	0.318	0.609	0.796	0.886	0.719	0.557	0.739	0.698
Spe	1.000	0.998	1.000	1.000	0.999	0.999	0.929	1.000	1.000	0.982	1.000	0.996	0.999	1.000	0.999	0.999	0.996	1.000	1.000	0.999	0.995
0.01	1	2	3	4	mean	1	2	3	4	mean	1	2	3	4	mean	1	2	3	4	mean	
Dice	90.001	84.213	75.411	52.485	75.527	73.361	78.513	93.009	65.937	77.705	59.755	87.164	69.408	45.136	65.366	80.774	87.242	73.534	57.458	74.752	73.338
HD	0.893	2.347	0.786	0.895	1.230	2.839	6.107	0.994	1.559	2.875	1.974	2.504	1.400	1.261	1.785	1.782	2.536	1.330	1.224	1.718	1.902
JC	0.164	0.200	0.104	0.057	0.131	0.299	0.443	0.287	0.168	0.299	0.122	0.238	0.109	0.057	0.131	0.202	0.330	0.154	0.089	0.194	0.189
RVE	0.070	0.146	0.201	0.194	0.153	0.291	2.238	0.076	0.238	0.711	0.395	0.193	0.277	0.311	0.294	0.286	0.088	0.154	0.205	0.183	0.335
Sen	0.898	0.874	0.691	0.494	0.739	0.697	0.791	0.910	0.642	0.760	0.580	0.904	0.652	0.428	0.641	0.822	0.889	0.709	0.586	0.752	0.723
Spe	1.000	0.997	1.000	1.000	0.999	0.999	0.924	1.000	0.999	0.981	1.000	0.995	1.000	1.000	0.998	0.999	0.995	1.000	1.000	0.998	0.994
0.001	1	2	3	4	mean	1	2	3	4	mean	1	2	3	4	mean	1	2	3	4	mean	
Dice	89.363	86.046	75.599	50.741	75.437	71.975	74.055	91.625	66.485	76.035	60.252	87.589	69.150	41.460	64.613	80.935	85.855	75.241	60.220	75.563	72.912
HD	0.985	1.913	0.917	0.810	1.157	2.996	6.236	1.035	1.554	2.955	2.038	2.228	1.369	1.245	1.720	1.775	2.398	1.279	1.163	1.654	1.872
JC	0.162	0.205	0.105	0.054	0.132	0.293	0.416	0.281	0.170	0.290	0.122	0.239	0.107	0.052	0.130	0.202	0.324	0.159	0.094	0.195	0.187
RVE	0.077	0.117	0.182	0.249	0.157	0.352	2.030	0.108	0.248	0.685	0.402	0.149	0.259	0.367	0.294	0.260	0.078	0.114	0.207	0.165	0.325
Sen	0.891	0.877	0.700	0.466	0.734	0.683	0.732	0.893	0.651	0.740	0.584	0.881	0.644	0.391	0.625	0.820	0.855	0.731	0.617	0.756	0.714
Spe	1.000	0.998	1.000	1.000	0.999	0.999	0.930	1.000	0.999	0.982	0.999	0.996	1.000	1.000	0.999	0.999	0.997	1.000	1.000	0.999	0.995

Organ indexes are numbers on the straight right side of the name of method.

Model performance is better when metrics are higher, except for HD and RVE.

Table S5. Ablation study on weight scheduler.

Client index (the next line) & Organ index (after name of method)																					
Strategy & Metric	1				2				3				4				Mean				
	1	2	3	4	mean	1	2	3	4	mean	1	2	3	4	mean	1		2	3	4	
TS	1	2	3	4	mean	1	2	3	4	mean	1	2	3	4	mean	1	2	3	4	mean	
Dice	90.162	87.442	76.888	49.430	75.980	72.955	76.875	94.070	69.066	78.242	58.440	89.017	75.613	42.264	66.334	80.019	86.902	76.442	62.072	76.359	74.229
HD	0.936	2.275	2.318	0.817	1.587	2.889	6.066	0.989	1.526	2.867	2.111	2.070	1.629	1.175	1.746	1.768	2.366	1.389	1.107	1.658	1.965
JC	0.164	0.210	0.106	0.053	0.133	0.298	0.433	0.292	0.177	0.300	0.119	0.245	0.118	0.053	0.134	0.200	0.329	0.161	0.098	0.197	0.191
RVE	0.069	0.084	0.156	0.288	0.149	0.320	1.990	0.053	0.231	0.649	0.431	0.103	0.251	0.390	0.294	0.270	0.079	0.133	0.175	0.164	0.314
Sen	0.903	0.877	0.725	0.451	0.739	0.694	0.767	0.937	0.685	0.771	0.566	0.891	0.719	0.397	0.643	0.817	0.871	0.753	0.635	0.769	0.731
Spe	1.000	0.998	1.000	1.000	0.999	0.999	0.932	1.000	0.999	0.997	1.000	0.997	0.999	1.000	0.999	0.999	0.997	1.000	1.000	0.999	0.995
BD	1	2	3	4	mean	1	2	3	4	mean	1	2	3	4	mean	1	2	3	4	mean	
Dice	90.054	85.203	73.070	52.624	75.238	73.605	79.252	93.431	67.569	78.464	58.398	87.818	72.080	45.090	65.846	79.404	87.661	75.007	58.221	75.073	73.655
HD	0.884	2.983	1.917	0.901	1.671	2.827	6.017	1.026	1.545	2.854	1.954	2.450	1.491	1.283	1.794	1.755	2.464	1.423	1.205	1.712	2.008
JC	0.164	0.203	0.099	0.057	0.131	0.301	0.447	0.289	0.173	0.302	0.119	0.240	0.113	0.057	0.132	0.198	0.332	0.157	0.090	0.194	0.190
RVE	0.069	0.118	0.207	0.194	0.147	0.295	2.220	0.072	0.244	0.708	0.426	0.173	0.279	0.343	0.305	0.282	0.081	0.135	0.223	0.180	0.335
Sen	0.898	0.871	0.676	0.499	0.736	0.702	0.803	0.923	0.671	0.775	0.563	0.904	0.689	0.426	0.646	0.809	0.894	0.733	0.600	0.759	0.729
Spe	1.000	0.998	1.000	1.000	0.999	0.999	0.925	1.000	0.999	0.981	1.000	0.995	1.000	1.000	0.998	0.999	0.996	1.000	1.000	0.998	0.994
RG	1	2	3	4	mean	1	2	3	4	mean	1	2	3	4	mean	1	2	3	4	mean	
Dice	89.983	83.416	74.119	54.278	75.449	73.284	77.649	94.167	67.751	78.213	59.423	87.513	70.165	45.833	65.734	80.209	87.297	74.953	58.421	75.220	73.654
HD	0.944	3.106	2.341	0.971	1.840	2.872	6.073	1.071	1.555	2.893	1.995	2.415	1.944	1.309	1.916	1.742	2.485	1.513	1.220	1.740	2.097
JC	0.164	0.198	0.101	0.059	0.130	0.300	0.438	0.292	0.173	0.301	0.121	0.239	0.108	0.058	0.131	0.200	0.331	0.157	0.090	0.195	0.189
RVE	0.083	0.111	0.250	0.194	0.159	0.293	2.209	0.069	0.244	0.704	0.414	0.177	0.387	0.339	0.329	0.290	0.078	0.211	0.236	0.204	0.349
Sen	0.904	0.849	0.717	0.519	0.747	0.702	0.780	0.943	0.682	0.777	0.577	0.895	0.683	0.441	0.649	0.823	0.881	0.752	0.606	0.765	0.735
Spe	1.000	0.998	0.999	1.000	0.999	0.999	0.925	1.000	0.999	0.981	1.000	0.995	0.999	1.000	0.998	0.999	0.996	0.999	0.999	0.998	0.994
Client index (the next line) & Organ index (after name of method)																					
Final epoch & Metric	1				2				3				4				Mean				
	1	2	3	4	mean	1	2	3	4	mean	1	2	3	4	mean	1		2	3	4	
150	1	2	3	4	mean	1	2	3	4	mean	1	2	3	4	mean	1	2	3	4	mean	
Dice	89.037	83.958	74.620	51.831	74.861	71.923	74.138	92.544	66.905	76.378	62.249	87.084	71.308	42.420	65.765	81.640	85.712	74.988	60.166	75.626	73.158
HD	1.204	3.000	2.408	0.817	1.857	2.960	6.235	1.072	1.553	2.955	2.133	2.189	1.629	1.244	1.799	1.697	2.361	1.408	1.158	1.656	2.067
JC	0.161	0.197	0.102	0.056	0.129	0.292	0.417	0.285	0.171	0.291	0.125	0.238	0.110	0.053	0.132	0.204	0.323	0.158	0.094	0.195	0.187
RVE	0.108	0.157	0.188	0.230	0.171	0.392	1.982	0.089	0.247	0.677	0.369	0.131	0.254	0.391	0.286	0.245	0.084	0.154	0.219	0.175	0.327
Sen	0.892	0.866	0.698	0.484	0.735	0.679	0.729	0.914	0.666	0.747	0.601	0.865	0.674	0.403	0.636	0.827	0.849	0.737	0.623	0.759	0.719
Spe	1.000	0.997	1.000	1.000	0.999	0.999	0.931	1.000	0.999	0.982	0.999	0.997	1.000	1.000	0.999	0.999	0.997	1.000	1.000	0.999	0.995
200	1	2	3	4	mean	1	2	3	4	mean	1	2	3	4	mean	1	2	3	4	mean	
Dice	90.162	87.442	76.888	49.430	75.980	72.955	76.875	94.070	69.066	78.242	58.440	89.017	75.613	42.264	66.334	80.019	86.902	76.442	62.072	76.359	74.229
HD	0.936	2.275	2.318	0.817	1.587	2.889	6.066	0.989	1.526	2.867	2.111	2.070	1.629	1.175	1.746	1.768	2.366	1.389	1.107	1.658	1.965
JC	0.164	0.210	0.106	0.053	0.133	0.298	0.433	0.292	0.177	0.300	0.119	0.245	0.118	0.053	0.134	0.200	0.329	0.161	0.098	0.197	0.191
RVE	0.069	0.084	0.156	0.288	0.149	0.320	1.990	0.053	0.231	0.649	0.431	0.103	0.251	0.390	0.294	0.270	0.079	0.133	0.175	0.164	0.314
Sen	0.903	0.877	0.725	0.451	0.739	0.694	0.767	0.937	0.685	0.771	0.566	0.891	0.719	0.397	0.643	0.817	0.871	0.753	0.635	0.769	0.731
Spe	1.000	0.998	1.000	1.000	0.999	0.999	0.932	1.000	0.999	0.983	1.000	0.997	0.999	1.000	0.999	0.999	0.997	1.000	1.000	0.999	0.995
250	1	2	3	4	mean	1	2	3	4	mean	1	2	3	4	mean	1	2	3	4	mean	
Dice	90.046	83.004	77.278	52.935	75.816	72.447	79.672	93.434	67.472	78.256	58.184	86.879	74.119	46.158	66.335	79.815	87.472	77.062	58.387	75.684	74.023
HD	0.905	2.335	1.494	0.945	1.420	2.858	6.040	1.101	1.562	2.890	1.908	2.517	1.866	1.315	1.902	1.724	2.545	1.511	1.231	1.753	1.991
JC	0.164	0.196	0.105	0.057	0.130	0.296	0.450	0.288	0.172	0.302	0.118	0.237	0.115	0.058	0.132	0.199	0.331	0.160	0.090	0.195	0.190
RVE	0.070	0.133	0.203	0.197	0.151	0.342	2.268	0.066	0.251	0.732	0.427	0.182	0.392	0.337	0.334	0.263	0.086	0.215	0.246	0.202	0.355
Sen	0.896	0.854	0.722	0.510	0.746	0.691	0.807	0.928	0.679	0.776	0.561	0.896	0.705	0.448	0.653	0.813	0.886	0.753	0.610	0.766	0.735
Spe	1.000	0.997	1.000	1.000	0.999	0.999	0.923	1.000	0.999	0.980	1.000	0.995	0.999	1.000	0.998	0.999	0.995	0.999	0.999	0.998	0.994
Client index (the next line) & Organ index (after name of method)																					
U _r & Metric	1				2				3				4				Mean				
	1	2	3	4	mean	1	2	3	4	mean	1	2	3	4	mean	1		2	3	4	
0.6	1	2	3	4	mean	1	2	3	4	mean	1	2	3	4	mean	1	2	3	4	mean	
Dice	90.087	86.578	75.214	48.588	75.117	72.938	77.279	91.823	68.181	77.555	58.373	89.477	72.041	41.848	65.435	80.097	86.761	76.434	62.076	76.342	73.612
HD	0.976	2.313	1.540	0.756	1.396	2.916	6.124	1.070	1.525	2.908	2.193	2.227	1.394	1.153	1.742	1.814	2.397	1.218	1.104	1.633	1.920
JC	0.164	0.207	0.104	0.051	0.131	0.298	0.435	0.281	0.175	0.297	0.119	0.246	0.111	0.052	0.132	0.201	0.328	0.161	0.098	0.197	0.189
RVE	0.067	0.113	0.176	0.330	0.172	0.313	2.030	0.095	0.240	0.670	0.429	0.126	0.226	0.395	0.294	0.269	0.083	0.121	0.201	0.168	0.326
Sen	0.899	0.883	0.702	0.432	0.729	0.695	0.774	0.896	0.666	0.758	0.568	0.900	0.673	0.386	0.632	0.823	0.874	0.741	0.629	0.767	0.722
Spe	1.000	0.998	1.000	1.000	0.999	0.999	0.930	1.000	1.000	0.982	1.000	0.997	1.000	1.000	0.999	0.999	0.996	1.000	1.000	0.999	0.995
0.7	1	2	3	4	mean	1	2	3	4	mean	1	2	3	4	mean	1	2	3	4	mean	
Dice	90.162	87.442	76.888	49.430	75.980	72.955	76.875	94.070	69.066	78.242	58.440	89.017	75.613	42.264	66.334	80.019	86.902	76.442	62.072	76.359	74.229
HD	0.936	2.275	2.318	0.817	1.587	2.889	6.066	0.989	1.526	2.867	2.111	2.070	1.629	1.175	1.746	1.768	2.366	1.389	1.107	1.658	1.965
JC	0.164	0.210	0.106	0.053	0.133	0.298	0.433	0.292	0.177	0.300	0.119	0.245	0.118	0.053	0.134	0.200	0.329	0.161	0.098	0.197	0.191
RVE	0.069	0.084	0.156	0.288	0.149	0.320	1.990	0.053	0.231	0.649	0.431	0.103	0.251	0.390	0.294	0.270	0.079	0.133	0.175	0.164	0.314
Sen	0.903	0.877	0.725																		

Table S6. Ablation study on uncertainty-based aggregation.

Part & Metric		Client index (the next line) & Organ index (after name of method)																				Mean
		1					2					3					4					
Whole		1	2	3	4	mean	1	2	3	4	mean	1	2	3	4	mean	1	2	3	4	mean	
Dice		89.152	87.143	72.443	55.928	76.167	72.077	80.032	92.170	68.436	78.179	55.467	88.943	68.425	44.227	64.266	78.831	86.120	75.791	60.651	75.348	73.490
HD		1.019	2.313	1.171	0.927	1.357	2.959	6.003	1.079	1.642	2.921	1.933	2.425	1.845	1.370	1.893	1.734	2.569	1.306	1.260	1.717	1.972
JC		0.162	0.209	0.100	0.060	0.133	0.294	0.451	0.284	0.174	0.301	0.113	0.244	0.107	0.055	0.130	0.196	0.325	0.159	0.094	0.194	0.190
RVE		0.095	0.147	0.203	0.206	0.163	0.335	2.010	0.085	0.299	0.682	0.459	0.142	0.323	0.342	0.317	0.242	0.087	0.135	0.260	0.181	0.336
Sen		0.875	0.886	0.668	0.550	0.745	0.680	0.802	0.911	0.732	0.781	0.533	0.912	0.655	0.448	0.637	0.788	0.877	0.741	0.648	0.764	0.732
Spe		1.000	0.997	1.000	1.000	0.999	0.999	0.932	1.000	0.999	0.983	1.000	0.996	0.999	1.000	0.999	0.999	0.995	1.000	0.999	0.998	0.995
Decoder		1	2	3	4	mean	1	2	3	4	mean	1	2	3	4	mean	1	2	3	4	mean	
Dice		89.189	87.566	74.843	55.024	76.655	71.651	79.422	92.767	68.377	78.054	55.613	88.663	71.228	43.742	64.812	78.643	85.612	76.312	60.216	75.196	73.679
HD		0.988	2.413	1.342	0.849	1.398	2.940	6.004	1.133	1.629	2.927	1.973	2.468	1.906	1.249	1.899	1.750	2.574	1.356	1.226	1.726	1.988
JC		0.162	0.211	0.103	0.059	0.134	0.290	0.448	0.285	0.174	0.300	0.114	0.243	0.111	0.054	0.130	0.196	0.323	0.161	0.093	0.193	0.189
RVE		0.101	0.112	0.170	0.199	0.145	0.339	1.971	0.080	0.301	0.673	0.458	0.118	0.323	0.368	0.317	0.275	0.083	0.137	0.260	0.189	0.331
Sen		0.872	0.884	0.706	0.529	0.748	0.673	0.796	0.926	0.729	0.781	0.535	0.900	0.679	0.438	0.638	0.787	0.867	0.752	0.640	0.761	0.732
Spe		1.000	0.998	1.000	1.000	0.999	0.999	0.933	1.000	0.999	0.983	1.000	0.997	0.999	1.000	0.999	0.999	0.996	1.000	0.999	0.999	0.995
Encoder		1	2	3	4	mean	1	2	3	4	mean	1	2	3	4	mean	1	2	3	4	mean	
Dice		89.160	86.205	73.917	56.563	76.461	71.797	77.977	92.006	68.408	77.547	54.908	88.393	70.014	44.558	64.468	78.398	86.128	75.169	60.078	74.943	73.355
HD		0.988	2.688	0.829	0.966	1.368	2.876	6.055	1.053	1.626	2.903	1.993	2.466	1.514	1.278	1.813	1.791	2.597	1.357	1.288	1.758	1.961
JC		0.162	0.205	0.102	0.061	0.132	0.292	0.439	0.283	0.174	0.297	0.112	0.241	0.110	0.056	0.130	0.195	0.325	0.158	0.093	0.193	0.188
RVE		0.092	0.177	0.197	0.211	0.169	0.331	1.993	0.095	0.303	0.681	0.468	0.144	0.298	0.353	0.316	0.277	0.087	0.153	0.246	0.191	0.339
Sen		0.878	0.887	0.679	0.551	0.749	0.678	0.784	0.907	0.730	0.775	0.531	0.905	0.666	0.447	0.637	0.787	0.874	0.737	0.641	0.760	0.730
Spe		1.000	0.997	1.000	1.000	0.999	0.999	0.932	1.000	0.999	0.983	1.000	0.997	1.000	1.000	0.999	0.999	0.996	1.000	0.999	0.998	0.995

Organ indexes are numbers on the straight right side of the name of method.

Model performance is better when metrics are higher, except for HD and RVE.

Table S7. Ablation study on global main teacher.

Strategy & Metric		Client index (the next line) & Organ index (after name of method)																				Mean
		1					2					3					4					
Pretrained		1	2	3	4	mean	1	2	3	4	mean	1	2	3	4	mean	1	2	3	4	mean	
Dice		90.114	84.690	72.959	51.983	74.937	72.890	79.384	93.662	66.448	78.096	59.062	88.036	68.126	42.890	64.528	79.517	87.911	75.399	56.123	74.738	73.075
HD		0.857	2.593	0.810	0.910	1.292	2.770	6.033	0.993	1.527	2.831	1.869	2.590	1.552	1.310	1.830	1.730	2.548	1.291	1.206	1.694	1.912
JC		0.164	0.200	0.101	0.056	0.130	0.296	0.449	0.290	0.169	0.301	0.119	0.239	0.107	0.054	0.130	0.197	0.333	0.158	0.086	0.194	0.189
RVE		0.065	0.176	0.223	0.196	0.165	0.310	2.211	0.063	0.240	0.706	0.409	0.221	0.343	0.348	0.330	0.249	0.093	0.125	0.210	0.169	0.343
Sen		0.897	0.892	0.677	0.485	0.738	0.692	0.803	0.926	0.645	0.766	0.571	0.920	0.640	0.402	0.633	0.807	0.904	0.734	0.561	0.752	0.722
Spe		1.000	0.997	1.000	1.000	0.999	0.999	0.925	1.000	0.999	0.981	1.000	0.994	0.999	1.000	0.998	0.999	0.995	1.000	1.000	0.998	0.994
Global		1	2	3	4	mean	1	2	3	4	mean	1	2	3	4	mean	1	2	3	4	mean	
Dice		85.067	82.719	76.878	53.277	74.485	69.884	79.873	92.888	66.808	77.363	67.640	88.265	73.222	47.373	69.125	81.954	85.995	75.902	59.939	75.947	74.230
HD		2.812	6.117	2.720	1.854	3.376	2.858	6.063	1.290	1.598	2.952	3.772	3.205	2.803	2.008	2.947	2.755	2.984	1.914	1.686	2.335	2.903
JC		0.151	0.193	0.107	0.057	0.127	0.273	0.447	0.285	0.170	0.294	0.134	0.240	0.113	0.059	0.136	0.204	0.323	0.159	0.093	0.195	0.188
RVE		0.321	0.234	0.753	0.435	0.436	0.394	1.598	0.072	0.298	0.591	0.229	0.165	0.614	0.478	0.371	0.414	0.082	0.248	0.248	0.248	0.412
Sen		0.847	0.878	0.766	0.522	0.753	0.634	0.787	0.934	0.642	0.749	0.673	0.912	0.735	0.507	0.707	0.841	0.865	0.774	0.622	0.776	0.746
Spe		0.999	0.996	0.998	0.999	0.998	0.999	0.945	1.000	0.999	0.986	0.998	0.995	0.998	0.999	0.998	0.998	0.996	0.999	0.999	0.998	0.995
Intersection		1	2	3	4	mean	1	2	3	4	mean	1	2	3	4	mean	1	2	3	4	mean	
Dice		89.913	87.246	75.142	58.777	77.770	71.843	77.264	93.326	67.922	77.589	59.374	87.560	68.836	46.827	65.649	80.884	86.757	74.798	61.954	76.098	74.277
HD		0.923	1.928	0.900	1.001	1.188	2.771	6.104	1.003	1.546	2.856	2.123	2.729	1.629	1.379	1.965	1.805	2.536	1.338	1.274	1.738	1.937
JC		0.163	0.209	0.104	0.064	0.135	0.291	0.436	0.288	0.174	0.298	0.121	0.238	0.107	0.059	0.131	0.203	0.328	0.158	0.097	0.196	0.190
RVE		0.068	0.095	0.185	0.191	0.135	0.341	2.054	0.072	0.251	0.680	0.418	0.206	0.259	0.347	0.308	0.262	0.082	0.132	0.216	0.173	0.324
Sen		0.900	0.885	0.698	0.566	0.762	0.674	0.773	0.921	0.675	0.761	0.573	0.901	0.652	0.462	0.647	0.825	0.876	0.731	0.649	0.770	0.735
Spe		1.000	0.998	1.000	1.000	0.999	0.999	0.929	1.000	0.999	0.982	1.000	0.995	1.000	1.000	0.998	0.999	0.996	1.000	1.000	0.999	0.995

Organ indexes are numbers on the straight right side of the name of method.

Model performance is better when metrics are higher, except for HD and RVE.

Table S8. Complete result for strategies of sUSAM.

Strategy & Metric	Client index (the next line) & Organ index (after name of method)																				Mean
	1					2					3					4					
(1)	1	2	3	4	mean	1	2	3	4	mean	1	2	3	4	mean	1	2	3	4	mean	
Dice	89.056	87.866	78.359	48.093	75.844	83.081	79.221	90.457	57.690	77.612	68.886	88.081	69.481	38.603	66.263	85.400	87.724	74.219	55.043	75.597	73.829
HD	1.085	1.561	0.794	0.718	1.039	2.408	6.069	1.098	1.632	2.801	2.019	2.631	1.401	1.127	1.795	1.857	2.932	1.321	1.174	1.821	1.864
JC	0.161	0.212	0.110	0.052	0.134	0.340	0.447	0.275	0.143	0.301	0.140	0.239	0.106	0.047	0.133	0.216	0.330	0.155	0.084	0.196	0.191
RVE	0.073	0.068	0.124	0.360	0.156	0.280	2.057	0.095	0.343	0.694	0.307	0.146	0.254	0.374	0.270	0.226	0.098	0.157	0.264	0.186	0.327
Sen	0.887	0.881	0.759	0.430	0.739	0.787	0.802	0.884	0.525	0.750	0.670	0.902	0.656	0.360	0.647	0.861	0.907	0.721	0.516	0.751	0.722
Spe	1.000	0.998	1.000	1.000	0.999	1.000	0.929	1.000	1.000	0.982	0.999	0.996	1.000	1.000	0.999	0.999	0.995	1.000	1.000	0.998	0.995
(2)	1	2	3	4	mean	1	2	3	4	mean	1	2	3	4	mean	1	2	3	4	mean	
Dice	88.112	85.961	76.718	52.858	75.912	78.615	76.530	89.125	60.981	76.313	67.829	85.355	69.328	41.341	65.963	83.853	86.615	72.927	57.625	75.255	73.361
HD	1.357	1.553	1.117	0.801	1.207	2.581	6.415	1.259	1.607	2.965	2.231	3.059	1.951	1.231	2.118	1.942	3.231	1.596	1.170	1.985	2.069
JC	0.159	0.205	0.107	0.057	0.132	0.316	0.430	0.269	0.152	0.292	0.136	0.231	0.106	0.051	0.131	0.210	0.326	0.151	0.089	0.194	0.187
RVE	0.097	0.087	0.231	0.194	0.152	0.329	2.096	0.107	0.307	0.710	0.300	0.146	0.338	0.325	0.277	0.191	0.080	0.180	0.200	0.162	0.325
Sen	0.866	0.838	0.757	0.495	0.739	0.725	0.753	0.882	0.572	0.733	0.643	0.843	0.672	0.399	0.639	0.826	0.866	0.719	0.561	0.743	0.714
Spe	0.999	0.999	1.000	1.000	0.999	1.000	0.927	0.999	1.000	0.982	0.999	0.996	0.999	1.000	0.999	0.999	0.996	0.999	1.000	0.999	0.995
(3)	1	2	3	4	mean	1	2	3	4	mean	1	2	3	4	mean	1	2	3	4	mean	
Dice	89.315	84.561	75.661	50.342	74.970	71.804	76.503	93.050	66.334	76.923	58.716	87.325	70.761	41.486	64.572	81.227	85.450	74.157	59.398	75.058	72.881
HD	0.941	2.400	0.917	0.778	1.259	2.791	6.141	1.040	1.558	2.883	1.896	2.523	1.548	1.170	1.784	1.661	2.438	1.320	1.157	1.644	1.893
JC	0.162	0.200	0.105	0.054	0.130	0.290	0.432	0.287	0.169	0.295	0.119	0.237	0.109	0.051	0.129	0.204	0.322	0.156	0.093	0.193	0.187
RVE	0.070	0.127	0.176	0.272	0.161	0.349	2.033	0.074	0.252	0.677	0.420	0.159	0.274	0.368	0.305	0.227	0.080	0.165	0.203	0.169	0.328
Sen	0.879	0.865	0.711	0.458	0.728	0.669	0.757	0.923	0.653	0.751	0.559	0.877	0.678	0.393	0.627	0.813	0.853	0.734	0.605	0.751	0.714
Spe	1.000	0.998	1.000	1.000	0.999	1.000	0.930	1.000	0.999	0.982	1.000	0.996	1.000	1.000	0.999	0.999	0.996	1.000	1.000	0.999	0.995
(4)	1	2	3	4	mean	1	2	3	4	mean	1	2	3	4	mean	1	2	3	4	mean	
Dice	89.898	85.934	73.955	51.902	75.422	72.841	78.147	92.656	66.228	77.468	59.050	88.062	68.214	43.595	64.730	79.909	87.912	75.289	56.800	74.978	73.150
HD	0.886	2.052	0.793	0.891	1.155	2.840	6.088	1.001	1.541	2.868	1.969	2.508	1.400	1.315	1.798	1.763	2.508	1.233	1.225	1.682	1.876
JC	0.164	0.205	0.107	0.056	0.132	0.296	0.441	0.286	0.169	0.298	0.120	0.240	0.107	0.055	0.130	0.200	0.333	0.158	0.088	0.195	0.189
RVE	0.066	0.128	0.214	0.204	0.153	0.306	2.188	0.076	0.229	0.700	0.406	0.205	0.280	0.322	0.303	0.283	0.087	0.135	0.214	0.180	0.334
Sen	0.890	0.893	0.675	0.484	0.735	0.688	0.788	0.909	0.642	0.757	0.571	0.915	0.639	0.406	0.633	0.808	0.901	0.729	0.570	0.752	0.719
Spe	1.000	0.998	1.000	1.000	0.999	0.999	0.925	1.000	0.999	0.981	1.000	0.995	1.000	1.000	0.998	0.999	0.995	1.000	1.000	0.998	0.994
(5)	1	2	3	4	mean	1	2	3	4	mean	1	2	3	4	mean	1	2	3	4	mean	
Dice	89.529	84.727	76.069	49.922	75.062	73.099	76.691	93.864	67.759	77.853	58.920	88.507	72.711	42.560	65.675	79.970	87.155	76.630	61.661	76.354	73.736
HD	1.033	2.749	0.948	0.785	1.379	2.841	6.141	1.002	1.530	2.879	2.256	2.312	1.641	1.158	1.842	1.853	2.404	1.296	1.133	1.671	1.943
JC	0.162	0.200	0.106	0.053	0.130	0.298	0.433	0.290	0.174	0.299	0.120	0.243	0.114	0.053	0.133	0.200	0.330	0.162	0.097	0.197	0.190
RVE	0.093	0.143	0.177	0.285	0.174	0.335	2.056	0.060	0.236	0.672	0.404	0.154	0.279	0.373	0.302	0.278	0.077	0.122	0.194	0.168	0.329
Sen	0.904	0.883	0.711	0.450	0.737	0.697	0.765	0.934	0.663	0.764	0.576	0.896	0.698	0.400	0.643	0.822	0.879	0.753	0.624	0.770	0.729
Spe	1.000	0.997	1.000	1.000	0.999	0.999	0.929	1.000	1.000	0.982	0.999	0.996	0.999	1.000	0.999	0.999	0.996	1.000	1.000	0.999	0.995
(6)	1	2	3	4	mean	1	2	3	4	mean	1	2	3	4	mean	1	2	3	4	mean	
Dice	89.846	82.857	75.490	49.649	74.461	73.496	76.523	93.876	67.588	77.871	59.113	88.522	73.592	41.519	65.686	80.467	86.866	76.002	60.874	76.052	73.518
HD	1.057	3.105	1.007	0.766	1.484	2.807	6.119	1.020	1.518	2.866	2.250	2.408	1.759	1.150	1.892	1.795	2.364	1.430	1.108	1.674	1.979
JC	0.163	0.194	0.105	0.053	0.129	0.300	0.432	0.290	0.173	0.299	0.120	0.243	0.114	0.052	0.132	0.201	0.329	0.160	0.096	0.197	0.189
RVE	0.091	0.195	0.194	0.299	0.195	0.317	2.013	0.065	0.242	0.659	0.411	0.141	0.313	0.392	0.314	0.296	0.078	0.153	0.186	0.178	0.337
Sen	0.902	0.878	0.712	0.447	0.735	0.703	0.764	0.939	0.652	0.765	0.578	0.892	0.703	0.384	0.639	0.832	0.872	0.755	0.606	0.766	0.726
Spe	1.000	0.997	1.000	1.000	0.999	0.999	0.931	1.000	1.000	0.982	0.999	0.996	0.999	1.000	0.999	0.999	0.996	1.000	1.000	0.999	0.995
(7)	1	2	3	4	mean	1	2	3	4	mean	1	2	3	4	mean	1	2	3	4	mean	
Dice	88.075	85.074	76.997	54.502	76.162	80.481	77.577	88.778	61.513	77.087	64.175	83.632	67.529	43.325	64.665	82.431	85.277	71.514	57.243	74.116	73.008
HD	1.079	3.088	0.962	0.753	1.471	2.496	6.427	1.222	1.615	2.940	2.153	3.847	1.758	1.206	2.241	1.871	3.743	1.430	1.187	2.058	2.178
JC	0.159	0.202	0.107	0.059	0.132	0.324	0.437	0.266	0.153	0.295	0.129	0.223	0.103	0.054	0.127	0.205	0.318	0.147	0.088	0.190	0.186
RVE	0.069	0.124	0.139	0.202	0.133	0.319	2.028	0.122	0.302	0.693	0.346	0.242	0.291	0.381	0.315	0.141	0.119	0.172	0.198	0.158	0.325
Sen	0.857	0.858	0.750	0.534	0.750	0.740	0.777	0.880	0.595	0.748	0.601	0.860	0.658	0.435	0.639	0.802	0.873	0.705	0.575	0.738	0.719
Spe	1.000	0.997	1.000	1.000	0.999	1.000	0.929	0.999	0.999	0.982	0.999	0.994	0.999	1.000	0.998	0.999	0.994	0.999	1.000	0.998	0.994
(8)	1	2	3	4	mean	1	2	3	4	mean	1	2	3	4	mean	1	2	3	4	mean	
Dice	89.468	86.396	72.558	55.431	75.963	72.648	78.573	93.068	68.255	78.136	55.325	88.577	70.853	45.212	64.992	78.437	86.464	74.982	60.753	75.159	73.563
HD	1.017	2.511	1.138	0.887	1.388	3.120	6.008	1.110	1.641	2.970	1.965	2.464	2.028	1.253	1.927	1.777	2.488	1.454	1.236	1.739	2.006
JC	0.162	0.205	0.100	0.060	0.132	0.297	0.443	0.287	0.174	0.300	0.113	0.242	0.111	0.056	0.130	0.195	0.327	0.157	0.094	0.193	0.189
RVE	0.107	0.149	0.223	0.214	0.173	0.314	1.988	0.083	0.328	0.678	0.467	0.135	0.355	0.338	0.324	0.291	0.083	0.169	0.277	0.205	0.345
Sen	0.883	0.888	0.679	0.542	0.748	0.694	0.790	0.928	0.731	0.786	0.535	0.906	0.687	0.460	0.647	0.792	0.880	0.747	0.656	0.769	0.738
Spe	1.000	0.997	1.000	1.000	0.999	0.999	0.932	1.000	0.999	0.983	1.000	0.996	0.999	1.000	0.999	0.999	0.996	1.000	1.000	0.999	0.998
(9)	1	2	3	4	mean	1	2	3	4	mean	1	2	3	4	mean	1	2	3	4	mean	
Dice	89.607	86.188	75.868	56.591	77.064	72.590	78.745	93.043	68.564	78.236	56.931	88.331	70.639	46.224	65.531	78.799	86.347	75.005	61.2		

Table S9. Hyper-parameter ablation for sUSAM.

Perturbation radius & Metric	Client index (the next line) & Organ index (after name of method)																				
	1					2					3					4					Mean
	1	2	3	4	mean	1	2	3	4	mean	1	2	3	4	mean	1	2	3	4	mean	
0.6	88.789	84.057	73.915	52.409	74.793	72.391	72.412	91.661	67.626	76.022	62.499	86.911	70.869	42.980	65.815	81.889	85.269	74.171	60.902	75.558	73.047
HD	1.279	2.428	0.964	0.831	1.375	2.989	6.251	1.065	1.584	2.972	2.433	2.203	1.562	1.281	1.870	1.978	2.341	1.307	1.205	1.707	1.981
JC	0.160	0.198	0.101	0.056	0.129	0.295	0.407	0.281	0.173	0.289	0.126	0.238	0.109	0.053	0.131	0.204	0.321	0.155	0.095	0.194	0.186
RVE	0.147	0.148	0.192	0.211	0.174	0.353	1.980	0.104	0.233	0.668	0.357	0.129	0.258	0.360	0.276	0.309	0.086	0.133	0.236	0.191	0.327
Sen	0.905	0.865	0.680	0.500	0.737	0.699	0.713	0.903	0.684	0.750	0.620	0.859	0.669	0.422	0.643	0.849	0.843	0.725	0.643	0.765	0.724
Spe	0.999	0.997	1.000	1.000	0.999	0.999	0.931	1.000	0.999	0.982	0.999	0.997	1.000	1.000	0.999	0.999	0.997	1.000	1.000	0.999	0.995
0.7	1	2	3	4	mean	1	2	3	4	mean	1	2	3	4	mean	1	2	3	4	mean	
Dice	89.529	84.727	76.069	49.922	75.062	73.099	76.691	93.864	67.759	77.853	58.920	88.507	72.711	42.560	65.675	79.970	87.155	76.630	61.661	76.354	73.736
HD	1.033	2.749	0.948	0.785	1.379	2.841	6.141	1.002	1.530	2.879	2.256	2.312	1.641	1.158	1.842	1.853	2.404	1.296	1.133	1.671	1.943
JC	0.162	0.200	0.106	0.053	0.130	0.298	0.433	0.290	0.174	0.299	0.120	0.243	0.114	0.053	0.133	0.200	0.330	0.162	0.097	0.197	0.190
RVE	0.093	0.143	0.177	0.285	0.174	0.335	2.056	0.060	0.236	0.672	0.404	0.154	0.279	0.373	0.302	0.278	0.077	0.122	0.194	0.168	0.329
Sen	0.904	0.883	0.711	0.450	0.737	0.697	0.765	0.934	0.663	0.764	0.576	0.896	0.698	0.400	0.643	0.822	0.879	0.753	0.624	0.770	0.729
Spe	1.000	0.997	1.000	1.000	0.999	0.999	0.929	1.000	1.000	0.982	0.999	0.996	0.999	1.000	0.999	0.999	0.996	1.000	1.000	0.999	0.995
0.8	1	2	3	4	mean	1	2	3	4	mean	1	2	3	4	mean	1	2	3	4	mean	
Dice	89.563	81.818	73.000	54.332	74.678	71.880	77.954	92.785	67.677	77.574	58.873	87.737	70.434	44.521	65.391	80.880	87.264	75.637	60.457	76.060	73.426
HD	0.881	3.826	0.817	0.859	1.596	2.858	6.104	1.022	1.528	2.878	1.953	2.862	1.442	1.212	1.867	1.713	2.496	1.228	1.175	1.653	1.999
JC	0.163	0.191	0.101	0.059	0.128	0.292	0.441	0.286	0.173	0.298	0.120	0.239	0.109	0.056	0.131	0.203	0.330	0.159	0.095	0.197	0.189
RVE	0.071	0.278	0.220	0.207	0.194	0.380	2.094	0.075	0.247	0.699	0.416	0.195	0.260	0.366	0.309	0.224	0.081	0.141	0.173	0.155	0.339
Sen	0.880	0.881	0.677	0.508	0.737	0.678	0.779	0.914	0.660	0.758	0.567	0.895	0.670	0.424	0.639	0.822	0.885	0.737	0.620	0.766	0.725
Spe	1.000	0.996	1.000	1.000	0.999	0.999	0.928	1.000	0.999	0.982	1.000	0.995	1.000	1.000	0.998	0.999	0.996	1.000	1.000	0.999	0.995
0.9	1	2	3	4	mean	1	2	3	4	mean	1	2	3	4	mean	1	2	3	4	mean	
Dice	89.705	82.774	72.666	53.104	74.562	71.986	77.983	93.409	66.928	77.576	57.547	86.915	69.881	45.579	64.980	80.307	87.796	76.619	58.002	75.681	73.200
HD	0.910	2.553	0.971	0.898	1.333	2.815	6.092	1.023	1.570	2.875	1.937	2.840	1.652	1.274	1.926	1.698	2.559	1.250	1.215	1.680	1.954
JC	0.163	0.196	0.099	0.058	0.129	0.292	0.440	0.288	0.171	0.298	0.117	0.237	0.109	0.058	0.130	0.201	0.333	0.162	0.090	0.196	0.188
RVE	0.073	0.165	0.197	0.176	0.153	0.329	2.264	0.073	0.241	0.727	0.436	0.226	0.318	0.325	0.326	0.268	0.088	0.134	0.205	0.174	0.345
Sen	0.887	0.863	0.673	0.502	0.731	0.680	0.784	0.925	0.665	0.763	0.553	0.905	0.667	0.439	0.641	0.812	0.895	0.750	0.598	0.764	0.725
Spe	1.000	0.997	1.000	1.000	0.999	0.999	0.922	1.000	0.999	0.980	1.000	0.994	0.999	1.000	0.998	0.999	0.995	1.000	1.000	0.998	0.994

Start epoch & Metric

Start epoch & Metric	Client index (the next line) & Organ index (after name of method)																				
	1					2					3					4					Mean
	1	2	3	4	mean	1	2	3	4	mean	1	2	3	4	mean	1	2	3	4	mean	
200	89.849	85.316	75.887	51.235	75.572	73.545	77.112	93.514	67.290	77.865	59.906	88.837	71.160	42.631	65.634	80.654	87.517	75.827	61.718	76.429	73.875
HD	1.013	2.652	1.073	0.810	1.387	2.795	6.135	1.041	1.543	2.878	2.216	2.409	1.781	1.224	1.907	1.814	2.443	1.357	1.164	1.694	1.967
JC	0.163	0.202	0.106	0.054	0.131	0.301	0.435	0.289	0.172	0.299	0.121	0.244	0.111	0.053	0.132	0.201	0.331	0.159	0.097	0.197	0.190
RVE	0.102	0.145	0.168	0.278	0.173	0.312	2.092	0.064	0.243	0.678	0.401	0.145	0.293	0.377	0.304	0.284	0.080	0.152	0.194	0.177	0.333
Sen	0.911	0.888	0.713	0.468	0.745	0.707	0.773	0.932	0.653	0.766	0.587	0.907	0.682	0.403	0.645	0.835	0.887	0.753	0.626	0.775	0.733
Spe	1.000	0.997	1.000	1.000	0.999	0.999	0.928	1.000	1.000	0.982	0.999	0.996	0.999	1.000	0.999	0.999	0.996	1.000	1.000	0.999	0.995
300	1	2	3	4	mean	1	2	3	4	mean	1	2	3	4	mean	1	2	3	4	mean	
Dice	89.529	84.727	76.069	49.922	75.062	73.099	76.691	93.864	67.759	77.853	58.920	88.507	72.711	42.560	65.675	79.970	87.155	76.630	61.661	76.354	73.736
HD	1.033	2.749	0.948	0.785	1.379	2.841	6.141	1.002	1.530	2.879	2.256	2.312	1.641	1.158	1.842	1.853	2.404	1.296	1.133	1.671	1.943
JC	0.162	0.200	0.106	0.053	0.130	0.298	0.433	0.290	0.174	0.299	0.120	0.243	0.114	0.053	0.133	0.200	0.330	0.162	0.097	0.197	0.190
RVE	0.093	0.143	0.177	0.285	0.174	0.335	2.056	0.060	0.236	0.672	0.404	0.154	0.279	0.373	0.302	0.278	0.077	0.122	0.194	0.168	0.329
Sen	0.904	0.883	0.711	0.450	0.737	0.697	0.765	0.934	0.663	0.764	0.576	0.896	0.698	0.400	0.643	0.822	0.879	0.753	0.624	0.770	0.729
Spe	1.000	0.997	1.000	1.000	0.999	0.999	0.929	1.000	1.000	0.982	0.999	0.996	0.999	1.000	0.999	0.999	0.996	1.000	1.000	0.999	0.995
400	1	2	3	4	mean	1	2	3	4	mean	1	2	3	4	mean	1	2	3	4	mean	
Dice	90.077	84.171	75.436	53.716	75.850	72.514	77.703	93.665	66.522	77.601	59.985	87.820	69.560	44.576	65.485	80.053	88.187	75.371	57.203	75.203	73.535
HD	0.859	3.096	0.835	0.920	1.428	2.822	6.115	1.004	1.546	2.872	1.893	2.686	1.691	1.289	1.890	1.724	2.586	1.320	1.205	1.708	1.975
JC	0.164	0.198	0.104	0.058	0.131	0.295	0.439	0.290	0.170	0.298	0.121	0.240	0.109	0.056	0.132	0.199	0.334	0.159	0.088	0.195	0.189
RVE	0.065	0.191	0.196	0.169	0.155	0.323	2.252	0.063	0.237	0.719	0.405	0.212	0.307	0.309	0.308	0.241	0.098	0.143	0.204	0.172	0.339
Sen	0.895	0.898	0.697	0.513	0.751	0.685	0.788	0.927	0.655	0.764	0.576	0.919	0.663	0.434	0.648	0.808	0.911	0.732	0.584	0.759	0.731
Spe	1.000	0.997	1.000	1.000	0.999	0.999	0.922	1.000	0.999	0.980	1.000	0.995	1.000	1.000	0.998	0.999	0.995	1.000	1.000	0.998	0.994

Organ indexes are numbers on the straight right side of the name of method.

Model performance is better when metrics are higher, except for HD and RVE.

Table S10. Comparison with SOTAs under setting 2.

Method & Metric	Client index (the next line) & Organ index (after name of method)																				Mean	Post
	1					2					3					4						
	1	2	3	4	mean	1	2	3	4	mean	1	2	3	4	mean	1	2	3	4	mean		
SOLO partial	86.597	80.353	78.451	63.418	77.205	80.222	96.593	64.549	41.904	70.817	83.817	86.602	47.438	57.571	68.857	86.267	87.972	49.282	43.355	66.719	70.899	70.944
HD	0.869	1.916	0.705	0.704	1.049	2.536	2.312	2.006	2.215	2.267	1.111	2.640	1.463	0.941	1.539	1.414	2.383	1.599	1.246	1.661	1.629	1.449
JC	0.155	0.190	0.112	0.071	0.132	0.333	0.570	0.182	0.099	0.296	0.183	0.233	0.070	0.075	0.140	0.224	0.336	0.093	0.064	0.179	0.187	0.187
RVE	0.111	0.124	0.145	0.179																		

Table S11. Comparison with SOTAs under setting 3.

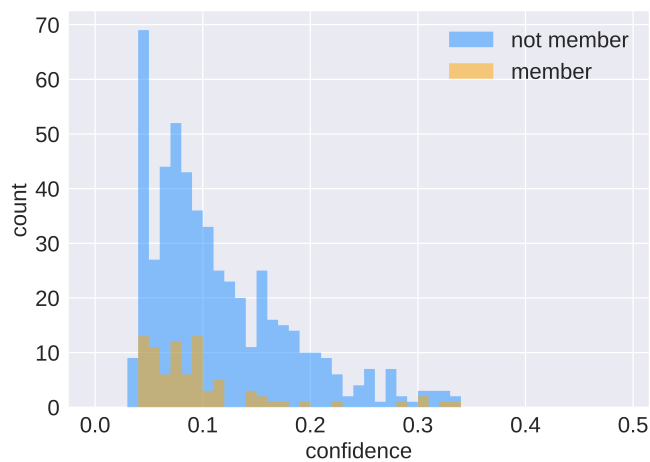
Method & Metric	Client index (the next line) & Organ index (after name of method)																				Mean	Post
	1					2					3					4						
SOLO partial	1	2	3	4	mean	1	2	3	4	mean	1	2	3	4	mean	1	2	3	4	mean		
Dice	83.130	91.808	66.233	71.113	78.071	94.319	77.109	77.739	24.397	68.391	67.871	85.653	81.382	22.628	64.384	86.879	83.395	69.573	26.200	66.512	69.339	69.693
HD	1.003	1.312	1.387	0.644	1.087	1.629	5.959	2.638	2.345	3.143	1.544	2.322	1.735	1.376	1.744	1.506	2.871	1.853	1.306	1.884	1.964	1.706
JC	0.150	0.225	0.086	0.083	0.136	0.413	0.424	0.221	0.056	0.279	0.147	0.230	0.126	0.027	0.133	0.225	0.308	0.141	0.037	0.178	0.181	0.183
RVE	0.112	0.059	0.366	0.135	0.168	0.056	0.842	0.844	0.547	0.572	0.318	0.141	0.318	0.551	0.332	0.480	0.098	0.267	0.574	0.355	0.357	0.341
Sen	0.816	0.930	0.633	0.693	0.768	0.946	0.762	0.908	0.223	0.710	0.679	0.873	0.806	0.204	0.641	0.901	0.833	0.709	0.230	0.668	0.697	0.694
Spe	1.000	0.999	0.999	1.000	1.000	1.000	0.968	0.996	0.999	0.991	1.000	0.997	0.999	1.000	0.999	0.999	0.996	0.999	1.000	0.999	0.997	0.997
FedAvg*	1	2	3	4	mean	1	2	3	4	mean	1	2	3	4	mean	1	2	3	4	mean		
Dice	86.362	90.381	77.539	65.820	80.026	92.694	79.490	83.124	25.580	70.222	73.052	86.870	78.673	30.003	67.150	86.030	85.495	69.783	28.162	67.368	71.192	71.523
HD	1.035	2.080	1.617	0.691	1.356	1.814	5.631	2.175	2.319	2.985	1.864	2.458	1.923	1.286	1.883	1.649	2.938	1.924	1.389	1.975	2.050	1.685
JC	0.155	0.220	0.107	0.075	0.139	0.401	0.438	0.244	0.059	0.286	0.157	0.234	0.122	0.036	0.137	0.221	0.318	0.142	0.040	0.180	0.186	0.187
RVE	0.093	0.093	0.324	0.157	0.167	0.081	0.831	0.605	0.493	0.503	0.240	0.139	0.387	0.451	0.304	0.401	0.099	0.302	0.427	0.307	0.320	0.294
Sen	0.853	0.919	0.779	0.650	0.800	0.929	0.784	0.917	0.237	0.717	0.734	0.891	0.780	0.279	0.671	0.907	0.864	0.711	0.262	0.686	0.719	0.716
Spe	1.000	0.998	0.999	1.000	0.999	0.999	0.969	0.997	0.999	0.991	0.999	0.996	0.999	1.000	0.999	0.999	0.995	0.999	1.000	0.998	0.997	0.997
UFPS(Ours)	1	2	3	4	mean	1	2	3	4	mean	1	2	3	4	mean	1	2	3	4	mean		
Dice	84.849	83.967	77.615	67.276	78.427	92.129	82.454	84.455	32.139	72.794	77.418	85.045	74.852	35.710	68.256	83.735	86.671	69.981	30.618	67.751	71.807	72.601
HD	3.194	3.500	2.875	1.176	2.686	1.879	6.047	1.954	2.418	3.075	3.587	3.235	2.678	2.000	2.875	2.736	3.392	2.261	1.857	2.562	2.800	1.951
JC	0.150	0.197	0.107	0.076	0.132	0.397	0.461	0.251	0.073	0.296	0.163	0.227	0.114	0.043	0.137	0.212	0.324	0.142	0.044	0.180	0.186	0.190
RVE	0.503	0.374	0.910	0.172	0.490	0.103	1.363	0.587	0.504	0.639	0.350	0.229	0.591	0.293	0.366	0.712	0.121	0.296	0.363	0.373	0.467	0.366
Sen	0.869	0.921	0.787	0.672	0.812	0.923	0.830	0.904	0.290	0.737	0.794	0.899	0.767	0.348	0.702	0.898	0.900	0.716	0.296	0.703	0.739	0.735
Spe	0.998	0.995	0.998	1.000	0.998	0.999	0.952	0.997	0.999	0.987	0.998	0.994	0.998	0.999	0.997	0.998	0.994	0.999	0.999	0.997	0.995	0.996

Organ indexes are numbers on the straight right side of the name of method.
 Model performance is better when metrics are higher, except for HD and RVE.

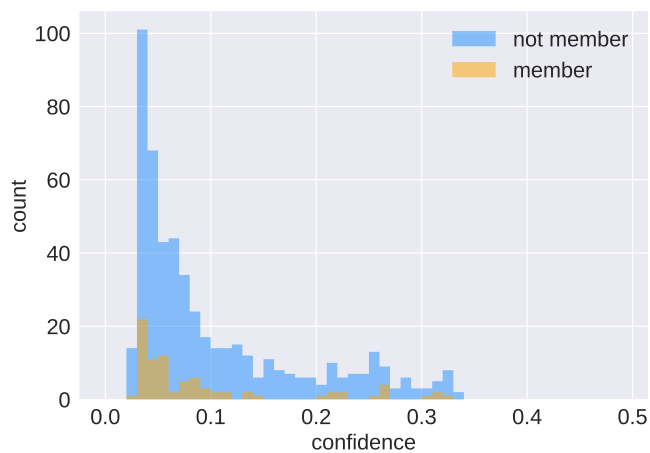
Table S12. Performance comparison between teacher models.

No aug	Kidney	Liver	Spleen	Pancreas	Mean
Client 1	91.43 / 0.77	86.71 / 1.44	0 / 1.61	0.51 / 1.11	47.01 / 2.23
Client 2	51.41 / 3.66	33.29 / 7.83	93.64 / 0.93	70.59 / 1.53	62.23 / 3.49
Client 3	43.56 / 2.81	93.73 / 1.71	0.21 / 2.19	10.73 / 1.40	37.06 / 2.03
Client 4	55.40 / 2.27	90.54 / 2.08	0.99 / 2.84	29.51 / 1.51	44.11 / 2.18
Mean	60.45 / 2.37	76.06 / 3.26	23.41 / 1.89	27.83 / 1.38	47.01 / 2.23
Aug	Kidney	Liver	Spleen	Pancreas	Mean
Client 1	91.48 / 0.80	85.92 / 1.21	53.94 / 1.22	45.35 / 0.85	69.17 / 1.02
Client 2	68.78 / 3.02	72.38 / 6.34	91.84 / 1.05	70.01 / 1.53	75.75 / 3.03
Client 3	53.09 / 2.11	90.20 / 1.74	64.66 / 1.27	34.43 / 1.35	60.59 / 1.62
Client 4	77.48 / 1.57	86.16 / 2.28	75.39 / 1.12	59.76 / 1.11	74.70 / 1.52
Mean	72.70 / 1.87	83.66 / 2.89	71.45 / 1.16	52.38 / 1.21	70.05 / 1.80
Aug+DP	Kidney	Liver	Spleen	Pancreas	Mean
Client 1	90.79 / 0.70	83.76 / 1.20	46.84 / 0.98	38.20 / 0.76	64.89 / 0.91
Client 2	51.93 / 3.42	68.73 / 5.96	86.12 / 1.17	68.12 / 1.52	68.72 / 3.01
Client 3	40.64 / 1.96	88.58 / 1.65	59.30 / 1.15	27.10 / 1.22	53.90 / 1.49
Client 4	70.59 / 1.63	84.50 / 2.26	72.73 / 1.08	55.26 / 1.07	70.77 / 1.51
Mean	63.48 / 1.92	81.39 / 2.76	66.24 / 1.09	47.17 / 1.14	64.57 / 1.73

Here we show Dice / HD (higher / lower numbers are better) on test sets.



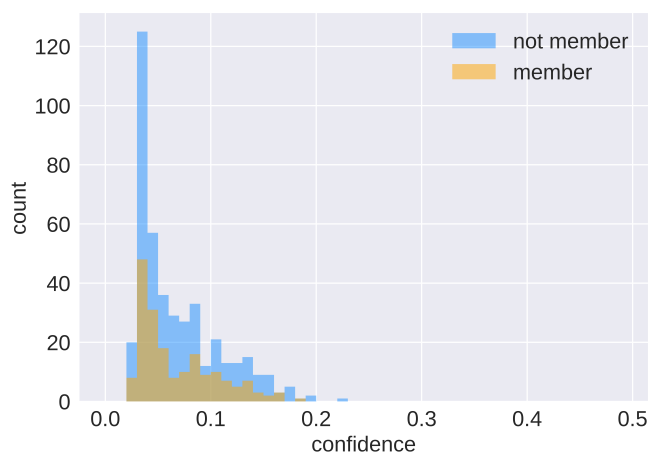
(a) teacher 1, no aug



(b) teacher 1, aug



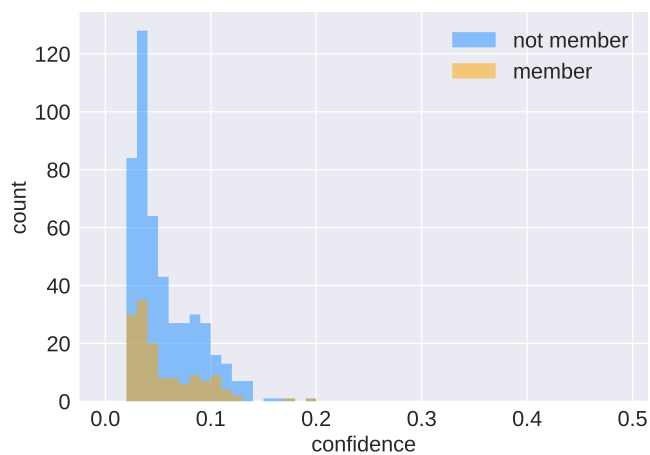
(c) teacher 2, no aug



(d) teacher 2, aug



(e) teacher 3, no aug



(f) teacher 3, aug

Figure S 5: Comparison of uncertainty.

Comparison of uncertainty for all clients when teacher models are trained with or without augmentation (aug).

Table S13. MIA attack performance on teacher models.

No aug	Client 1	Client 2	Client 3	Mean
Shadow	50.39 / 2.588	60.36 / 1.115	71.43 / 5.189	60.72 / 2.964
Attack class mean	68.06 / 57.75	69.61 / 66.11	53.05 / 36.40	63.57 / 53.42
Attack class 1	82.92 / 48.22	97.87 / 74.49	98.63 / 59.01	93.14 / 60.57
Aug	Client 1	Client 2	Client 3	Mean
Shadow	64.45 / 2.614	46.29 / 1.304	82.21 / 5.760	64.31 / 3.226
Attack class mean	78.32 / 78.56	68.12 / 67.18	76.23 / 72.74	74.22 / 72.82
Attack class 1	65.85 / 66.66	46.80 / 59.06	94.52 / 73.79	69.05 / 66.50
Aug + DP	Client 1	Client 2	Client 3	Mean
Shadow	59.11 / 2.722	45.46 / 1.396	80.72 / 5.465	61.76 / 3.194
Attack class mean	70.01 / 66.91	69.28 / 68.73	57.29 / 45.82	65.52 / 60.48
Attack class 1	63.41 / 51.99	51.06 / 61.93	95.89 / 60.86	70.12 / 58.26

Here we show Dice / HD (higher / lower numbers indicate better stimulation) for the shadow model and accuracy / F1 score (higher numbers indicate better attacks) for the attack model.

Class 1 refers to the label 'member'.

References

1. Aman Sinha, Hongseok Namkoong, and John Duchi. Certifiable distributional robustness with principled adversarial training. *arXiv preprint arXiv:1710.10571*, 2, 2017. <https://arxiv.org/abs/1710.10571>.
2. Peter L Bartlett and Shahar Mendelson. Rademacher and gaussian complexities: Risk bounds and structural results. In *Computational Learning Theory: 14th Annual Conference on Computational Learning Theory, COLT 2001 and 5th European Conference on Computational Learning Theory, EuroCOLT 2001 Amsterdam, The Netherlands, July 16–19, 2001 Proceedings 14*, pages 224–240. Springer, 2001. https://doi.org/10.1007/3-540-44581-1_15.
3. Thomas Mikosch, Aad van der Vaart, and Jon A. Wellner. *Weak Convergence and Empirical Processes: With Applications to Statistics*. Springer Science & Business Media, 1996. <https://link.springer.com/book/10.1007/978-1-4757-2545-2>.
4. Zhe Qu, Xingyu Li, Rui Duan, Yao Liu, Bo Tang, and Zhuo Lu. Generalized federated learning via sharpness aware minimization. In *International Conference on Machine Learning*, pages 18250–18280. PMLR, 2022. <https://proceedings.mlr.press/v162/qu22a.html>.
5. Haibo Yang, Minghong Fang, and Jia Liu. Achieving linear speedup with partial worker participation in non-iid federated learning. *arXiv preprint arXiv:2101.11203*, 2021. <https://arxiv.org/abs/2101.11203>.
6. Fabian Isensee, Paul F Jaeger, Simon AA Kohl, Jens Petersen, and Klaus H Maier-Hein. nnu-net: a self-configuring method for deep learning-based biomedical image segmentation. *Nature methods*, 18(2):203–211, 2021. <https://doi.org/10.1038/s41592-020-01008-z>.
7. Brendan McMahan, Eider Moore, Daniel Ramage, Seth Hampson, and Blaise Aguera y Arcas. Communication-efficient learning of deep networks from decentralized data. In *Artificial intelligence and statistics*, pages 1273–1282. PMLR, 2017. <https://www.nejm.org/doi/full/10.1056/NEJM200205233462118>.
8. M Jorge Cardoso, Wenqi Li, Richard Brown, Nic Ma, Eric Kerfoot, Yiheng Wang, Benjamin Murrey, Andriy Myronenko, Can Zhao, Dong Yang, et al. Monai: An open-source framework for deep learning in healthcare. *arXiv preprint arXiv:2211.02701*, 2022. <https://arxiv.org/abs/2211.02701>.
9. Ilya Loshchilov and Frank Hutter. Decoupled weight decay regularization. *arXiv preprint arXiv:1711.05101*, 2017. <https://arxiv.org/abs/1711.05101>.
10. Jean-Bastien Grill, Florian Strub, Florent Altché, Corentin Tallec, Pierre Richemond, Elena Buchatskaya, Carl Doersch, Bernardo Avila Pires, Zhaohan Guo, Mohammad Gheshlaghi Azar, et al. Bootstrap your own latent—a new approach to self-supervised learning. *Advances in neural information processing systems*, 33:21271–21284, 2020. https://proceedings.neurips.cc/paper_files/paper/2020/file/f3ada80d5c4ee70142b17b8192b2958e-Paper.pdf.
11. Simon Kornblith, Mohammad Norouzi, Honglak Lee, and Geoffrey Hinton. Similarity of neural network representations revisited. In *International Conference on Machine Learning*, pages 3519–3529. PMLR, 2019. <http://proceedings.mlr.press/v97/kornblith19a/kornblith19a.pdf>.
12. Reza Shokri, Marco Stronati, Congzheng Song, and Vitaly Shmatikov. Membership inference attacks against machine learning models. In *2017 IEEE symposium on security and privacy (SP)*, pages 3–18. IEEE, 2017. <https://doi.org/10.1109/SP.2017.41>.
13. Tomas Chobola, Dmitrii Usynin, and Georgios Kaissis. Membership inference attacks against semantic segmentation models. *arXiv preprint arXiv:2212.01082*, 2022. <https://arxiv.org/abs/2212.01082>.
14. Cynthia Dwork. Differential privacy. In *International colloquium on automata, languages, and programming*, pages 1–12. Springer, 2006. https://link.springer.com/chapter/10.1007/11787006_1.